

THS 7HB816 2 2W>

This is to certify that the dissertation entitled

ASYMPTOTIC NEAR-TO-FAR-ZONE TRANSFORMATION FOR PERIODIC CONFORMAL ANTENNAS EMBEDDED IN CANONICAL STRUCTURES

presented by

JORGE M VILLA-GIRON

has been accepted towards fulfillment of the requirements for the

Ph. D degree in Electrical and Computer Engineering

Major Professor's Signature

Maych 21, 2008

MSU is an affirmative-action, equal-opportunity employer

Date

LIBRARY Michigan State University

PLACE IN RETURN BOX to remove this checkout from your record. **TO AVOID FINES** return on or before date due. **MAY BE RECALLED** with earlier due date if requested.

DATE DUE	DATE DUE	DATE DUE
	—	

5/08 K:/Proj/Acc&Pres/CIRC/DateDue indd

ASYMPTOTIC NEAR-TO-FAR-ZONE TRANSFORMATION FOR PERIODIC CONFORMAL ANTENNAS EMBEDDED IN CANONICAL STRUCTURES

By

Jorge M. Villa-Giron

A DISSERTATION

Submitted to
Michigan State University
in partial fulfillment of the requirements
for the degree of

DOCTOR OF PHILOSOPHY

Electrical and Computer Engineering

2008

ABSTRACT

ASYMPTOTIC NEAR-TO-FAR-ZONE TRANSFORMATION FOR PERIODIC CONFORMAL ANTENNAS EMBEDDED IN CANONICAL STRUCTURES

By

Jorge M. Villa-Giron

Conformal antennas are important to the aerospace community because of their aerodynamic characteristics and their versatility for electronic scanning. Computational electromagnetic methods such as the Finite Element-Boundary Integral method have been used extensively to obtain estimations of radiation and scattering performance of antennas on planar, elliptical and prolate spheroid surfaces. Typically, in formulating these methods, either an infinite structure approximation or reciprocity has been used to accomplish the near-to-far-zone transformation. At times, the need for such transformation has been ignored all-together. In cases where a Green's function—that enforced cylinder boundary conditions—was used, calculations of the far-zone field in the paraxial region were inaccurate. Several researchers have been working in obtaining integral solutions that overcome the problems in the paraxial and shadow zone using GTD and UTD techniques.

In this dissertation, an asymptotic periodic dyadic Green's function will be derived. A different asymptotic approximation for the periodic Green's function will be used to accomplish the near-to-far-zone transformation. This results will be validated by testing expression for large radii against similar results for planar structures.

To My Inspirations, Sebastian and Nivia

ACKNOWLEDGMENTS

I would like to thank several people who have helped me through the development of my PhD. First, I would like to mention three key people and acknowledge them for helping me during my doctoral work and were integral part of my development. Special thanks to my three advisors: Dr. B. Shanker, Dr. Leo Kempel, and Dr. Edward Rothwell. Thank you so much Shanker for teaching me how to think critically, for encouraging me when I needed it the most, for teaching me electromagnetic theory; you do not imagine how excited and pleased I was while sitting in your class listening to you. Many thanks to you because not only you shared your knowledge, but also your friendship; thank you for sharing the secrets of the Russian beer and the spicy food, thank you for inviting me into your house, and for helping me to discover how good I am in sports, jogging and basketball. These are memories I will never forget. I do not know how to say thank you to you, Leo, I have never seen a person as pro-student as you are. My family and I appreciate everything you have done for us. You are one of the great role models I want to follow everyday and you are a great example of becoming a well balanced human being that can be not only a successful researcher, but also a manager. Dr Rothwell thanks for being there for me; being a lab instructor for you was an invaluable experience for me and it allowed me to develop a different way to view the electromagnetic theory; your comments were extremely helpful to understand deeply my research topic.

Second, I thank the opportunity of being part of MSU's Computational Electromagnetic Group during my degree; sharing time and space with great persons is

invaluable. Many thanks to Dr. Kobidze and Dr. Gao were always there to answer basic electromagnetic questions and wiling to help. Thanks to my friend Dr. Pedro Barba for dedicating time explaining the principles of computational electromagnetics, I enjoyed the time we spent at Beaners discussing finite elements topics. Thanks to Dr. Chuan for helping me debug my codes and for showing what is in reality a hardworker. Naveen and Vikram, thanks for sharing your culture and knowledge with me, I admire you very much. Thanks Andrew Baczewski and Ozgur Tuncer for your sincere friendship and for sharing great times at RCE B-102.

I am extremely grateful for the assistance of Dr. Barbara O'Kelly and Dr. Pierce Pierre for providing me an opportunity to be part of this great institution. You helped me begin to realize my biggest dream, become an expert in a technical area and earn a PhD degree from a national recognized institution. Thank you so much for all the tools you provided me for my success and thanks to you I have never worried about money during my PhD. That helped a lot. Thank you Barbara for you friendship and always looking after me along with Dr. Pierre.

My dissertation would have not been possible without the unconditional support of my family. I can not find words to express my infinite gratitude to my parents: Dumar Villa and Leonor Giron, my son Sebastian and my wife Nivia for supporting and understanding how important this was for me. You all helped me accomplish my biggest dream.

TABLE OF CONTENTS

LIST OF FIGURES		
KEY T	O SYMBOLS AND ABBREVIATIONS	ix
CHAPT Introdu	TER 1	1
1.1	Literature Review	2
1.2	Asymptotic Solution for the Electromagnetic Fields due to an Aperture on a Circular Cylinder using UTD	6
1.3	Electromagnetic Fields in the Shadow and Transition Region	8
CHAPT Electron	TER 2 magnetic fields in terms of Green's Functions	17
2.1	Derivation of Green's Functions	20
2.2	Approximation of Green's Function On-Surface	33
2.3	Approximation of Green's Function in the Far Zone	40
CHAP7 Modifie	TER 3 d Modal Solution for the Dyadic Green's Function	63
3.1	Exact Modal and Asymptotic Solutions	64
3.2	Numerical Results and Discussions	70
3.3	Singly Surface Periodic Structure in \hat{z}	80
CHAP7 Conclus	TER 4 ions and Future Work	93
RIRI IC	OCR A PHV	06

LIST OF FIGURES

Figure 1.1	Diffraction of surface rays	4
Figure 1.2	Infinite circular cylinder with an aperture source \mathbf{M}	6
Figure 1.3	Shadow, transition and illuminated regions adjacent to a magnetic dipole on a perfectly conducting, convex surface	7
Figure 1.4	Strip formed by surface rays	8
Figure 1.5	Coordinate system of a surface diffracted ray	11
Figure 1.6	Diffracted Wave front	13
Figure 1.7	Spread of a surface diffracted ray	14
Figure 2.1	Watson transform integration contour c formed by paths c_1 and c_2	35
Figure 3.1	Complex k_z plane	65
Figure 3.2	Contour of integration dictated by the radiation condition	66
Figure 3.3	Definition of the Branch Cut	67
Figure 3.4	Integration around the Branch Cut	68
Figure 3.5	Magnitude convergence for exact modal solution and modified modal solution	72
Figure 3.6	Phase convergence for exact modal solution and modified modal solution	74
Figure 3.7	(a) Magnitude for exact modal solution and modified modal solution; (b) Relative Error; $n=3$ and $R=50\lambda$	75
Figure 3.8	(a) Magnitude for exact modal solution and modified modal solution; (b) Relative Error; $n=3$ and $R=100\lambda$	76
Figure 3.9	(a) Phase for exact modal solution and modified modal solution; (b) Relative Error; $n = 3$ and $R = 50\lambda \dots \dots \dots$	77
Figure 3.10	(a) Phase for exact modal solution and modified modal solution; (b) Relative Error; $n = 3$ and $R = 100\lambda$	79
Figure 3.11	Magnitude convergence for modified modal solution and steepest descent solution	85
Figure 3.12	Phase convergence for modified modal solution and steepest descent solution	87
Figure 3.13	(a) Magnitude for modified modal solution and steepest descent solution; (b) Relative error; $n = 10$, $R = 50\lambda$	88
Figure 3.14	(a) Magnitude for modified modal solution and steepest descent solution; (b) Relative error; $n=10,\ R=100\lambda$	89

Figure 3.15	(a) Phase for modified modal solution and steepest descent solution; (b) Relative error; $n = 10$, $R = 50\lambda$	90
Figure 3.16	(a) Phase for modified modal solution and steepest descent solution; (b) Relative error; $n=10,R=100\lambda$	91
Figure 3.17	Singly surface periodic structure in \hat{z}	92

KEY TO SYMBOLS AND ABBREVIATIONS

CEM: Computational Electromagnetics

FE-BI: Finite Element-Boundary Integral

GTD: Geometric Theory of Diffraction

UTD: Uniform Theory of Diffraction

EMS: Exact Modal Solution

MMS: Modified Modal Solution

CHAPTER 1

INTRODUCTION

The interest in developing antennas that can be mounted on structures with a convex surface such as airplanes, automobiles, cell phones, or laptops in mobile communication systems, has increased significantly over the past few decades. These types of antennas are known as conformal antennas. Consequently, studies to understand radiation of these antennas in the presence of mounting platform has increased as well. The analysis of these antennas is critical as the performance "in situ" is very different from that of a stand alone structure. These antennas offer several advantages; a potential listing is given next. Conformal antennas can help the aerodynamics of the structure on which it is mounted and reduces its cost and weight [1]. Arrays of these antennas permit faster electronic scan than a traditional mechanical scan. Compared to mechanically scanned arrays, small aerodynamic drag and less space occupancy are advantages of conformal arrays [2, 3].

Canonical shapes such as cylinders and prolate spheroids are acceptable approximations to surface that the antennas are typically mounted up on, and can be used to model structures with singly and doubly surfaces, respectively [4, 5]. One analytic solution to fields due to sources radiating in the presence of canonical shapes exist. Computational electromagnetic methods have also been used to obtain an approximate solution to the problem [6, 7]. These techniques have only been efficient when analyzing electrically small structures, or arrays with small number of elements [8, 9].

This thesis proceeds along the following lines: Different methods for analyzing high frequencies methods will be presented in the reminder of this chapter. The Geometric Theory of Diffraction (GTD) is a technique that finds a solution for high frequencies [10]. A complete derivation of the GTD method for a circular cylinder,

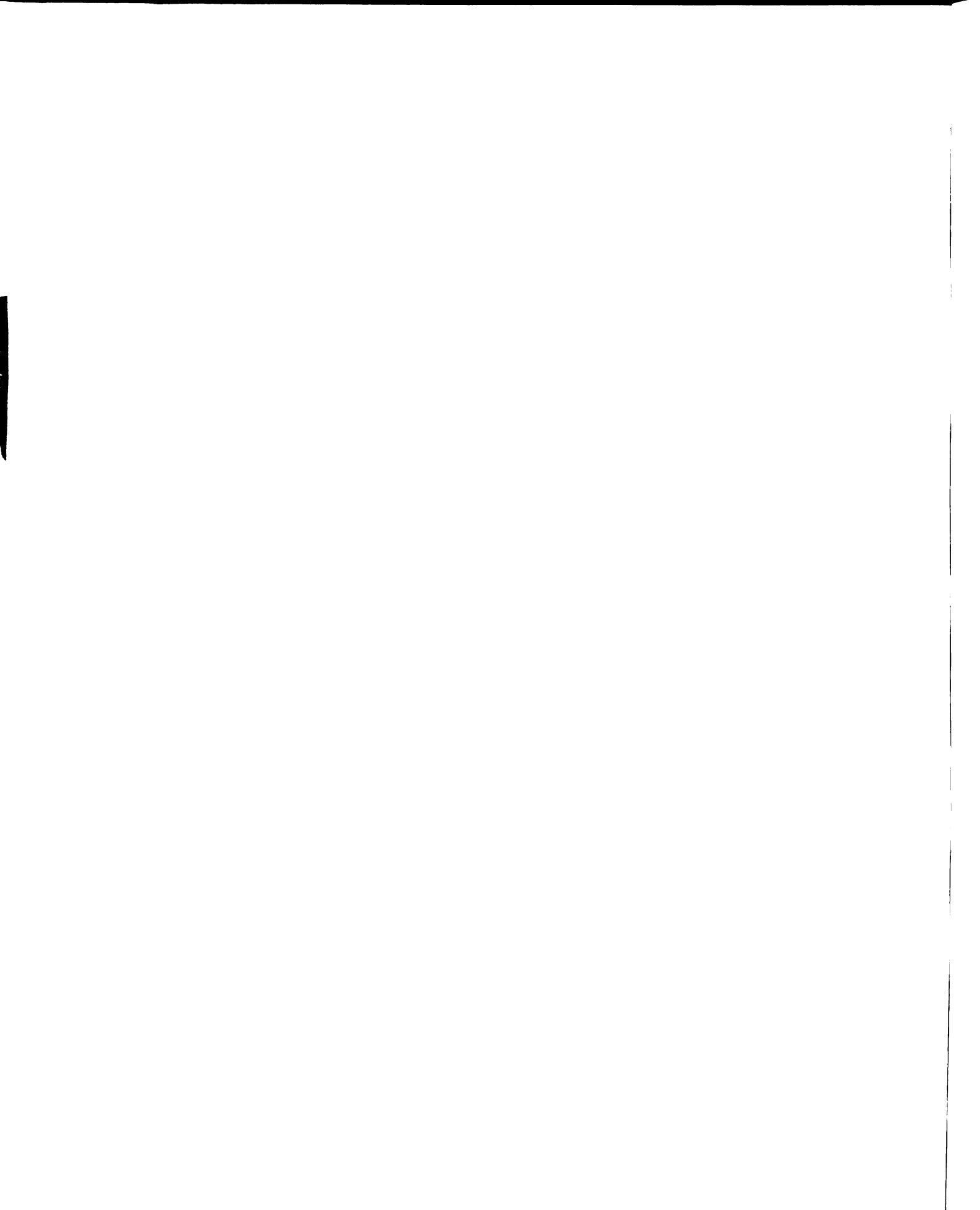
developed by Keller [10], will be expanded in Section 1.2.

The canonical and asymptotic Green's function for a circular cylinder was obtained and its procedure is described in Chapter 2. After this, the function was modified to increase efficiency at high frequencies on the surface of the cylinder and also in the far field zone using Watson's technique [11]. Finally the resultant integral equation is evaluated by the method of steepest descent. It is important to mention the final expression is not valid in the paraxial zone [12, 13, 14, 15], when the observation angle is close to the surface but far away from the source ($\theta = 0$ or $\theta = \pi$ and $R \gg 10\lambda$).

Chapter 3 contains the derivation of a modified modal solution. Validation of this solution against the exact modal solution for an infinite circular cylinder of a small radius ($a = 0.01\lambda$) is shown. A comparison between the steepest descent solution and the modified modal solution for the infinite circular cylinder of big radius ($a = 10\lambda$) is presented. A new asymptotic solution for an elliptical cylinder is derived, based in Keller's method and using the modified modal solution for a circular cylinder matching the GTD approximation constants. Conclusions and future work will be presented in Chapter 4.

1.1 Literature Review

Modeling conformal antennas is a challenge. Not only it is necessary to model the antenna "per se" but the platform that it is mounted upon as well. Several approximate methods have been proposed to analyze these antennas, and these depend of its platform and the behavior of the antenna. The first studies assumed, that the antenna was mounted on an infinite circular cylinder [16]. The fields were expressed in terms of infinite Fourier series of the form $\sum_{m} C_{m} \cos(m\phi)$, with C_{m} as a function of the radius, ρ (in cylindrical coordinates). Wait and Kahana [17] obtained the radiation pattern for circumferential half-wave slots with ka = 2, 3, 5, and for different elevation angles. Similar results were obtained by Bailin [18] for large circular



cylinders. The solutions are obtained in terms of harmonic series using integer order Bessel functions. This solution is poorly convergent for large arguments of the Bessel functions (when $ka \gg 1$).

Watson [19] developed a method for large values of ka, where he transformed the poor converging harmonic series into a contour integral, deforming the integration path for capturing individual terms poles which represent creeping waves. This new contour integral is expressed in the form of infinite but rapid convergent series. The problem with Watson's method is that it can be only used for some canonical shapes. For a slotted cylinder antenna, the residue series proposed by Watson is highly convergent in the direction away from the slot; known as the deep or shadow region. However, better results were obtained for the region forward to the slot, or the illuminated region, when using physical and geometrical optics [20, 21]. These methods, by Watson, assumes that there are no surface currents in the deep or shadow region and also approximate the induced current in the illuminated region by the current that would be induced on the local tangent plane. While good results were obtained at the illuminated region, incorrect results were obtained from the shadow and the transition region, which is the boundary between the shadow and illuminated region. With the assumption that fields propagate along rays Keller developed the Geometrical Theory of Diffraction (GTD) [10]. This theory includes the effects of diffraction which are not considered in the geometrical optics.

Diffraction happens when an incident ray is tangential to a convex surface, or when it hits edges, or vertices of boundary surfaces, creating new rays called diffracted rays, see Figure 1.1. The total field, defined in the geometrical optics, is a sum of the incident and reflected rays. A diffraction coefficient can also be obtained and used to obtain the diffracted ray by multiplying the incident ray with the diffraction coefficient [10, 22]. This coefficient depends on the type of structure or material the ray is hitting upon or traveling on, for instance, in Figure 1.1, \mathbf{r}' is the surface ray

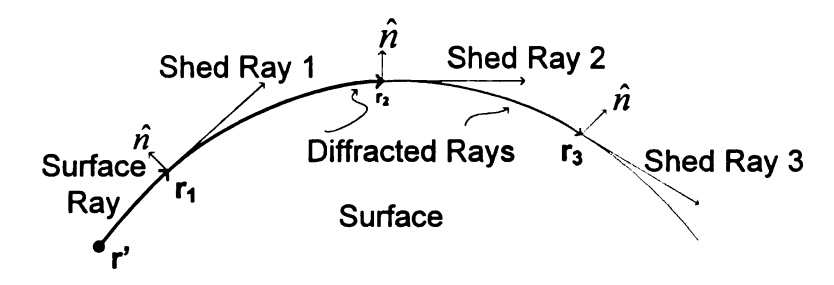


Figure 1.1. Diffraction of surface rays

vector launched at the source point, \mathbf{r}_i for i=1,2,3... are the shed rays and \hat{n} is the unit vector normal to the surface at the diffraction points. Laws for geometrical optics were modified and extended at the new GTD. The generalized Fermat's principle is one of them. The modified principle says the least time path is the same minimum distance path. It emphasizes that a surface-diffracted ray between two points is a curve where the optical length is stationary among all curves between the same points having an arc on the boundary surface [10]. The optical length then defined as the product of the geometrical distance and the refractive index (assuming a constant refractive index).

An extension in the GTD was made by Pathak et al. [23] and he called this new method Uniform GTD (UTD) [24]. This method introduces a new term, dyadic torsion factor [25]. This includes the torsional surface rays that may be excited by apertures and monopoles. All the ray fields are expressed in terms of Fock functions improving the solution in the transition region including the boundary with the shadow region, where the GTD failed [26], and reducing it geometric optics in the lit or illuminated region.

The incremental fields, $d\mathbf{E}^m(\mathbf{r}|\mathbf{r}')$ and $d\mathbf{H}^m(\mathbf{r}|\mathbf{r}')$ are excited by the aperture. These surface fields travel along the surface. The path they follow is known as the geodesic or shortest path of propagation. It is described by a partial differential equation theory for rays on surfaces for homogeneous medium, fulfilling the extended

Fermat's principle [10]. The dyadic torsion factor, $\overline{\mathbf{T}}^{\mathbf{F}}(\mathbf{r}|\mathbf{r}')$, proposed by Pathak, relationes the incremental fields, $d\mathbf{E}^{m}(\mathbf{r}|\mathbf{r}')$ and $d\mathbf{H}^{m}(\mathbf{r}|\mathbf{r}')$, where \mathbf{F} is either \mathbf{E} or \mathbf{H} depending of the problem being solved, and the differential magnetic current $d\mathbf{M}$ by [23]

$$d\mathbf{F}(\mathbf{r}|\mathbf{r}') = \frac{-jk}{4\pi} d\mathbf{M}(\mathbf{r}') \cdot \overline{\mathbf{T}}^{\mathbf{F}}(\mathbf{r}|\mathbf{r}') Df \frac{e^{-jks}}{s}$$
(1.1)

where $d\mathbf{F}(\mathbf{r}|\mathbf{r}')$ is either $d\mathbf{E}^m(\mathbf{r}|\mathbf{r}')$ or $d\mathbf{H}^m(\mathbf{r}|\mathbf{r}')$, k is the wave number, the geodesic path between the source and the observation point is described by s. The surface ray divergence factor, Df, represents the change in the width of the surface ray strip, and is given by

$$Df = \sqrt{\frac{s \, d\psi_0}{\rho_c \, d\psi}} \tag{1.2}$$

The term $d\psi_0$ is the angle between the surface rays adjacent to the central surface ray from $\mathbf{r'}$ to \mathbf{r} . $d\psi$ is the angle between the backward tangent rays to the adjacent rays at the observation point, \mathbf{r} . The distance between \mathbf{r}_c and \mathbf{r} is called the tangent (or geodesic) radius of curvature of the geodesic circle at \mathbf{r} [25].

The dyadic torsion factor, $\overline{\mathbf{T}}(\mathbf{r}|\mathbf{r}')$, was introduced because the field on the surface is not just the surface ray field between the source and the observation point. It is a function of the launching of the surface ray field at the source, the variation of the surface ray field from \mathbf{r}' to \mathbf{r} , and its attachment to the surface. All these additional effects are modeled by the dyadic torsion factor, $\overline{\mathbf{T}}(\mathbf{r}|\mathbf{r}')$ and is defined as:

$$\overline{\mathbf{T}}(\mathbf{r}|\mathbf{r}') = T_1 \hat{t}\hat{t}' + T_2 \hat{t}\hat{b}' + T_3 \hat{t}\hat{n}' + T_4 \hat{b}\hat{t}' + T_5 \hat{b}\hat{b}' + T_6 \hat{b}\hat{n}' + T_7 \hat{n}\hat{t}' + T_8 \hat{n}\hat{b}' + T_9 \hat{n}\hat{n}'$$
(1.3)

where \hat{n} is unit vector normal to the surface at any point, \hat{t} a tangential unit vector to the surface, and \hat{b} as the cross product between \hat{t} and \hat{n} , named the binormal unit vector. For a differential magnetic current that is tangential to the convex surface,

(1.3) reduces to

$$\overline{\mathbf{T}}(\mathbf{r}|\mathbf{r}') = T_1 \hat{t}\hat{t}' + T_2 \hat{t}\hat{b}' + T_4 \hat{b}\hat{t}' + T_5 \hat{b}\hat{b}' + T_7 \hat{n}\hat{t}' + T_8 \hat{n}\hat{b}'$$
(1.4)

as $d\mathbf{M}(\mathbf{r}) \cdot \hat{n} = 0$.

1.2 Asymptotic Solution for the Electromagnetic Fields due to an Aperture on a Circular Cylinder using UTD

Next, a method to find the field produced by a magnetic current due to an aperture on an uniformly circular cylinder is presented. The problem that we will attempt to solve is to find the electromagnetic field produced by an aperture in the convex surface of an infinite circular cylinder. It is to assumed the external medium is free space. The problem is shown in Figure 1.2. It is known that the tangential component of the

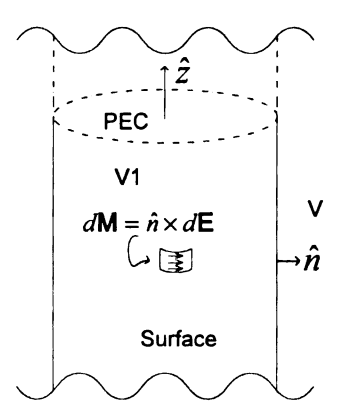


Figure 1.2. Infinite circular cylinder with an aperture source M

electric field \mathbf{E} , is zero everywhere on the cylinder surface except at the aperture. The tangential component of \mathbf{E} on the aperture S, can be expressed in terms of differential magnetic current $d\mathbf{M}$ as in (1.5). It is assumed that this current is known and is given

by

$$d\mathbf{M}(\mathbf{r}') = \mathbf{E}_{a}(\mathbf{r}') \times \hat{\mathbf{n}} dA \tag{1.5}$$

Here, dA is an element of area in the aperture, $\mathbf{E}_a(\mathbf{r'})$ represents the electric field at a point $\mathbf{r'}$ inside the aperture. Electric and magnetic fields can be found at some point \mathbf{r} outside the surface then integrating the incremental fields $d\mathbf{E}^m(\mathbf{r}|\mathbf{r'})$ and $d\mathbf{H}^m(\mathbf{r}|\mathbf{r'})$, over the aperture as in 1.7.

$$\mathbf{E}^{m}(\mathbf{r}) = \int_{Sa} \int d\mathbf{E}^{m}(\mathbf{r}|\mathbf{r}')$$
 (1.6)

$$\mathbf{H}^{m}(\mathbf{r}) = \int \int d\mathbf{H}^{m}(\mathbf{r}|\mathbf{r}')$$
 (1.7)

This equations is evaluated using UTD to find the field. Figure 1.3 shows how the differential magnetic current $d\mathbf{M}$, together with the tangent plane at this point, divides the area in two regions. These regions are the shadow and the illuminated regions, with a transition region separating them. UTD's expression for electric field is obtained for both, shadow and illuminated regions, and also provides a smooth transition between the shadow and the illuminated region. In the next three subsections, the procedure to obtain expressions for the fields in each region is explained.

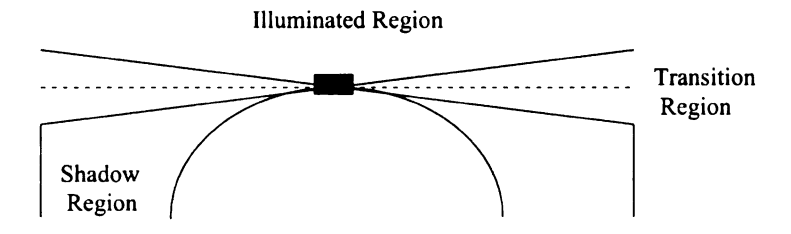


Figure 1.3. Shadow, transition and illuminated regions adjacent to a magnetic dipole on a perfectly conducting , convex surface

1.3 Electromagnetic Fields in the Shadow and Transition Region

The electric fields in the shadow region are expressed in terms of rays. These rays are excited by the magnetic current source $d\mathbf{M}$, and they propagate along the surface from the lit or illuminated region into the deep or shadow region. The surface ray has associated an amplitude A(s) and a phase $\phi(s)$ which varies with space, and can be expressed as

$$a(s) = A(s) \exp[j(\phi_0 - ks)] \exp(jwt)$$
(1.8)

The principle of conservation of energy, applied to a narrow band is used to determine A(s) along the surface [27]. Due to the diffraction, the surface ray sheds energy as they move, meaning that surface ray diffracts tangentially, decaying as it travels in the direction of propagation [23]. Figure 1.1 depicts this effect. The energy is proportional to A(s) and to the cross section area at s. For this case it would be just the width w(s) of the band, as in Figure 1.4. The energy between two points inside the strip is



Figure 1.4. Strip formed by surface rays

$$A^{2}(s+\Delta s)w(s+\Delta s) - A^{2}(s)w(s) = -2\alpha(s)A^{2}(s)w(s)\Delta s$$
 (1.9)

The energy lost, due to shedding is described by the factor $2\alpha(s)$. It can be shown that the derivative of A(s) is



$$\frac{d}{ds}[A^{2}(s)w(s)] = -2\alpha(s)[A^{2}(s)w(s)]$$
 (1.10)

Integrating with respect to s from s_0 to s

$$\int_{A^{2}(s)w(s)}^{A^{2}(s)w(s)} \frac{d[A^{2}(s')w(s')]}{[A^{2}(s')w(s')]} = -2\int_{s_{0}}^{s} \alpha(s')ds'$$

$$\Rightarrow \ln\left[\frac{A^{2}(s)w(s)}{A^{2}(s_{0})w(s_{0})}\right] = -2\int_{s_{0}}^{s} \alpha(s')ds'$$

$$\Rightarrow A(s) = A(s_{0})\sqrt{\frac{w(s_{0})}{w(s)}} \exp\left(-\int_{s_{0}}^{s} \alpha(s')ds'\right) \tag{1.11}$$

Suppressing the time dependence and solving it at s equal to s_0 results in

$$A(s_0) = a(s_0) \exp[-j(\phi_0 - ks_0)] \tag{1.12}$$

Substituting (1.12) in (1.11)

$$A(s) = a(s_0) \exp(-j(\phi_0 - ks_0)) \sqrt{\frac{w(s_0)}{w(s)}} \exp\left(-\int_{s_0}^{s} \alpha(s') ds'\right)$$
(1.13)

Using (1.13) and (1.8), it can be shown that

$$a(s) = a(s_0) \exp(-j(\phi_0 - ks_0)) \sqrt{\frac{w(s_0)}{w(s)}} \exp\left(-\int_{s_0}^s \alpha(s')ds'\right) \exp(j(\phi_0 - ks))$$

$$\Rightarrow a(s) = a(s_0) \sqrt{\frac{w(s_0)}{w(s)}} \exp(-jk(s - s_0)) \exp\left(-\int_{s_0}^s \alpha(s')ds'\right)$$
(1.14)

The width of the strip can be written in terms of arc length, $\Delta w(s) = d\eta(s)$. The arc length is determined by the distance s and the angle, $d\psi_0$, formed by the surface rays as in

$$a(s) = a(s_0)\sqrt{s_0}\sqrt{\frac{d\psi_0}{d\eta}}\exp\left(-jks - \int_{s_0}^s \alpha(s')ds'\right)$$
(1.15)

The dependence of the above expression on s_0 is assumed by writing $\lim_{s_0\to 0} a(s_0)\sqrt{s_0} = C'$. Using C' in (1.15) it is obtained

$$a(s) = C' \sqrt{\frac{d\psi_0}{d\eta}} \exp\left(-jks - \int_0^s \alpha(s')ds'\right)$$
 (1.16)

The proportional constant C' represents the strength of the source. The next step is to associate a direction to the surface ray and to relate it directly with the current source. Because this method should work for any shape, the canonical coordinate systems already defined cannot be used at this moment. The coordinate system that is used here is composed by an unit vector \hat{n} that is normal to the surface at any point, a tangential unit vector to the surface \hat{t} that points to the direction of propagation of the surface ray, as it is shown in Figure 1.5. To complete the set of our coordinate

system, we must define an unit vector perpendicular both to \hat{n} and also to \hat{t} . This unit vector is known as the binormal unit vector, and it is defined as $\hat{b} = \hat{t} \times \hat{n}$. As before, $\hat{b}, \hat{t}, \hat{n}$ represent the observation point and $\hat{b}', \hat{t}', \hat{n}'$ the source point. The source $d\mathbf{M}$ is expressed in terms of the new coordinate system as follows

$$d\mathbf{M} = \hat{b}'(\hat{b}' \cdot d\mathbf{M}) + \hat{t}'(\hat{t}' \cdot d\mathbf{M})$$
(1.17)

From the analysis of canonical problems, it is found that the source current excites an

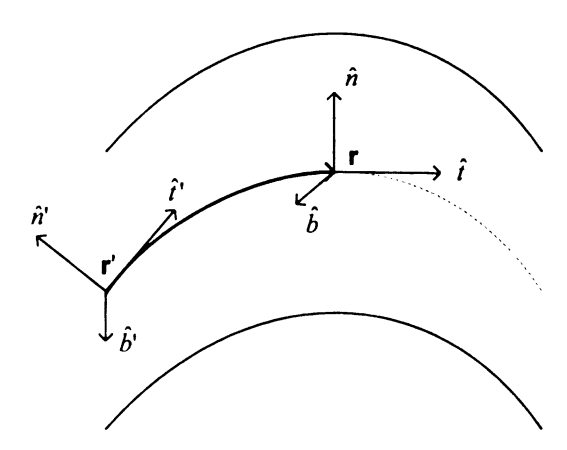


Figure 1.5. Coordinate system of a surface diffracted ray.

infinite number of modes for the normal component of field and another set of infinite modes for the tangential component of the field. Those sets are independent of each other, and they satisfy the different boundary condition. This definition allows us to define C' in terms of the boundary condition for a single mode, as shown in (1.18).

$$C_p' = CL_p^{h,s}(s_0) \left[\hat{b}' \cdot d\mathbf{M} + \hat{t}' \cdot d\mathbf{M} \right]$$
 (1.18)

Here, $L_p^{h,s}$ denotes the launching coefficient, and it depends on the boundary condi-

tion it satisfies and on mode. The constant C does not depend of the mode or the boundary condition. This constant is used to fix the final expression with the one obtained from the canonical problem.

The normal component of the electric field, $\hat{n} \cdot d\mathbf{E}$, has to satisfy the Newmann boundary condition, and is

$$\hat{n} \cdot d\mathbf{E}_{p} = CL_{p}^{h}(s_{0}) \left[\hat{b}' \cdot d\mathbf{M} + \hat{t}' \cdot d\mathbf{M} \right] \sqrt{\frac{d\psi_{0}}{d\eta}} \exp \left(-jks - \int_{0}^{s} \alpha_{p}^{h}(s') ds' \right)$$
(1.19)

where \mathbf{E}_p is the contribution of a single p mode of the total electric field \mathbf{E} . The tangential component of the electric field $\hat{b} \cdot d\mathbf{E}$, that is also perpendicular to the surface ray trajectory, \hat{t} , is obtained by satisfying the Dirichlet boundary condition as in (1.20).

$$\hat{b} \cdot d\mathbf{E}_{p} = CL_{p}^{s}(s_{0}) \left[\hat{b}' \cdot d\mathbf{M} + \hat{t}' \cdot d\mathbf{M} \right] \sqrt{\frac{d\psi_{0}}{d\eta}} \exp \left(-jks - \int_{0}^{s} \alpha_{p}^{s}(s')ds' \right)$$
(1.20)

It is obvious that this component vanishes on the surface; however, this term is important to calculate the electric field outside the surface. The total electric field on any point \mathbf{r} on the surface due to a source point \mathbf{r}' is written as

$$d\mathbf{E}(\mathbf{r}|\mathbf{r}') = \hat{n} d\mathbf{E}_n(\mathbf{r}|\mathbf{r}') + \hat{b} d\mathbf{E}_d(\mathbf{r}|\mathbf{r}')$$
(1.21)

With (1.21), dE is calculated for any given point on the surface, and using GTD dE is calculated for points outside the surface.

Keller [10] developed the GTD and shows that the wavefront of a surface diffracted field in any point \mathbf{r}_s outside the surface, can be represented in terms of other wavefront diffracted field at some point \mathbf{r}_0 . This is presented in Figure 1.6. The relation between

wavefronts is given by

$$d\mathbf{E}(\mathbf{r}_s|\mathbf{r}') \sim d\mathbf{E}(\mathbf{r}_0|\mathbf{r}')\sqrt{\frac{\rho_1^d \rho_2^d}{(\rho_1^d + s_0)(\rho_2^d + s_0)}} e^{-jks_0}$$
 (1.22)

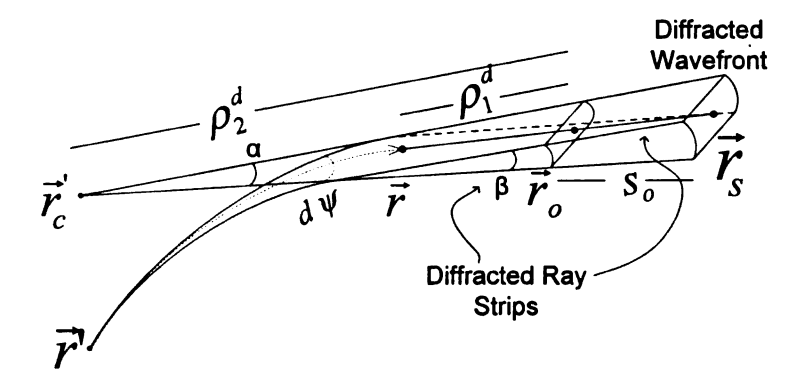


Figure 1.6. Diffracted Wave front

By moving the reference point \mathbf{r}_0 to the diffraction point \mathbf{r} , Pathak [2] relates $d\mathbf{E}(\mathbf{r}_s|\mathbf{r}')$ directly to the source $d\mathbf{M}$. As shown in Figure 1.6 and Figure 1.7, when $\mathbf{r}_0 \to \mathbf{r}$, $\rho_1^d \to 0$, $\rho_2^d \to \rho_c$ and $s_0 \to s$, the following expression is obtained

$$\lim_{\rho_1^d \to 0} \sqrt{\rho_1^d} d\mathbf{E}(\mathbf{r}_0 | \mathbf{r}') \sim d\mathbf{E}(\mathbf{r} | \mathbf{r}') D(\mathbf{r})$$
(1.23)

where $D(\mathbf{r})$ is the attachment coefficient when the field is shedding or escaping from the surface object or it is defined as the diffraction coefficient when the field is tangentially hitting the surface object. This is due to the reciprocity, which states a source \mathbf{M} located at \mathbf{r}' produces a field in \mathbf{r}_0 equal to the field at \mathbf{r}_0 when the source is place at \mathbf{r}_0 . The coefficient $D(\mathbf{r})$ depends on two factors: the nature of the field

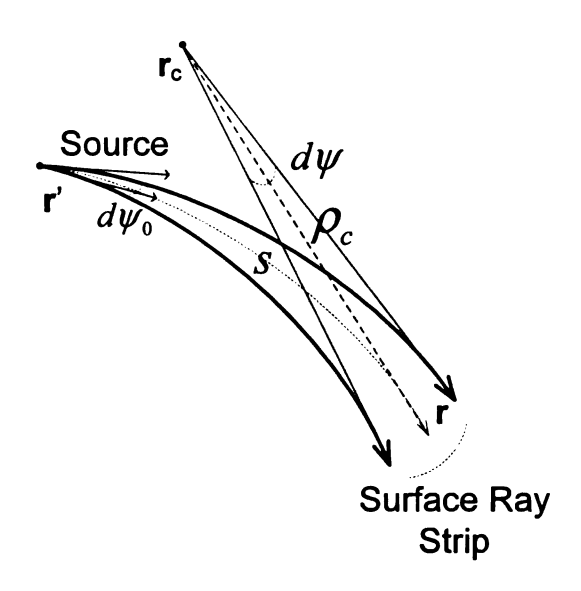


Figure 1.7. Spread of a surface diffracted ray

and the infinitesimal area around the object. Equation (1.23) can be rewritten as

$$\lim_{\rho_1^d \to 0} \sqrt{\rho_1^d} d\mathbf{E}(\mathbf{r}_0 | \mathbf{r}') \sim d\mathbf{M}(\mathbf{r}') \cdot \overline{\mathbf{T}}(\mathbf{r} | \mathbf{r}')$$
(1.24)

replacing (1.24) into (1.22)

$$d\mathbf{E}(\mathbf{r}_s|\mathbf{r'}) \sim \mathbf{L}(\mathbf{r}|\mathbf{r'})\sqrt{\frac{\rho_c}{s(\rho_c+s)}} e^{-jks}$$
 (1.25)

where $\mathbf{L}(\mathbf{r}|\mathbf{r}')$ is a linear transfer function, and it is defined as

$$\mathbf{L}(\mathbf{r}|\mathbf{r}') \sim d\mathbf{M}(\mathbf{r}') \cdot \overline{\mathbf{T}}(\mathbf{r}|\mathbf{r}')$$
 (1.26)

 $\overline{\mathbf{T}}(\mathbf{r}|\mathbf{r}')$ is the dyadic transfer function and using (1.19), (1.20), (1.21), (1.23), (1.24),

and (1.26) can be written as

$$T_{ij}(\mathbf{r}|\mathbf{r}') \sim C \sum_{p} L_{p}(\mathbf{r}') D_{p}(\mathbf{r}) \sqrt{\frac{d\psi_{0}}{d\eta}} \exp\left(-jks_{D} - \int_{0}^{s_{D}} \alpha_{p}(s') ds'\right)$$
 (1.27)

where i and j are the \hat{t} , \hat{n} and \hat{b} components defined before for source and observation points. Equation (1.25) can be expressed in terms of the source point $d\mathbf{M}$ and the dyadic transfer function that relates the physical phenomenons from the diffracted point to the source point as

$$d\mathbf{E}(\mathbf{r}_{s}|\mathbf{r}') \sim d\mathbf{M}(\mathbf{r}') \cdot \overline{\mathbf{T}}(\mathbf{r}|\mathbf{r}') \sqrt{\frac{\rho_{c}}{s(\rho_{c}+s)}} e^{-jks}$$
 (1.28)

The attachment coefficient $D_p(\mathbf{r})$, the attenuation constant $\alpha_p(s')$, and the constant C are obtained by comparing (1.28) to the asymptotic solution of canonical problems. The asymptotic series expansion demonstrates a highly convergence when the observation point is in the shadow region, and just few terms are normally needed to obtain an acceptable accuracy. However, as the observation point moves to the boundary between the transition and the shadow region more terms will be needed to obtain the same accuracy. This problem is solved by changing the series representation using Fock integral representation [28], which describes creeping waves, as the observation point moves from the shadow to the transition region. The dyadic transfer function on (1.28) can be written for the TE_t case as

$$\overline{\mathbf{T}}(\mathbf{r}|\mathbf{r}') = C \left[T_a(\mathbf{r}')H\hat{b}'\hat{n} + T_b(\mathbf{r}')S\hat{t}'\hat{b} + T_c(\mathbf{r}')H\hat{b}'\hat{b} + T_d(\mathbf{r}')S\hat{t}'\hat{n} \right]$$

$$\sqrt{\frac{d\psi_0}{d\eta}} \left[\frac{\rho_g(\mathbf{r})}{\rho_g(\mathbf{r}')} \right]^{\frac{1}{6}} e^{-jks_D}$$
(1.29)

The torsion factor $T_k(\mathbf{r}')$ for k=a,b,c,d,H and S are all related to the hard and soft boundary conditions and satisfy the Robin boundary condition for the TE_t

case. Pathak et al. [23] found that a circular cylinder $T_a(\mathbf{r}')$ and $T_b(\mathbf{r}')$ are equal to 1, $T_d(\mathbf{r}')$ is equal to zero and $T_c(\mathbf{r}') = \sin 2\alpha'/a \sin^2 \alpha'$. Pathak also obtained the surface radius of curvature $\rho_g(\mathbf{r}') = a/\sin^2 \alpha'$ for a circular cylinder.

In this Chapter, we have obtained semianalytic methods that can be used for analyzing sources near canonical prefect electrical conducting objects. In the next chapters, we derive dyadic Green's functions that may be integrated within differential equation solvers

CHAPTER 2

ELECTROMAGNETIC FIELDS IN TERMS OF GREEN'S FUNCTIONS

Unique electric or magnetic fields at any observation point are obtained by solving a second-order differential equation subject to specific boundary conditions. As said in Chapter 1, the usual solution for this type of problem is an infinite series, but these ones usually converge slowly. For that reason, a closed form solution would be useful.

A Green's function is a solution of the partial differential equation when using a unit source as the driving function subject to appropriate boundary condition [29]. The solution for the partial differential equation with the actual forcing function, is then given by the convolution of the Green's function with the actual forcing function. Hence, the Green's function serves as the transfer function of the system.

In this chapter, we explain the manner in which a closed form integral equation that relates the magnetic field due to an aperture on a circular cylinder may be obtained, using a dyadic Green's function. The electromagnetic field, is governed by the vector wave equation (2.1), the boundary conditions at the surface of the cylinder and the radiation condition.

$$\nabla \times \nabla \times \mathbf{F} - k_0^2 \mathbf{F} = 0 \tag{2.1}$$

where the vector field \mathbf{F} can be either \mathbf{E} or \mathbf{H} . The dyadic Green's function $\overline{\mathbf{G}}$ must solve the same differential equation, but using a unit source as a driving function, as shown in (2.2)

$$\nabla \times \nabla \times \overline{\mathbf{G}} - k_0^2 \overline{\mathbf{G}} = \overline{\mathbf{I}} \delta(\mathbf{r} - \mathbf{r}')$$
 (2.2)

multiplying (2.1) by $\overline{\mathbf{G}}$ and (2.2) by \mathbf{F} , subtracting the results and grouping the terms,

it gives the differential equation (2.3)

$$\mathbf{F} \cdot (\nabla \times \nabla \times \overline{\mathbf{G}}) - (\nabla \times \nabla \times \mathbf{F}) \cdot \overline{\mathbf{G}} = \mathbf{F} \cdot \overline{\mathbf{I}} \delta(\mathbf{r} - \mathbf{r}')$$
 (2.3)

using the identity (2.4)

$$\nabla \times (\mathbf{A} \times \mathbf{B}) = \mathbf{B} \cdot (\nabla \times \mathbf{A}) - \mathbf{A} \cdot (\nabla \times \mathbf{B})$$
$$\mathbf{B} \cdot (\nabla \times \mathbf{A}) = \nabla \times (\mathbf{A} \times \mathbf{B}) - \mathbf{A} \cdot (\nabla \times \mathbf{B})$$
(2.4)

with $\mathbf{A} = \nabla \times \overline{\mathbf{G}}$ and $\mathbf{B} = \mathbf{F}$ for the first term in the left hand side of (2.3) and using $\mathbf{A} = \nabla \times \mathbf{F}$ and $\mathbf{B} = \overline{\mathbf{G}}$ for the second term, produces

$$\nabla \cdot \nabla \times \overline{\mathbf{G}} \times \mathbf{F} - \nabla \cdot \nabla \times \mathbf{F} \times \overline{\mathbf{G}} = \mathbf{F} \cdot \overline{\mathbf{I}} \delta(\mathbf{r} - \mathbf{r}')$$
 (2.5)

Using $\mathbf{A} \times \mathbf{B} = -\mathbf{B} \times \mathbf{A}$ and grouping terms, (2.5) becomes

$$-\nabla \cdot [\mathbf{F} \times \nabla \times \overline{\mathbf{G}} + \nabla \times \mathbf{F} \times \overline{\mathbf{G}}] = \mathbf{F} \cdot \overline{\mathbf{I}} \delta(\mathbf{r} - \mathbf{r'})$$
 (2.6)

(2.6) is the integrated over the volume exterior to the surface (the region in which fields are sought)

$$-\iiint_{V} \nabla \cdot [\mathbf{F} \times \nabla \times \overline{\mathbf{G}} + \nabla \times \mathbf{F} \times \overline{\mathbf{G}}] dV = \iiint_{V} \mathbf{F} \cdot \overline{\mathbf{I}} \delta(\mathbf{r} - \mathbf{r}') dV$$
 (2.7)

and using the divergence theorem, (2.7) is converted in (2.8)

$$- \iint_{S} \hat{\mathbf{n}} \cdot [\mathbf{F} \times \nabla \times \overline{\mathbf{G}} + \nabla \times \mathbf{F} \times \overline{\mathbf{G}}] dS = -\mathbf{F}(\mathbf{r}')$$
 (2.8)

If **F** is **H**, using Faraday's Law for a source free region $(\nabla \times \mathbf{H} = jw\epsilon_0 \mathbf{E})$, (2.8) can

be written as

$$\mathbf{H}(\mathbf{r'}) = \iint_{S} \hat{n} \times \mathbf{H} \cdot \nabla \times \overline{\mathbf{G}} \, dS + jw\epsilon_{0} \iint_{S} \hat{n} \times \mathbf{E} \cdot \overline{\mathbf{G}} \, dS$$
 (2.9)

Because the cylinder is a perfect electric conductor (PEC), the Green's function is chosen such that the normal derivative $\nabla \times \overline{\mathbf{G}}$ is equal to zero (satisfying the Newman boundary condition) on the surface of the cylinder. Then, the first integral is zero. Also, as the tangential component of the electric field, $\hat{n} \times \mathbf{E}$, on the PEC surface is zero, the only region the integral can be non zero is at the aperture. For these reasons, (2.9) reduce to

$$\mathbf{H}(\mathbf{r'}) = jw\epsilon_0 \iint_{S_a} \hat{n} \times \mathbf{E} \cdot \overline{\mathbf{G}} \ dS$$
 (2.10)

where Sa is the aperture on the cylinder surface. Due to symmetry of the Green's function, (2.10) can be written as in

$$\mathbf{H}(\mathbf{r}) = jw\epsilon_0 \iint_{Sa} \hat{n} \times \mathbf{E}(\mathbf{r'}) \cdot \overline{\mathbf{G}}(\mathbf{r'} \mid \mathbf{r}) \ dS'$$
 (2.11)

interchanging source and observation points. To relate the dyadic Green's function to the torsion factor of Chapter 1, it is recognized that by replacing $d\mathbf{F}(\mathbf{r})$ by $d\mathbf{H}(\mathbf{r})$ in (1.1) and with $\mathbf{M} = \hat{n} \times \mathbf{E}$ as the magnetic source on the surface, the relation between the dyadic torsion factor and the dyadic Green's function is defined as

$$\varsigma \overline{\mathbf{T}}(\mathbf{r'} \mid \mathbf{r}) = \overline{\mathbf{G}}(\mathbf{r'} \mid \mathbf{r})$$
(2.12)

2.1 Derivation of Green's Functions

To relate and derive the relations of the dyadic Green's function, we should start introducing the concept of dyadic electric and magnetic field and rewriting the Maxwell equation in terms of these fields. First, there are three orthogonal current distributions, \mathbf{J}_i , with (i=1,2,3) which produce three sets of harmonically oscillating fields in the same environment and at the same frequency. In this way, we would have fields such as \mathbf{E}_i and \mathbf{H}_i [29]. However, if the coordinates x, y, z are replaced by x_1, x_2, x_3 , the magnetic and electric fields could be written in the dyadic form

$$\overline{\mathbf{F}} = \sum_{j=1}^{3} \sum_{i=1}^{3} F_{ij} \tag{2.13}$$

where **F** could be either **E** or **H**. The dyadic electric field can be represented or called the electric dyadic Green's function

$$\overline{\mathbf{E}} = \overline{\mathbf{G}}_{e} \tag{2.14}$$

whereas the magnetic dyadic Green's function is given as

$$jw\mu_0\overline{\mathbf{H}} = \overline{\mathbf{G}}_m \tag{2.15}$$

Normalizing the current moment, it is found that

$$jw\mu_0 \overline{\mathbf{J}} = \overline{\mathbf{I}}\delta(\mathbf{R} - \mathbf{R'}) \tag{2.16}$$

Maxwell's equations can be rewritten in terms of the new notation as:

$$\nabla \times \overline{\mathbf{G}}_{e0}(\mathbf{R}|\mathbf{R}') = \overline{\mathbf{G}}_{m0}(\mathbf{R}|\mathbf{R}') \tag{2.17}$$

$$\nabla \times \overline{\mathbf{G}}_{m0}(\mathbf{R}|\mathbf{R}') = \overline{\mathbf{I}}\delta(\mathbf{R} - \mathbf{R}') + k^2 \overline{\mathbf{G}}_{e0}(\mathbf{R}|\mathbf{R}')$$
 (2.18)

$$\nabla \cdot \overline{\mathbf{G}}_{e0}(\mathbf{R}|\mathbf{R'}) = \frac{1}{k^2} \nabla \cdot [\overline{\mathbf{I}}\delta(\mathbf{R} - \mathbf{R'})]$$
 (2.19)

$$\nabla \cdot \overline{\mathbf{G}}_{m0}(\mathbf{R}|\mathbf{R'}) = 0 \tag{2.20}$$

The subscript zero is used to indicate that only the free-space radiation boundary condition is enforced. The dyadic magnetic Green's function, $\overline{\mathbf{G}}_{m0}$, may be decomposed into two terms, $\overline{\mathbf{G}}_{m0}^+$ and $\overline{\mathbf{G}}_{m0}^-$, such that

$$\overline{\mathbf{G}}_{m0} = \overline{\mathbf{G}}_{m0}^{+} U(\rho - \rho') + \overline{\mathbf{G}}_{m0}^{-} U(\rho' - \rho) \tag{2.21}$$

This is because $\overline{\mathbf{G}}_{m0}$ has a singularity at $\rho = \rho'$ where again ρ' denotes the source radius. The unit step functions for cylindrical coordinates are defined as

$$U(\rho - \rho') = \begin{cases} 1, & \text{if } \rho > \rho' \\ 0, & \text{if } \rho < \rho' \end{cases}$$
 (2.22)

$$U(\rho' - \rho) = \begin{cases} 1, & \text{if } \rho' > \rho \\ 0, & \text{if } \rho' < \rho \end{cases}$$
 (2.23)

Taking curl is applied to (2.21), results in

$$\nabla \times \overline{\mathbf{G}}_{m0} = \nabla \times [\overline{\mathbf{G}}_{m0}^+ U(\rho - \rho') + \overline{\mathbf{G}}_{m0}^- U(\rho' - \rho)]$$
 (2.24)

Applying the identity (2.25)

$$\nabla \times (a\overline{\mathbf{B}}) = a\nabla \times \overline{\mathbf{B}} - \overline{\mathbf{B}} \times \nabla a \tag{2.25}$$

on (2.24) and using $\mathbf{A} \times \mathbf{B} = -\mathbf{B} \times \mathbf{A}$, yields

$$\nabla \times \overline{\mathbf{G}}_{m0} = (\nabla \times \overline{\mathbf{G}}_{m0}^{+})U(\rho - \rho') + \nabla U(\rho - \rho') \times \overline{\mathbf{G}}_{m0}^{+}$$
$$+ (\nabla \times \overline{\mathbf{G}}_{m0}^{-})U(\rho' - \rho) + \nabla U(\rho' - \rho) \times \overline{\mathbf{G}}_{m0}^{-} \qquad (2.26)$$

Evaluating the divergence of the step functions, we have

$$\nabla U(\rho - \rho') = \hat{\rho} \frac{\partial U}{\partial \rho} + \hat{\phi} \frac{\partial U}{\rho \partial \phi} + \hat{z} \frac{\partial U}{\partial z} = \hat{\rho} \delta(\rho - \rho')$$
 (2.27)

$$\nabla U(\rho' - \rho) = \hat{\rho}\delta(-1(\rho - \rho'))\partial_{\rho}(-\rho) = \frac{-1}{|-1|}\hat{\rho}\delta(\rho - \rho')$$
 (2.28)

Substituting (2.27) and (2.28) on (2.26), results in

$$\nabla \times \overline{\mathbf{G}}_{m0} = (\nabla \times \overline{\mathbf{G}}_{m0}^{+})U(\rho - \rho') + \hat{\rho}\delta(\rho - \rho') \times \overline{\mathbf{G}}_{m0}^{+}$$

$$+ (\nabla \times \overline{\mathbf{G}}_{m0}^{-})U(\rho' - \rho) - \hat{\rho}\delta(\rho - \rho') \times \overline{\mathbf{G}}_{m0}^{-}$$

$$= (\nabla \times \overline{\mathbf{G}}_{m0}^{+})U(\rho - \rho') + (\nabla \times \overline{\mathbf{G}}_{m0}^{-})U(\rho' - \rho)$$

$$+ \hat{\rho}\delta(\rho - \rho') \times (\overline{\mathbf{G}}_{m0}^{+} - \overline{\mathbf{G}}_{m0}^{-})$$
(2.29)

Using the boundary condition for a magnetic field $\hat{\rho} \times (\overline{\mathbf{H}}_{m0}^+ - \overline{\mathbf{H}}_{m0}^-) = \overline{\mathbf{J}}_s$, in terms of the dyadic functions, substituting (2.15) and (2.16), we have

$$\hat{n} \times (\overline{\mathbf{G}}_{m0}^{+} - \overline{\mathbf{G}}_{m0}^{-}) = \overline{\mathbf{I}}_{s} \delta(\mathbf{r} - \mathbf{r}')$$
(2.30)

where $\bar{\mathbf{I}}_s$ is the surface idem factor and $\delta(\mathbf{r} - \mathbf{r'})$ is the surface delta function. Converting (2.30) to cylindrical coordinates, $\hat{n} = \hat{\rho}$ and $\delta(\mathbf{r} - \mathbf{r'}) = \delta(\phi - \phi')\delta(z - z')$. Substituting $\bar{\mathbf{I}}_s$ by $\bar{\mathbf{I}} - \hat{\rho}\hat{\rho}$, yields

$$\hat{\rho} \times (\overline{\mathbf{G}}_{m0}^{+} - \overline{\mathbf{G}}_{m0}^{-}) = (\overline{\mathbf{I}} - \hat{\rho}\hat{\rho})\delta(\phi - \phi')\delta(z - z') \tag{2.31}$$

Multiplying both sides of (2.31) by $\delta(\rho - \rho')$

$$\hat{\rho}\delta(\rho - \rho') \times (\overline{\mathbf{G}}_{m0}^{+} - \overline{\mathbf{G}}_{m0}^{-}) = (\overline{\mathbf{I}} - \hat{\rho}\hat{\rho})\delta(\rho - \rho')\delta(\phi - \phi')\delta(z - z') \tag{2.32}$$

and substituting (2.32) into (2.29), yields

$$\nabla \times \overline{\mathbf{G}}_{m0} = (\nabla \times \overline{\mathbf{G}}_{m0}^{+})U(\rho - \rho') + (\nabla \times \overline{\mathbf{G}}_{m0}^{-})U(\rho' - \rho) + (\overline{\mathbf{I}} - \hat{\rho}\hat{\rho})\delta(\rho - \rho')\delta(\phi - \phi')\delta(z - z')$$
(2.33)

Using (2.18) in (2.33), we have

$$\bar{\mathbf{I}}\delta(\rho - \rho')\delta(\phi - \phi')\delta(z - z') + k_0^2 \overline{\mathbf{G}}_{e0} = (\nabla \times \overline{\mathbf{G}}_{m0}^+)U(\rho - \rho') + (\bar{\mathbf{I}} - \hat{\rho}\hat{\rho})\delta(\rho - \rho')\delta(\phi - \phi')\delta(z - z') + (\nabla \times \overline{\mathbf{G}}_{m0}^-)U(\rho' - \rho)$$
(2.34)

and simplifying (2.34), the expression for the electric dyadic Green's function for free space can be written as

$$\overline{\mathbf{G}}_{e0}(\mathbf{R}|\mathbf{R}') = \frac{1}{k_0^2} [(\nabla \times \overline{\mathbf{G}}_{m0}^+) U(\rho - \rho') + (\nabla \times \overline{\mathbf{G}}_{m0}^-) U(\rho' - \rho) - \hat{\rho}\hat{\rho}\delta(\mathbf{R} - \mathbf{R}')]$$
(2.35)

An expression for $\overline{\mathbf{G}}_{e0}(\mathbf{R}|\mathbf{R}')$ in terms of eigenfunctions must be found, but we will not do this directly. First, $\overline{\mathbf{G}}_{m0}(\mathbf{R}|\mathbf{R}')^{\pm}$ will be written in terms of eigenfunctions, and then, the expression will replace $\overline{\mathbf{G}}_{m0}(\mathbf{R}|\mathbf{R}')^{\pm}$ in (2.35). To do this, the curl is applied to (2.18), obtaining:

$$\nabla \times \nabla \times \overline{\mathbf{G}}_{m0}(\mathbf{R}|\mathbf{R}') = \nabla \times [\overline{\mathbf{I}}\delta(\mathbf{R} - \mathbf{R}')] + k_0^2 \nabla \times \overline{\mathbf{G}}_{e0}(\mathbf{R}|\mathbf{R}')$$
 (2.36)

and using (2.17) in (2.36), we obtain

$$\nabla \times \nabla \times \overline{\mathbf{G}}_{m0}(\mathbf{R}|\mathbf{R}') - k_0^2 \overline{\mathbf{G}}_{m0}(\mathbf{R}|\mathbf{R}') = \nabla \times [\overline{\mathbf{I}}\delta(\mathbf{R} - \mathbf{R}')]$$
 (2.37)

Equation (2.37) shows that $\overline{\mathbf{G}}_{m0}(\mathbf{R}|\mathbf{R}')$ is also a solution for the dyadic wave equation. For this reason, a solution for $\overline{\mathbf{G}}_{m0}(\mathbf{R}|\mathbf{R}')$ could be found in terms of eigenfunctions. The eigenfunctions will be formed on vector wave functions [30]. These functions are a set of eigenfunctions that can be found using scalar wave functions, φ_1 and φ_2 as the generation functions. In this work, two kinds of vector wave functions will be used: \mathbf{M} and \mathbf{N} . These two, in addition to \mathbf{L} , were introduced by Hansen [30]. To construct \mathbf{M} , it is assumed that φ_1 is a solution for the scalar Helmholtz equation

$$\nabla^2 \varphi_1 + k^2 \varphi_1 = 0 \tag{2.38}$$

and that there is a function F such that

$$\mathbf{F} = \nabla \times (\varphi_1 \hat{p}) \tag{2.39}$$

where \hat{p} is the pilot vector. It can be verified that **F** satisfies the vector wave equation.

$$\nabla \times \nabla \times \mathbf{F} - k^2 \mathbf{F} = 0 \tag{2.40}$$

Using (2.39) in (2.40), and factorizing the curl in the equation:

$$\nabla \times \nabla \times (\nabla \times (\varphi_1 \hat{p})) - k^2 \nabla \times (\varphi_1 \hat{p}) = 0$$
 (2.41)

$$\nabla \times \left[\nabla \times \nabla \times (\varphi_1 \hat{p}) - k^2 \varphi_1 \hat{p}\right] = 0 \tag{2.42}$$

using the identity (2.43)

$$\nabla \times \nabla \times \mathbf{A} = \nabla(\nabla \cdot \mathbf{A}) - \nabla^2 \mathbf{A} \tag{2.43}$$

in (2.42) results in

$$\nabla \times \left[\nabla (\nabla \cdot \varphi_1 \hat{p}) - \nabla^2 \varphi_1 \hat{p} - k^2 \varphi_1 \hat{p} \right] = 0 \tag{2.44}$$

Using $\nabla \cdot (a\mathbf{B}) = a\nabla \mathbf{B} + \mathbf{B}\nabla a$ in (2.44) simplified it as

$$\nabla \times \left[\nabla (\varphi_1 \nabla \cdot \hat{p} + \hat{p} \triangle \varphi_1) - \nabla^2 \varphi_1 \hat{p} - k^2 \varphi_1 \hat{p} \right] = 0 \tag{2.45}$$

Because $\nabla \cdot \hat{p} = 0$, (2.45) reduces to

$$\nabla \times \left[\nabla (\hat{p} \triangle \varphi_1) - \nabla^2 \varphi_1 \hat{p} - k^2 \varphi_1 \hat{p} \right] = 0 \tag{2.46}$$

and again to

$$\nabla \times \left[-\nabla^2 \varphi_1 \hat{p} - k^2 \varphi_1 \hat{p} \right] = 0 \tag{2.47}$$

Factorizing $-\hat{p}$ from (2.47), it is obtained

$$\nabla \times [(\nabla^2 \varphi_1 - k^2 \varphi_1)\hat{p}] = 0 \tag{2.48}$$

If φ_1 is a solution for the Helmholtz equation (2.38), then (2.48) is zero, which means that **F** is a solution for the vector wave equation (2.39). One set of vector eigenfunctions is given by

$$\mathbf{M} = \nabla \times (\varphi_1 \hat{p}) \tag{2.49}$$

The other set of vector eigenfunctions is given by

$$\mathbf{N} = \frac{1}{k} \nabla \times \nabla \times (\varphi_2 \hat{p}) \tag{2.50}$$

Using (2.50) in the vector wave equation (2.40) and factorizing, it is obtained

$$\nabla \times \nabla \times \left[\frac{1}{k}\nabla \times \nabla \times (\varphi_2 \hat{p})\right] - k^2 \left[\frac{1}{k}\nabla \times \nabla \times (\varphi_2 \hat{p})\right] = 0$$

$$\Rightarrow \nabla \times \nabla \times \left[\frac{1}{k}\nabla \times \nabla \times (\varphi_2 \hat{p}) - k\varphi_2 \hat{p}\right] = 0$$
(2.51)

Using identity (2.43) with (2.51), it becomes

$$\nabla \times \nabla \times \left[\frac{1}{k}(\nabla(\nabla \cdot \varphi_2 \hat{p}) - \nabla^2 \varphi_2 \hat{p}) - k\varphi_2 \hat{p}\right] = 0$$
 (2.52)

applying $\nabla \cdot (a\mathbf{B}) = a\nabla \mathbf{B} + \mathbf{B}\nabla a$ to (2.52), it becomes

$$\nabla \times \nabla \times \left[\frac{1}{k}(\nabla(\varphi_2\nabla \cdot \hat{p} + \hat{p}\nabla\varphi_2) - \nabla^2\varphi_2\hat{p}) - k\varphi_2\hat{p}\right] = 0$$
 (2.53)

with $\nabla \cdot \hat{p} = 0$, (2.53) reduces to

$$\nabla \times \nabla \times \left[\frac{1}{k} (\nabla \hat{p} \nabla \varphi_2 - \nabla^2 \varphi_2 \hat{p}) - k \varphi_2 \hat{p} \right] = 0$$

$$\Rightarrow \nabla \times \nabla \times \left[-\frac{1}{k} \nabla^2 \varphi_2 \hat{p} - k \varphi_2 \hat{p} \right] = 0$$

$$\Rightarrow \nabla \times \nabla \times \left[-\frac{\hat{p}}{k} (\nabla^2 \varphi_2 - k^2 \varphi_2) \right] = 0$$
(2.54)

As before, if φ_2 is a solution for the Helmholtz equation (2.38), then (2.54) is zero, which means that **N** is also a solution for the vector wave equation. If $\varphi_1 = \varphi_2$, **M** can be written in terms of **N** by placing (2.49) in (2.50)

$$\mathbf{N} = \frac{1}{k} \nabla \times \mathbf{M} \tag{2.55}$$

This can be shown by a rather simple development. The vector wave equation in terms of M is expressed as

$$\nabla \times \nabla \times \mathbf{M} - k^2 \mathbf{M} = 0 \tag{2.56}$$

Finally, substituting (2.55) into (2.56)

$$k\nabla \times \mathbf{N} - k^2 \mathbf{M} = 0 \tag{2.57}$$

and so

$$\nabla \times \mathbf{N} = k\mathbf{M} \tag{2.58}$$

To find an expression for $\overline{\mathbf{G}}_{m0}(\mathbf{R}|\mathbf{R}')$ in terms of vector wave equations, only the first two vector wave functions, \mathbf{M} and \mathbf{N} , called the solenoidal vector wave functions are necessary. Conversely, if we want to find an expression for $\overline{\mathbf{G}}_{e0}(\mathbf{R}|\mathbf{R}')$, the three vector wave functions, \mathbf{M} , \mathbf{N} and \mathbf{L} will be necessary. For convenience, $\overline{\mathbf{G}}_{m0}(\mathbf{R}|\mathbf{R}')$ is first derived, then $\overline{\mathbf{G}}_{e0}(\mathbf{R}|\mathbf{R}')$ is represented in terms of $\overline{\mathbf{G}}_{m0}(\mathbf{R}|\mathbf{R}')$. To expand $\overline{\mathbf{G}}_{m0}$ in terms of the solenoidal vector wave functions, it is convenient to follow the Ohm-Rayleigh method. The method is explained in [31] on page 179, or in a more applied way by [29], renamed as the $\overline{\mathbf{G}}_m$ method. Basically, it says that a source function, $\nabla \times [\overline{\mathbf{I}}\delta(\mathbf{R} - \mathbf{R}')]$, can be written in an expansion by simply finding the appropriate vector wave functions that enforces the boundary condition.

$$\nabla \times [\bar{\mathbf{I}}\delta(\mathbf{R} - \mathbf{R}')] = \int_{0}^{\infty} dk_{\rho} \int_{-\infty}^{\infty} dk_{z} \sum_{n=0}^{\infty} [\mathbf{N}(k_{z})\mathbf{A}(k_{z}) + \mathbf{M}(k_{z})\mathbf{B}(k_{z})]$$
(2.59)

Integrating the scalar product between $N'(-k_z)$ and (2.59) over the entire volume,

$$\iiint_{0} \mathbf{N}'(-k_{z}) \cdot \nabla \times [\overline{\mathbf{I}}\delta(\mathbf{R} - \mathbf{R}')]dV =$$

$$\int_{0}^{\infty} dk_{\rho} \int_{-\infty}^{\infty} dk_{z} \sum_{n=0}^{\infty} \iiint_{0} \mathbf{N}'(-k_{z}) \cdot [\mathbf{N}(k_{z})\mathbf{A}(k_{z})\mathbf{M}(k_{z})\mathbf{B}(k_{z})]dV \qquad (2.60)$$

and using the orthogonal properties for $\mathbf{M}(k_z)$ and $\mathbf{N}(k_z)$ proposed by [29] in page 150, $\mathbf{A}(k_z)$ and $\mathbf{B}(k_z)$ are obtained as

$$\mathbf{A}(k_z) = \frac{2 - \delta_0}{4\pi^2 \lambda} \mathbf{M}'(-k_z) \tag{2.61}$$

$$\mathbf{B}(k_z) = \frac{2 - \delta_0}{4\pi^2 \lambda} \mathbf{N}'(-k_z) \tag{2.62}$$

The source function can this be represented as

$$\nabla \times [\overline{\mathbf{I}}\delta(\mathbf{R} - \mathbf{R}')] = \int_{0}^{\infty} dk_{\rho} \int_{-\infty}^{\infty} dk_{z} \sum_{n=0}^{\infty} \frac{2 - \delta_{0}}{4\pi^{2}\lambda} [\mathbf{N}(k_{z})\mathbf{M}'(-k_{z}) + \mathbf{M}(k_{z})\mathbf{N}'(-k_{z}))]$$
(2.63)

Then $\overline{\mathbf{G}}_{m0}$ is written as a function of the terms obtained in (2.63). Furthermore, the integral with respect to k_{ρ} can be eliminated. This is because our problem involves an infinite cylinder [29]. Then function, $\overline{\mathbf{G}}_{m0}$ is expressed as

$$\overline{\mathbf{G}}_{m0}^{\pm}(\mathbf{R}|\mathbf{R}') = \frac{-jk}{8\pi} \int_{-\infty}^{\infty} dk_z \sum_{n=-\infty}^{\infty} \frac{1}{k_{\rho}^{2}}$$

$$\left\{ \begin{bmatrix} \mathbf{N}^{(2)}(k_z)\mathbf{M}'(-k_z) + \mathbf{M}^{(2)}(k_z)\mathbf{N}'(-k_z) \end{bmatrix}, & \text{if } \rho > \rho' \\ \begin{bmatrix} \mathbf{N}(k_z)\mathbf{M}'^{(2)}(-k_z) + \mathbf{M}(k_z)\mathbf{N}'^{(2)}(-k_z) \end{bmatrix}, & \text{if } \rho < \rho' \end{bmatrix} \right\}$$
(2.64)

where the superscript "(2)" means that the vector wave equation is in terms of second

kind Hankel functions. Taking the curl of $\overline{\mathbf{G}}_{m0}^+$ and $\overline{\mathbf{G}}_{m0}^-$ we obtain

$$\nabla \times \overline{\mathbf{G}}_{m0}^{+}(\mathbf{R}|\mathbf{R}') = \frac{-jk}{8\pi} \int_{-\infty}^{\infty} dk_z \sum_{n=-\infty}^{\infty} \frac{1}{k_{\rho}^{2}}$$
$$\{\nabla \times \mathbf{N}^{(2)}(k_z)\mathbf{M}'(-k_z) + \nabla \times \mathbf{M}^{(2)}(k_z)\mathbf{N}'(-k_z)\} , \quad \rho > \rho' \qquad (2.65)$$

$$\nabla \times \overline{\mathbf{G}}_{m0}^{-}(\mathbf{R}|\mathbf{R}') = \frac{-jk}{8\pi} \int_{-\infty}^{\infty} dk_z \sum_{n=-\infty}^{\infty} \frac{1}{k_{\rho}^{2}}$$
$$\{\nabla \times \mathbf{N}(k_z)\mathbf{M}'^{(2)}(-k_z) + \nabla \times \mathbf{M}(k_z)\mathbf{N}'^{(2)}(-k_z)\} , \quad \rho < \rho' \qquad (2.66)$$

replacing (2.55) and (2.58) in (2.65), the following is obtained

$$\nabla \times \overline{\mathbf{G}}_{m0}^{+}(\mathbf{R}|\mathbf{R}') = \frac{-jk^2}{8\pi} \int_{-\infty}^{\infty} \sum_{n=-\infty}^{\infty} \frac{1}{k_{\rho}^2}$$

$$\{\mathbf{M}^{(2)}(k_z)\mathbf{M}'(-k_z) + \mathbf{N}^{(2)}(k_z)\mathbf{N}'(-k_z)\}dk_z \quad , \qquad \rho > \rho'$$
(2.67)

Using identical steps as before, replacing (2.55) and (2.58) in (2.66), it can be expressed as

$$\nabla \times \overline{\mathbf{G}}_{m0}^{-}(\mathbf{R}|\mathbf{R}') = \frac{-jk^2}{8\pi} \int_{-\infty}^{\infty} \sum_{n=-\infty}^{\infty} \frac{1}{k_{\rho}^2}$$

$$\{\mathbf{M}(k_z)\mathbf{M}'^{(2)}(-k_z) + \mathbf{N}(k_z)\mathbf{N}'^{(2)}(-k_z)\}dk_z \quad , \quad \rho < \rho'$$
(2.68)

Using (2.67) and (2.68) in (2.35), the field expression is obtained

$$\overline{\mathbf{G}}_{e0}(\mathbf{R}|\mathbf{R}') = -\frac{1}{k^2}\hat{\rho}\hat{\rho}\delta(\mathbf{R} - \mathbf{R}') + \frac{-j}{8\pi} \int_{-\infty}^{\infty} dk_z \sum_{n=-\infty}^{\infty} \frac{1}{k_{\rho}^2}$$

$$\left\{ \begin{bmatrix} \mathbf{N}^{(2)}(k_z)\mathbf{M}'(-k_z) + \mathbf{M}^{(2)}(k_z)\mathbf{N}'(-k_z) \end{bmatrix}, \quad \rho > \rho' \\ \left[\mathbf{N}(k_z)\mathbf{M}'^{(2)}(-k_z) + \mathbf{M}(k_z)\mathbf{N}'^{(2)}(-k_z) \right], \quad \rho < \rho' \right\}$$
(2.69)

Finally, to obtain the second-kind dyadic Green's function, $\overline{\mathbf{G}}_{e2}$, the scattering superposition method can be used [29]. A scattered wave term has to be added to the free-space dyadic Green's function previously obtained, as we see in the following equation

$$\overline{\mathbf{G}}_{e2}(\mathbf{R}|\mathbf{R}') = \overline{\mathbf{G}}_{e0}(\mathbf{R}|\mathbf{R}') + \overline{\mathbf{G}}_{2s}(\mathbf{R}|\mathbf{R}')$$
(2.70)

This scattered wave term, $\overline{\mathbf{G}}_{es}$, must satisfy the boundary condition for the specific problem, where $\hat{\rho} \times \nabla \times \overline{\mathbf{G}}_{e2} = 0$ at $\rho = a$ on the cylinder surface. The Neumann boundary condition can only be satisfied if the vector wave functions from the observation point are the same as those used in $\overline{\mathbf{G}}_{e0}$ for $\rho < \rho'$, $\mathbf{M}'^{(2)}(-k_z)$ and $\mathbf{N}'^{(2)}(-k_z)$. The radiation condition of outgoing waves can be satisfied also by $\mathbf{M}^{(2)}(k_z)$ and $\mathbf{N}^{(2)}(k_z)$ from the observation point. The expression for $\overline{\mathbf{G}}_{es}$ is then deduced from the expression of $\overline{\mathbf{G}}_{e0}$ as in

$$\overline{\mathbf{G}}_{2s}(\mathbf{R}|\mathbf{R}') = \frac{-j}{8\pi} \int_{-\infty}^{\infty} dk_z \sum_{n=-\infty}^{\infty} \frac{1}{k_{\rho}^2} \left\{ a_{\eta} \mathbf{M}^{(2)}(k_z) \mathbf{M}'^{(2)}(-k_z) + b_{\eta} \mathbf{N}^{(2)}(k_z) \mathbf{N}'^{(2)}(-k_z) \right\} , \quad \rho > \rho' \qquad (2.71)$$

The coefficients a_η and b_η are found by making $\overline{\mathbf{G}}_{e2}$ satisfying the Neumann boundary

condition at the cylinder surface

$$\hat{\rho} \times \nabla \times [\mathbf{M} + a_{\eta} \mathbf{M}^{(2)} + \mathbf{N} + b_{\eta} \mathbf{N}^{(2)}]_{\rho = a} = 0'$$
(2.72)

Next, to obtain the vector wave function, the scalar wave function

$$\varphi(\rho,\phi,z) = J_n(k_\rho\rho)e^{jn\phi}e^{jk_zz} \tag{2.73}$$

is used [32]. Using (2.73) into (2.49), which defines one of the two groups of solenoidal vector wave functions, with pilot vector $\hat{p} = \hat{z}$, the vector wave function **M** is obtained

$$\mathbf{M} = \nabla \times (\hat{z}J_{n}(k_{\rho}\rho)e^{jn\phi}e^{jk_{z}z})$$

$$= \frac{1}{\rho}\frac{\partial\varphi}{\partial\phi}\hat{\rho} - \frac{\partial\varphi}{\partial\rho}\hat{\phi}$$

$$= \frac{k_{\rho}}{(k_{\rho}\rho)}\frac{\partial\varphi}{\partial\phi}\hat{\rho} - k_{\rho}\frac{\partial\varphi}{\partial(k_{\rho}\rho)}\hat{\phi}$$
(2.74)

For convenience, we define $x = k_{\rho}\rho$, and rewrite (2.74) as

$$\mathbf{M} = \frac{k_{\rho}}{x} \frac{\partial (J_{n}(x)e^{jn\phi}e^{jk_{z}z})}{\partial \phi} \hat{\rho} - k_{\rho} \frac{\partial (J_{n}(x)e^{jn\phi}e^{jk_{z}z})}{\partial x} \hat{\phi}$$

$$= \frac{jnk_{\rho}}{x} J_{n}(x)e^{jn\phi}e^{jk_{z}z} \hat{\rho} - k_{\rho} \frac{\partial J_{n}(x)}{\partial x}e^{jn\phi}e^{jk_{z}z} \hat{\phi}$$

$$= k_{\rho}e^{jn\phi}e^{jk_{z}z} [jn\frac{J_{n}(x)}{x} \hat{\rho} - \frac{\partial J_{n}(x)}{\partial x} \hat{\phi}]$$
(2.75)

Using (2.58) with $\mathbf{N} = \frac{1}{k} \nabla \times \mathbf{M}$, we obtain \mathbf{M} , as

$$\mathbf{N} = \frac{1}{k_0} \nabla \times \left[k_\rho e^{jn\phi} e^{jk_z z} \left[jn \frac{J_n(x)}{x} \hat{\rho} - \frac{\partial J_n(x)}{\partial x} \hat{\phi} \right] \right]$$

$$= \frac{k_\rho}{k_0} e^{jn\phi} e^{jk_z z} \left[jk_z \frac{\partial J_n(x)}{\partial x} \hat{\rho} - nk_z \frac{J_n(x)}{x} \hat{\phi} + \frac{n^2}{\rho} \frac{J_n(x)}{x} \hat{z} - \frac{1}{\rho} \frac{\partial x \frac{\partial J_n(x)}{\partial x} \hat{z}}{\partial x} \hat{z} \right]$$

$$= \frac{k_\rho}{k_0} e^{jn\phi} e^{jk_z z} \left[jk_z \frac{\partial J_n(x)}{\partial x} \hat{\rho} - nk_z \frac{J_n(x)}{x} \hat{\phi} - k_\rho J_n(x) \hat{z} \right]$$
(2.76)

We define $\mathbf{M}'(-k_z)$, $\mathbf{M}^{(2)}(k_z)$, $\mathbf{N}'(-k_z)$, and $\mathbf{N}^{(2)}(k_z)$ from 2.75 and 2.76 as

$$\mathbf{M}'(-k_z) = k_{\rho}e^{-jn\phi'}e^{-jk_zz'}\left[-jn\frac{J_n(x')}{x'}\hat{\rho}' - \frac{\partial J_n(x')}{\partial x}\hat{\phi}'\right]$$
(2.77)

$$\mathbf{M}^{(2)}(k_z) = k_\rho e^{jn\phi} e^{jk_z z} \left[jn \frac{H_n^{(2)}(x)}{x} \hat{\rho} - \frac{\partial H_n^{(2)}(x)}{\partial x} \hat{\phi} \right]$$
(2.78)

$$\mathbf{N}'(-k_z) = \frac{k\rho}{k_0} e^{-jn\phi'} e^{-jk_z z'}$$

$$\left[-jk_z \frac{\partial J_n(x')}{\partial x} \hat{\rho}' - nk_z \frac{J_n(x')}{x'} \hat{\phi} - k_\rho J_n(x') \hat{z}' \right]$$
(2.79)

$$\mathbf{N}^{(2)}(k_z) = \frac{k_{\rho}}{k_0} e^{jn\phi} e^{jk_z z} \left[jk_z \frac{\partial H_n^{(2)}(x)}{\partial x} \hat{\rho} - nk_z \frac{H_n^{(2)}(x)}{x} \hat{\phi} - k_{\rho} H_n^{(2)}(x) \hat{z} \right]$$
(2.80)

Finally, substituting (2.77), (2.78), (2.79) and (2.78) into (2.72), we can find a_{η} and b_{η}

$$a_{\eta} = \frac{-J_n}{H_n^{(2)}(\gamma)}$$

$$b_{\eta} = \frac{\frac{-\partial J_n}{\partial \gamma}}{\frac{\partial H_n^{(2)}(\gamma)}{\partial \gamma}}$$
(2.81)

where $\gamma = k_{\rho}a$. The complete expression for $\overline{\mathbf{G}}_{2s}$ is obtained by substituting (2.81)

into (2.71)

$$\overline{\mathbf{G}}_{2s}(\mathbf{R}|\mathbf{R}') = \frac{-j}{8\pi} \int_{-\infty}^{\infty} dk_z \sum_{n=-\infty}^{\infty} \frac{1}{k_{\rho}^{2}}$$

$$\left\{ \frac{-J_n}{H_n^{(2)}(\gamma)} \mathbf{M}'^{(2)}(-k_z) + \frac{\frac{-\partial J_n}{\partial \gamma}}{\frac{\partial H_n^{(2)}(\gamma)}{\partial \gamma}} \mathbf{N}^{(2)}(k_z) \mathbf{N}'^{(2)}(-k_z) \right\} , \quad \rho > \rho'$$
(2.82)

Evaluating (2.82) and (2.69) in (2.70), and expressing $\partial H_n^{(2)}(\gamma)/\partial \gamma$ as $H_n^{\prime(2)}(\gamma)$, yields the expression for the electric dyadic Green's function of the second kind for a perfect conducting circular cylinder

$$\overline{G}_{e2}(\rho, \phi, z | \rho', \phi', z') = \frac{1}{(2\pi)^{2}} \sum_{n=-\infty}^{\infty} e^{jn\overline{\phi}} \int_{-\infty}^{\infty} dk_{z} e^{-jk_{z}\overline{z}} \\
\times \left\{ \left[\frac{-jnH_{n}^{(2)}(x)}{\gamma_{x}H_{n}^{(2)}(\gamma)} + \frac{jn}{\gamma^{2}} \left(\frac{k_{z}}{k_{0}} \right)^{2} \frac{H_{n}^{\prime(2)}(x)}{H_{n}^{\prime(2)}(\gamma)} \right] \hat{\rho}\hat{\phi}' - j \left[\frac{k_{z}k_{\rho}H_{n}^{\prime(2)}(x)}{\gamma_{k_{0}}^{2}H_{n}^{\prime(2)}(\gamma)} \right] \hat{\rho}\hat{z}' \\
+ \left[\frac{H_{n}^{\prime(2)}(x)}{\gamma_{n}^{2}H_{n}^{(2)}(\gamma)} - \left(\frac{nk_{z}}{k_{0}\gamma} \right)^{2} \frac{H_{n}^{(2)}(x)}{xH_{n}^{\prime(2)}(\gamma)} \right] \hat{\phi}\hat{\phi}' + \left[\frac{nk_{z}k_{\rho}H_{n}^{(2)}(x)}{\gamma_{x}k_{0}^{2}H_{n}^{\prime(2)}(\gamma)} \right] \hat{\phi}\hat{z}' \\
+ \left[\frac{nk_{z}k_{\rho}H_{n}^{(2)}(x)}{\gamma_{2}^{2}k_{0}^{2}H_{n}^{\prime(2)}(\gamma)} \right] \hat{z}\hat{\phi}' - \frac{1}{\gamma} \left[\left(\frac{k_{\rho}}{k_{0}} \right)^{2} \frac{H_{n}^{\prime(2)}(x)}{H_{n}^{\prime(2)}(\gamma)} \right] \hat{z}\hat{z}' \right\} \tag{2.83}$$

where $\overline{\phi} = \phi - \phi'$ and $\overline{z} = z - z'$.

2.2 Approximation of Green's Function On-Surface

As it was said in Section 2.1, (2.83) represents the dyadic Green's function as a series of eigenfunction. In this section, $\overline{\mathbf{G}}_{2s}$ will be specialized for the case where both the observation and source points are on the surface. Then, x would also be equal to $k_{\rho}\rho$ and $\rho=a$, where a is the cylinder radius. Also, using the boundary condition,

the radial components of $\overline{\mathbf{G}}_{e2}$ will not be necessary and can be suppressed in (2.83). Using those conditions, the dyadic Green's function on the surface can be written as

$$\overline{G}_{e2}(\rho,\phi,z|a,\phi',z') = \frac{1}{(2\pi)^2} \sum_{n=-\infty}^{\infty} e^{jn\overline{\phi}} \int_{-\infty}^{\infty} dk_z e^{-jk_z\overline{z}} \\
\left\{ \frac{1}{\gamma} \left[\frac{H_n'^{(2)}(\gamma)}{H_n^{(2)}(\gamma)} - \left(\frac{nk_z}{k_0\gamma} \right)^2 \frac{H_n^{(2)}(\gamma)}{H_n'^{(2)}(\gamma)} \right] \hat{\phi} \hat{\phi}' \left[\frac{nk_z k_\rho H_n^{(2)}(\gamma)}{\gamma^2 + k_0^2 H_n'^{(2)}(\gamma)} \right] \hat{\phi} \hat{z}' \right. \\
+ \left[\frac{nk_z k_\rho H_n^{(2)}(\gamma)}{\gamma^2 k_0^2 H_n'^{(2)}(\gamma)} \right] \hat{z} \hat{\phi}' - \frac{1}{\gamma} \left[\left(\frac{k_\rho}{k_0} \right)^2 \frac{H_n^{(2)}(\gamma)}{H_n'^{(2)}(\gamma)} \right] \hat{z} \hat{z}' \right\} \tag{2.84}$$

Equation (2.84) is exact for any cylinder radius. However, for cylinder of large radius, (2.84) is very slowly convergent. The Hankel function of large order has to be computed to obtain a reasonable approximation. This order is approximately 2ka series terms to obtain a good accuracy. To solve this, and to avoid the time consumption by evaluating computationally the Hankel function, the Watson transform is used [33, 34]. Watson showed that an infinite series of the form $\sum_{-\infty}^{\infty} f(n)e^{-jn\pi}$ could be represented by a complex integral of the form $\oint_{\mathcal{C}} (f(v)/\sin(v\pi))dv$. If we assume that f(v) vanishes at $-\infty$ and ∞ the integral can be rewritten as $\int_{c_1+c_2} (f(v)/\sin(v\pi))dv$. He also proposed that this integral may be evaluated if the residues at each pole are taken. The surface of the cylinder is part of the shadow region. Watson showed that in this zone, few terms are needed to obtain an accurate and highly convergent expression [34]. Physically, this method of pole residues represents the creeping waves, which are launched by the surface ray when it is travelling in the direction of propagation. The original Watson transform is the first part of (2.85), but it can be

modified to be used with the series that we have in (2.84) as follows,

$$2j\sum_{-\infty}^{\infty} f(n)e^{-jn\pi} = \int_{c_1+c_2} \frac{f(v)}{\sin(v\pi)} dv$$

$$2j\sum_{-\infty}^{\infty} f(n)e^{jn\overline{\phi}}e^{-jn\pi} = \int_{c_1+c_2} \frac{f(v)e^{jv\overline{\phi}}}{\sin(v\pi)} dv$$

$$2j\sum_{-\infty}^{\infty} f(n)e^{jn\overline{\phi}}e^{-jn\pi}e^{jn\pi} = \int_{c_1+c_2} \frac{f(v)e^{jv\overline{\phi}}e^{jv\pi}}{\sin(v\pi)} dv$$

$$\sum_{-\infty}^{\infty} f(n)e^{jn(\overline{\phi}+\frac{\pi}{2})} = \frac{1}{2j}\int_{c_1+c_2} \frac{f(v)e^{jv(\overline{\phi}+\pi)}}{\sin(v\pi)} dv \qquad (2.85)$$

where c_1 and c_2 comprise the closed path of the integration contour, see Figure 2.1 [34]. The $\hat{z}\hat{z}'$ component of (2.84) represents the \hat{z} component of the surface field produced by the \hat{z} component of the magnetic dipole source. Taking this component

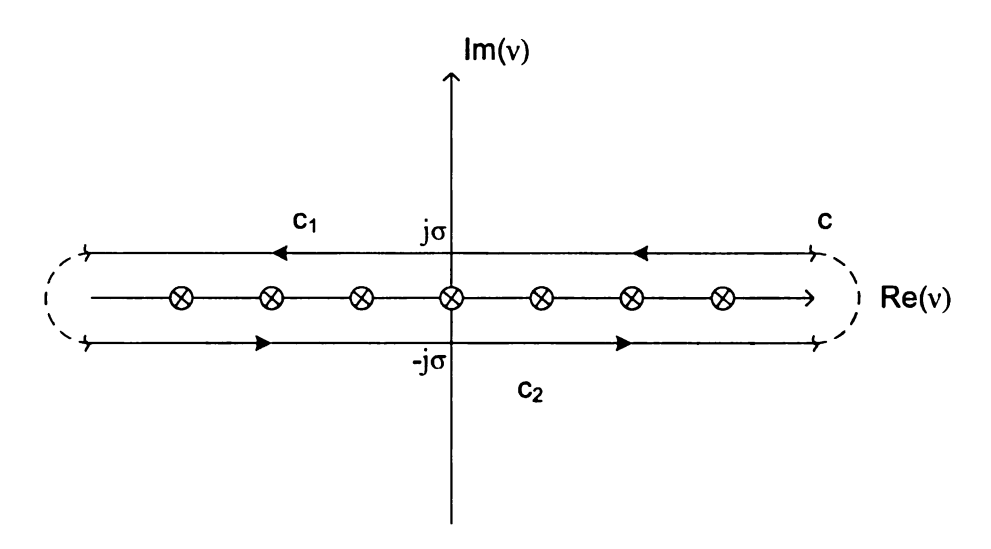


Figure 2.1. Watson transform integration contour c formed by paths c_1 and c_2

$$G_{e2}^{zz} = -\frac{1}{(2\pi)^2} \sum_{n=-\infty}^{\infty} e^{jn\overline{\phi}} \int_{-\infty}^{\infty} dk_z e^{-jk_z \overline{z}} \frac{k_\rho}{ak_0^2} \frac{H_n^{(2)}(\gamma)}{H_n^{\prime(2)}(\gamma)}$$
(2.86)

and applying the Watson transform obtained in (2.85) with $f(v) = H_v^{(2)}(\gamma)/H_v^{(2)}(\gamma)$ and c_1 from $-\infty - j\sigma$ to $\infty - j\sigma$ and c_2 from $\infty + j\sigma$ to $\infty - j\sigma$, we have the following result

$$G_{e2}^{zz} = \frac{1}{(2\pi)^2} \frac{j}{2} \int_{-\infty}^{\infty} \frac{k\rho}{ak_0^2} e^{-jk_z \overline{z}} dk_z \int_{c_1+c_2} \frac{e^{jv(\overline{\phi}+\pi)} H_v^{(2)}(\gamma)}{\sin(v\pi) H_v^{\prime(2)}(\gamma)}$$

$$= \frac{1}{(2\pi)^2} \frac{j}{2} \int_{-\infty}^{\infty} \frac{k\rho}{ak_0^2} e^{-jk_z \overline{z}} dk_z \int_{-\infty-j\sigma}^{\infty-j\sigma} \frac{e^{jv(\overline{\phi}+\pi)} H_v^{(2)}(\gamma)}{\sin(v\pi) H_v^{\prime(2)}(\gamma)} dv$$

$$+ \int_{\infty+j\sigma}^{-\infty+j\sigma} \frac{e^{jv(\overline{\phi}+\pi)} H_v^{(2)}(\gamma)}{\sin(v\pi) H_v^{\prime(2)}(\gamma)} dv \qquad (2.87)$$

Mapping ν to $-\nu$ in the third integral of (2.87), and inverting the integration limits, with $H_{-v}^{(2)}(\gamma) = e^{-jv\pi}H_v^{(2)}$ and $H_{-v}^{\prime(2)}(\gamma) = e^{-jv\pi}H_v^{\prime(2)}$, (2.87) may be rewritten as

$$G_{e2}^{zz} = \frac{1}{(2\pi)^2} \frac{j}{2} \int_{-\infty}^{\infty} \frac{k\rho}{ak_0^2} e^{-jk_z \overline{z}} dk_z$$

$$\left\{ \int_{-\infty - j\sigma}^{\infty - j\sigma} \frac{e^{jv(\overline{\phi} + \pi)} H_v^{(2)}(\gamma)}{\sin(v\pi) H_v^{\prime(2)}(\gamma)} dv - \int_{-\infty - j\sigma}^{\infty - j\sigma} \frac{e^{-jv(\overline{\phi} + \pi)} e^{-jv\pi} H_v^{(2)}(\gamma)}{-\sin(v\pi) e^{-jv\pi} H_v^{\prime(2)}(\gamma)} dv \right\}$$

$$= \frac{1}{(2\pi)^2} \frac{j}{2} \int_{-\infty}^{\infty} \frac{k\rho}{ak_0^2} e^{-jk_z \overline{z}} dk_z \int_{-\infty - j\sigma}^{\infty - j\sigma} \frac{\left[e^{jv(\overline{\phi} + \pi)} + e^{-jv(\overline{\phi} + \pi)}\right] H_v^{(2)}(\gamma)}{\sin(v\pi) H_v^{\prime(2)}(\gamma)} dv \quad (2.88)$$

To simplify (2.88), the Poisson's sum formula (2.89) can be used, where l is the number of times that the creeping wave encircles the cylinder. This equation varies depending on which path is chosen. In this case, the path c_1 was chosen, when $\sigma < 0$.

The procedure to obtain (2.89) is presented in [34] on p. 334. Using

$$\frac{e^{jv\pi}}{\sin(v\pi)} = 2j \sum_{l=0}^{\infty} e^{-j2lv\pi}$$
(2.89)

the term $e^{jv\pi}$ can be factorized in (2.88) as

$$G_{e2}^{zz} = \frac{1}{(2\pi)^2} \frac{j}{2} \int_{-\infty}^{\infty} \frac{k_{\rho}}{ak_0^2} e^{-jk_z \overline{z}} dk_z$$

$$\int_{-\infty - j\sigma}^{\infty - j\sigma} \frac{e^{jv\pi}}{\sin(v\pi)} \frac{\left[e^{jv(\overline{\phi} + \pi)} + e^{-jv(\overline{\phi} + \pi)}\right] H_v^{(2)}(\gamma)}{H_v^{(2)}(\gamma)} dv \qquad (2.90)$$

Replacing (2.89) with (2.90), it is express as

$$G_{e2}^{zz} = \frac{1}{(2\pi)^2} \frac{j}{2} \int_{-\infty}^{\infty} \frac{k\rho}{ak_0^2} e^{-jk_z \overline{z}} dk_z$$

$$\int_{-\infty - j\sigma}^{\infty - j\sigma} 2j \sum_{l=0}^{\infty} e^{-j2lv\pi} \frac{\left[e^{jv(\overline{\phi} + \pi)} + e^{-jv(\overline{\phi} + \pi)} \right] H_v^{(2)}(\gamma)}{H_v^{(2)}(\gamma)} dv$$

$$= \frac{-1}{(2\pi)^2} \int_{-\infty}^{\infty} \frac{k\rho}{ak_0^2} e^{-jk_z \overline{z}} dk_z$$

$$\sum_{l=0}^{\infty} \int_{-\infty - j\sigma}^{\infty - j\sigma} \frac{\left(e^{-jv(2l\pi + \overline{\phi} + 2\pi)} + e^{jv(\overline{\phi} - 2l\pi)} \right) H_v^{(2)}(\gamma)}{H_v^{(2)}(\gamma)} dv$$

$$H_v^{(2)}(\gamma)$$
(2.91)

is obtained for large radius cylinders. The orders of l larger than zero are negligible as the magnitude of the creeping wave, after a complete encirclement, has decayed

enough to ignore them. Taking the lowest term of l, the (2.91) is simplified as

$$G_{e2}^{zz} = \frac{-1}{(2\pi)^2} \int_{-\infty}^{\infty} \frac{k\rho}{ak_0^2} e^{-jk_z \overline{z}} dk_z \int_{-\infty - j\sigma}^{\infty - j\sigma} \frac{\left(e^{-jv(\overline{\phi} + 2\pi)} + e^{jv\overline{\phi}}\right) H_v^{(2)}(\gamma)}{H_v^{(2)}(\gamma)} dv \quad (2.92)$$

For the last Hankel functions, we can use the expansion for Hankel function with a large argument, in terms of Fock-type Airy functions as [8],

$$H_v^{(2)}(\gamma) \sim j \frac{w_2(\tau)}{m\sqrt{\pi}}$$
 (2.93)

$$H_v^{\prime(2)}(\gamma) \sim -j \frac{w_2^{\prime}(\tau)}{m^2 \sqrt{\pi}}$$
 (2.94)

where $w_2(\tau)$ as the Fock-type Airy functions of the second kind. Using the notation of Fock [28], the quantity τ is related to m as

$$\tau = \frac{1}{m}(\nu - \gamma) \tag{2.95}$$

Substituting (2.93) and (2.94) into (2.92), and with $v = m\tau + \gamma$ [33], we find that $dv = md\tau$ and (2.92) can be expressed as

$$G_{e2}^{zz} = \frac{-1}{(2\pi)^2} \int_{-\infty}^{\infty} \frac{k_{\rho}}{ak_0^2} e^{-jk_z \overline{z}} dk_z \int_{-\infty - j\sigma}^{\infty - j\sigma} \frac{\left(e^{-jv(\overline{\phi} + 2\pi)} + e^{jv\overline{\phi}}\right) j \frac{w_2(\tau)}{m\sqrt{\pi}}}{-j \frac{w_2'(\tau)}{m^2 \sqrt{\pi}}} dv$$

$$= \frac{1}{(2\pi)^2} \int_{-\infty}^{\infty} \frac{k_{\rho}}{ak_0^2} e^{-jk_z \overline{z}} dk_z \int_{-\infty - j\sigma}^{\infty - j\sigma} \frac{\left(e^{-jv(\overline{\phi} + 2\pi)} + e^{jv\overline{\phi}}\right) w_2(\tau)}{w_2'(\tau)} m dv$$

$$(2.96)$$

Considering only the short path term, $e^{jv\overline{\phi}}$, (2.96) can be written as

$$G_{e2}^{zz} = \frac{1}{(2\pi)^2} \int_{-\infty}^{\infty} \frac{k\rho}{ak_0^2} e^{-jk_z \overline{z}} dk_z \int_{\Gamma_1} \frac{e^{-j(m\tau + k\rho a)\overline{\phi}} w_2(\tau)}{w_2'(\tau)} m(m) d\tau$$

$$= \frac{1}{(2\pi)^2} \int_{-\infty}^{\infty} \frac{m^2 k\rho}{ak_0^2} e^{-jk_z \overline{z}} dk_z \int_{\Gamma_1} \frac{e^{-jm\tau \overline{\phi}} e^{-jk\rho a\overline{\phi}} w_2(\tau)}{w_2'(\tau)} d\tau \qquad (2.97)$$

Expressing above equation in polar coordinates,

$$k_{z} = k_{0} \sin \alpha$$

$$k_{\rho} = k_{0} \cos \alpha$$

$$a\overline{\phi} = s \cos \delta$$

$$\overline{z} = s \sin \delta$$

$$\beta = m\overline{\phi}$$
(2.98)

Simplifying this resulting expressions. Here, s is the geodesic distance, and δ is the angle subtended by the geodesic curve from the azimuthal plane of the cylinder at

the source point. Substituting (2.98) in (2.97) the final expression is given by

$$G_{e2}^{zz} = \frac{1}{(2\pi)^2} \int_{-\infty}^{\infty} \frac{m^2 k_{\rho}}{ak_0^2} e^{-jk_z \overline{z}} e^{-jk_{\rho} a \overline{\phi}} dk_z \int_{\Gamma_1} \frac{e^{-j\beta \tau} w_2(\tau)}{w_2'(\tau)} d\tau$$

$$= \frac{1}{(2\pi)^2} \int_{-\infty}^{\infty} \frac{m^2 k_0 \cos \alpha}{ak_0^2} e^{-jk_0 \sin \alpha (s \sin \delta)} e^{-jk_0 \cos \alpha (s \cos \delta)} dk_z$$

$$\int_{\Gamma_1} \frac{e^{-j\beta \tau} w_2(\tau)}{w_2'(\tau)} d\tau$$

$$= \frac{1}{(2\pi)^2} \int_{C\alpha} \frac{m^2 k_0 \cos \alpha}{ak_0^2} e^{-jk_0 \sin \alpha (s \sin \delta)} e^{-jk_0 \cos \alpha (s \cos \delta)} k_0 \cos \alpha d\alpha$$

$$\int_{\Gamma_1} \frac{e^{-j\beta \tau} w_2(\tau)}{w_2'(\tau)} d\tau$$

$$= \frac{1}{(2\pi)^2} \int_{C\alpha} \frac{m^2 \cos^2 \alpha}{a} e^{-jk_0 s \cos(\alpha - \delta)} d\alpha \int_{\Gamma_1} \frac{e^{-j\beta \tau} w_2(\tau)}{w_2'(\tau)} d\tau \qquad (2.99)$$

$$\nu(\beta) = \sqrt{\frac{j\beta}{4\pi}} \int_{\Gamma_1} \frac{e^{-j\beta\tau} w_2(\tau)}{w_2'(\tau)} d\tau$$
 (2.100)

$$G_{e2}^{zz} = \frac{1}{(2\pi)^2} \int_{C\alpha} \frac{m^2 \cos^2 \alpha}{a} \sqrt{\frac{4\pi}{j\beta}} \nu(\beta) e^{-jk_0 s \cos(\alpha - \delta)} d\alpha \qquad (2.101)$$

The remaining dyadic terms are given by $G_{e2}^{\phi\phi}$, $G_{e2}^{\phi z}$ and $G_{e2}^{z\phi}$

2.3 Approximation of Green's Function in the Far Zone

We start again with the expression for the expanded form of the electric dyadic Green's function of the second kind for an infinite PEC circular cylinder (2.83). In this case, only the source point will be on the cylinder surface at $\rho = a$. In contrast with the on-surface case presented in Section 2.2, the observation point can be in any point outside the surface including at an infinite distance from the cylinder. Because of this, $x = k_{\rho}\rho$ where $a < \rho < \infty$. For this case, (2.83) must be written as

$$G(\rho, \phi, z | a, \phi', z') = \frac{1}{(2\pi)^2} \sum_{n = -\infty}^{\infty} e^{jn\overline{\phi}} \int_{-\infty}^{\infty} dk_z e^{-jk_z \overline{z}}$$

$$\left\{ \left[\frac{-jnH_n^{(2)}(x)}{\gamma x H_n^{(2)}(\gamma)} + \frac{jn}{\gamma^2} \left(\frac{k_z}{k_0} \right)^2 \frac{H_n^{\prime(2)}(x)}{H_n^{\prime(2)}(\gamma)} \right] \hat{\rho} \hat{\phi}' - j \left[\frac{k_z k_\rho H_n^{\prime(2)}(x)}{\gamma k_0^2 H_n^{\prime(2)}(\gamma)} \right] \hat{\rho} \hat{z}' \right.$$

$$\left. + \left[\frac{H_n^{\prime(2)}(x)}{\gamma H_n^{(2)}(\gamma)} - \left(\frac{nk_z}{k_0 \gamma} \right)^2 \frac{H_n^{(2)}(x)}{x H_n^{\prime(2)}(\gamma)} \right] \hat{\phi} \hat{\phi}' + \left[\frac{nk_z k_\rho H_n^{(2)}(x)}{\gamma x k_0^2 H_n^{\prime(2)}(\gamma)} \right] \hat{\phi} \hat{z}' \right.$$

$$\left. + \left[\frac{nk_z k_\rho H_n^{(2)}(x)}{\gamma^2 k_0^2 H_n^{\prime(2)}(\gamma)} \right] \hat{z} \hat{\phi}' - \frac{1}{\gamma} \left[\left(\frac{k_\rho}{k_0} \right)^2 \frac{H_n^{(2)}(x)}{H_n^{\prime(2)}(\gamma)} \right] \hat{z} \hat{z}' \right\} \quad (2.102)$$

As noted in Section 2.2, this expression slowly converges for the case where the parameter $k_{\rho}\rho$ is large. Later, asymptotic expression will be derived similar to the surface case. To evaluated this Greens's function in the far-zone the Hankel function and its spectral derivative are approximated as

$$\lim_{\rho \to \infty} H_n^{\prime(2)}(x) \sim -jH_n^{(2)}(x) \tag{2.103}$$

$$\lim_{\rho \to \infty} \frac{H_n^{(2)}(x)}{x} \sim \lim_{\rho \to \infty} \frac{1}{e^{j\rho} \rho \sqrt{\rho}} = 0$$
 (2.104)

Substituting those in (2.102), it is written as

$$G(\rho, \phi, z | a, \phi', z') = \frac{1}{(2\pi)^2} \sum_{n = -\infty}^{\infty} e^{jn\overline{\phi}} \int_{-\infty}^{\infty} dk_z e^{-jk_z\overline{z}} \left\{ \left[\frac{n}{\gamma^2} \left(\frac{k_z}{k_0} \right)^2 \frac{H_n^{(2)}(x)}{H_n^{\prime(2)}(\gamma)} \right] \hat{\rho} \hat{\phi}' - \left[\frac{k_z k_\rho H_n^{(2)}(x)}{\gamma k_0^2 H_n^{\prime(2)}(\gamma)} \right] \hat{\rho} \hat{z}' - \left[\frac{jH_n^{(2)}(x)}{\gamma H_n^{(2)}(\gamma)} \right] \hat{\phi} \hat{\phi}' + \left[\frac{nk_z k_\rho H_n^{(2)}(x)}{\gamma^2 k_0^2 H_n^{\prime(2)}(\gamma)} \right] \hat{z} \hat{\phi}' - \frac{1}{\gamma} \left[\left(\frac{k_\rho}{k_0} \right)^2 \frac{H_n^{(2)}(x)}{H_n^{\prime(2)}(\gamma)} \right] \hat{z} \hat{z}' \right\} (2.105)$$

Using

$$H_n^{(2)}(x) \sim \sqrt{\frac{2}{\pi x}} e^{-jx} e^{jn\frac{\pi}{2}} e^{j\frac{\pi}{4}}$$
 (2.106)

factorizing it from the numerator on (2.105), and rewriting (2.105) grouping terms in function of the source points, we obtain

$$G(\rho, \phi, z | a, \phi', z') = \frac{2}{(2\pi)^2} \sum_{n = -\infty}^{\infty} e^{jn(\overline{\phi} + \frac{\pi}{2})}$$

$$\int_{-\infty}^{\infty} dk_z e^{-jk_z z'} \left\{ \frac{nk_z}{k_0 \gamma^2 H_n'^{(2)}(\gamma)} \left[\frac{k_z}{k_0} \hat{\rho} - \frac{k_\rho}{k_0} \hat{z} \right] \hat{\phi}' \right.$$

$$\left. + \frac{1}{k_0 a H_n'^{(2)}(\gamma)} \left[\frac{k_z}{k_0} \hat{\rho} - \frac{k_\rho}{k_0} \hat{z} \right] \hat{z}' - \frac{j}{\gamma H_n^{(2)}(\gamma)} \right\} \hat{\phi} \hat{\phi}' \frac{e^{jn\frac{\pi}{4}} e^{-j(k_\rho \rho + k_z z)}}{\sqrt{2\pi k_\rho \rho}}$$
(2.107)

Replacing $\left[\frac{k_z}{k_0}\hat{\rho} - \frac{k_\rho}{k_0}\hat{z}\right]$ with $\hat{\theta}$ in (2.107), and expressing it in terms of dyadic components resulting in

$$\overline{\mathbf{G}}_{e2} \sim \frac{2}{(2\pi)^2} \sum_{n=-\infty}^{\infty} e^{jn(\bar{\phi} + \frac{\pi}{2})} \left[G_{\theta\phi} \hat{\theta} \hat{\phi}' + G_{\theta z} \hat{\theta} \hat{z}' + G_{\phi\phi} \hat{\phi} \hat{\phi}' \right]$$
(2.108)

where

$$G_{e2}^{\theta\phi} = \int_{-\infty}^{\infty} \frac{e^{jk_z z'} e^{j\frac{\pi}{4}} nk_z}{(k_\rho a)^2 k_0 H_n^{\prime(2)}(k_\rho a)} \frac{e^{-j(k_\rho \rho + k_z z)}}{\sqrt{2\pi k_\rho \rho}} dk_z$$
 (2.109)

$$G_{e2}^{\theta z} = \int_{-\infty}^{\infty} \frac{e^{jk_z z'} e^{j\frac{\pi}{4}}}{k_{\rho} a H_n^{\prime(2)}(k_{\rho} a)} \frac{e^{-j(k_{\rho} \rho + k_z z)}}{\sqrt{2\pi k_{\rho} \rho}} dk_z$$
 (2.110)

$$G_{e2}^{\phi\phi} = \int_{-\infty}^{\infty} \frac{(-j)e^{jk_z z'}e^{j\frac{\pi}{4}}}{k_{\rho}aH_n^{(2)}(k_{\rho}a)} \frac{e^{-j(k_{\rho}\rho + k_z z)}}{\sqrt{2\pi k_{\rho}\rho}} dk_z$$
 (2.111)

Each dyadic component can be evaluated using the method of steepest descent. This method is used to calculate complex integrals with large parameters; in our case with $k\rho\rho$ large. This method works due to the fact that we can deform the contour of integration and the result will not change provided this function is analytic. We first need to find critical points of the integral. Then for those points, a path must be identified and finally, we must deform the contour to follow the paths [35]. We start from the canonical steepest descent integral which is given by:

$$G(k_z) \sim \int_{SDP} F(k_z) e^{\kappa g(k_z)} dk_z$$
 (2.112)

where κ is the large parameter and SDP is the contour that contains the saddle points. After applying the method, we will obtain a first order approximation of the form

$$G(k_z) \sim \frac{\sqrt{2\pi} F(k_z^s) e^{\kappa g(k_z^s)} e^{j\psi}}{|\kappa g''(k_z^s)|^{\frac{1}{2}}}$$
 (2.113)

with k_z^s as the saddle-point and ψ as the angle between the saddle-point and the intersection with the contour. For convenience, we change the parameters in (2.109) from cylindrical coordinates to spherical coordinates as

$$k_{\rho} = k_0 \sin(\theta), \quad \rho = R \sin(\theta), \quad z = R \cos(\theta)$$
 (2.114)

where θ is the angle between the z axis and the observation point in the far-zone. Taking $e^{-j(k_{\rho}\rho+k_{z}z)}$ from (2.109), replacing ρ and z from (2.114), and comparing this term with the canonical steepest descent integral, we can write it as

$$e^{-j(k_{\rho}R\sin(\theta) + k_{z}R\cos(\theta))} = e^{-jR(k_{\rho}\sin(\theta) + k_{z}\cos(\theta))} = e^{\kappa g(k_{z})}$$
(2.115)

with $\kappa=R$. Using $k_0^2=k_\rho^2+k_z^2$, we can substitute it on

$$g(k_z) = -j(k_\rho \sin(\theta) + k_z \cos(\theta)) \tag{2.116}$$

to obtain

$$g(k_z) = -j(\sqrt{k_0^2 - k_z^2}\sin(\theta) + k_z\cos(\theta))$$
 (2.117)

The saddle-point is obtained by setting the $\frac{dg(k_z)}{dk_z}|_{k_z=k_z^s}=0$. Thus,

$$\frac{dg(k_z)}{dk_z} = -j \left[\frac{-k_z \sin(\theta)}{(k_0^2 - k_z^2)^{\frac{1}{2}}} + \cos(\theta) \right]$$
 (2.118)

Therefore, when $\frac{dg(k_z)}{dk_z} = 0$, the value found for k_z is a saddle-point, k_z^s

$$-j \left[\frac{-k_z^s \sin(\theta)}{(k_0^2 - k_z^2)^{\frac{1}{2}}} + \cos(\theta) \right] = 0$$

$$k_z^s \sin(\theta) = (k_0^2 - k_z^2)^{\frac{1}{2}} \cos(\theta)$$

$$k_z^s \tan(\theta) = (k_0^2 - k_z^2)^{\frac{1}{2}}$$

$$(k_z^s)^2 = k_0^2 \cos(\theta)^2$$

$$k_z^s = k_0 \cos(\theta)$$
(2.119)

then function $g''(k_z)$ and $g(k_z)$ can be evaluated at the saddle-point $k_z = k_z^s = k_0 \cos(\theta)$ as

$$g''(k_z^s) = j\sin(\theta) \frac{k_0^2}{(k_0^2 - k_0^2\cos^2(\theta))^{\frac{3}{2}}}$$

$$= j\sin(\theta) \frac{k_0^2}{k_0^3(1 - \cos^2(\theta))^{\frac{3}{2}}}$$

$$= \frac{j}{k_0\sin^2(\theta)}$$
(2.120)

$$g(k_z^s) = -j[(k_0^2 - k_0^2 \cos^2(\theta))^{\frac{1}{2}} \sin(\theta) + k_0 \cos(\theta) \cos(\theta)]$$

$$= -j(k_0^2 [\sin^2(\theta) + \cos^2(\theta)]$$

$$= -jk_0$$
(2.121)

It follows that the function $F(k_z)$ would be written as

$$F(k_z) = \frac{e^{jk_z z'} e^{j\frac{\pi}{4}} nk_z}{(k_\rho a)^2 k_0 H_n^{\prime(2)}(k_\rho a) \sqrt{2\pi k_\rho \rho}}$$
(2.122)

with $k_{\rho} = k \sin(\theta)$

$$F(k_z^s) = \frac{e^{jk_0 \cos(\theta)z'} e^{j\frac{\pi}{4}n \cos(\theta)}}{(k \sin(\theta)a)^2 H_n'^{(2)}(k \sin(\theta)a) \sin(\theta)\sqrt{2\pi kR}}$$
(2.123)

Substituting equations (2.123), (2.121) and (2.120) into (2.113) resulting in

$$G_{e2}^{\theta\phi} \sim \frac{\sqrt{2\pi} \frac{e^{jk_0 \cos(\theta)z'} e^{j\frac{\pi}{4}n \cos(\theta)}}{(k \sin(\theta)a)^2 H_n^{\prime(2)}(k \sin(\theta)a) \sin(\theta)\sqrt{2\pi kR}} e^{R(-jk_0)} e^{j\psi}}{|R \frac{j}{k_0 \sin^2(\theta)}|^{\frac{1}{2}}}$$
(2.124)

with $\psi = \frac{\pi}{4}$

$$G_{e2}^{\theta\phi} \sim \frac{e^{jk_0\cos(\theta)z'}e^{j\frac{\pi}{4}}e^{j\frac{\pi}{4}}e^{R(-jk_0)}n\cos(\theta)\sqrt{k_0}}{(k\sin(\theta)a)^2H_n'^{(2)}(k\sin(\theta)a)\sqrt{kR}}$$

$$\sim \frac{je^{-jRk_0}\cos(\theta)e^{jk_0\cos(\theta)z'}}{R(ka\sin(\theta))^2}\frac{n}{H_n'^{(2)}(k\sin(\theta)a)}$$
(2.125)

We follow the same procedure for (2.110). Now, $g(k_z)^s$ and $g''(k_z)^s$ are the same as in (2.109), $F(k_z)$ is given by

$$F(k_z) = \frac{e^{jk_z z'} e^{j\frac{\pi}{4}}}{(k_0 a)^2 k_0 H_n^{\prime(2)}(k_\rho a) \sqrt{2\pi k_\rho \rho}}$$
(2.126)

and

$$F(k_z^s) = \frac{e^{jk_0\cos(\theta)z'}e^{j\frac{\pi}{4}}}{(k_0a)^2k_0H_n^{\prime(2)}(k_\rho a)\sqrt{2\pi k_\rho \rho}}$$
(2.127)

Replacing (2.113), we obtain:

$$G_{e2}^{\theta z} \sim \frac{\sqrt{2\pi} \frac{e^{jk_0 \cos(\theta)z'} e^{j\frac{\pi}{4}}}{(k_0a)^2 H_n^{\prime(2)}(k \sin(\theta)a) \sin(\theta) \sqrt{2\pi kR}} e^{R(-jk_0)} e^{j\psi}}{|R \frac{j}{k_0 \sin^2(\theta)}|^{\frac{1}{2}}}$$

$$\sim \frac{je^{-jRk_0} e^{jk_0 \cos(\theta)z'}}{R(ka)} \frac{1}{H_n^{\prime(2)}(k \sin(\theta)a)}$$
(2.128)

Finally for (2.111), $g(k_z^s)$ and $g''(k_z^s)$ are the same as in (2.109) and (2.110). $F(k_z)$ is

$$F(k_z) = \frac{-je^{jk_z z'} e^{j\frac{\pi}{4}}}{(k_\rho a) H_n'^{(2)}(k_\rho a) \sqrt{2\pi k_\rho \rho}}$$
(2.129)

and

$$F(k_z^s) = \frac{-je^{jk_0\cos(\theta)z'}e^{j\frac{\pi}{4}}}{(ka\sin(\theta))H_n^{\prime(2)}(ka\sin(\theta))\sin(\theta)\sqrt{2\pi kR}}$$
 (2.130)

There for, it can be verified that

$$G_{e2}^{\phi\phi} \sim \frac{\sqrt{2\pi} \frac{(-j)e^{jk_0\cos(\theta)z'}e^{j\frac{\pi}{4}}}{(ka\sin(\theta))H_n^{\prime(2)}(k\sin(\theta)a)\sin(\theta)\sqrt{2\pi kR}}e^{R(-jk_0)}e^{j\psi}}{|R\frac{j}{k_0\sin^2(\theta)}|^{\frac{1}{2}}}$$

$$\sim \frac{e^{-jRk_0}e^{jk_0\cos(\theta)z'}}{R(ka\sin(\theta))}\frac{1}{H_n^{\prime(2)}(k\sin(\theta)a)}$$
(2.131)

Summarizing, the three components of $\overline{\mathbf{G}}_{2s}$ after applying the steepest decent method can be written as

$$G_{e2}^{\theta\phi} \sim \frac{e^{-jRk_0}}{k_0R} \frac{j2k\cos(\theta)e^{jk_0\cos(\theta)z'}}{(2\pi)^2(ka\sin(\theta))^2} \sum_{n=-\infty}^{\infty} \frac{ne^{jn(\overline{\phi} + \frac{\pi}{2})}}{H_n'^{(2)}(ka\sin(\theta))}$$
(2.132)

$$G_{e2}^{\theta z} \sim \frac{e^{-jRk_0}}{Rk_0} \frac{j2e^{jk\cos(\theta)z'}}{(2\pi)^2 a} \sum_{n=-\infty}^{\infty} \frac{e^{jn(\overline{\phi} + \frac{\pi}{2})}}{H_n'^{(2)}(ka\sin(\theta))}$$
 (2.133)

$$G_{e2}^{\phi\phi} \sim \frac{e^{-jRk_0}}{Rk_0} \frac{2k_0 e^{jk} \cos(\theta) z'}{(2\pi)^2 (ka\sin(\theta))} \sum_{n=-\infty}^{\infty} \frac{e^{jn(\overline{\phi} + \frac{\pi}{2})}}{H_n^{\prime(2)}(ka\sin(\theta))}$$
(2.134)

Equations (2.132), (2.133) and (2.134) can be written into separate sums using $\sum_{-\infty}^{\infty} F(\gamma) = \sum_{-\infty}^{0} F(\gamma) + \sum_{0}^{\infty} F(\gamma) - F(0)$. Doing that for (2.132), substituting n by -n in the first summation and changing its intervals, the following equation

is obtained

$$G_{e2}^{\theta\phi} \sim \frac{e^{-jRk_0}}{k_0R} \frac{j2k_0\cos(\theta)e^{jk}\cos(\theta)z'}{(2\pi)^2(ka\sin(\theta))^2} \\ \left[\sum_{n=-\infty}^{0} \frac{ne^{jn\overline{\phi}}e^{jn\frac{\pi}{2}}}{H_n'^{(2)}(ka\sin(\theta))} + \sum_{n=0}^{\infty} \frac{ne^{jn\overline{\phi}}e^{jn\frac{\pi}{2}}}{H_n'^{(2)}(ka\sin(\theta))} - 0 \right] \\ \sim \frac{e^{-jRk_0}}{k_0R} \frac{j2k_0\cos(\theta)e^{jk}\cos(\theta)z'}{(2\pi)^2(ka\sin(\theta))^2} \\ \left[\sum_{n=0}^{\infty} \frac{-ne^{-jn\overline{\phi}}e^{-jn\frac{\pi}{2}}}{H_{-n}'^{(2)}(ka\sin(\theta))} + \sum_{n=0}^{\infty} \frac{ne^{jn\overline{\phi}}j^n}{H_n'^{(2)}(ka\sin(\theta))} \right]$$
(2.135)

Using the transform $H_{-n}^{\prime(2)}(\gamma) = e^{-j\pi n} H_n^{\prime(2)}(\gamma)$ for analytic functions [36] and substituting it in (2.135), we have

$$G_{e2}^{\theta\phi} \sim \frac{e^{-jRk_0}}{k_0R} \frac{j2k_0\cos(\theta)e^{jk}\cos(\theta)z'}{(2\pi)^2(ka\sin(\theta))^2} \\ \left[\sum_{n=0}^{\infty} \frac{-ne^{-jn\bar{\phi}}e^{-jn\frac{\pi}{2}}}{e^{-j\pi n}H_n'^{(2)}(ka\sin(\theta))} + \sum_{n=0}^{\infty} \frac{ne^{jn\bar{\phi}}j^n}{H_n'^{(2)}(ka\sin(\theta))} \right] \\ \sim \frac{e^{-jRk_0}}{k_0R} \frac{j2k_0\cos(\theta)e^{jk}\cos(\theta)z'}{(2\pi)^2(ka\sin(\theta))^2} \\ \left[\sum_{n=0}^{\infty} \frac{nj^n(-e^{-jn\bar{\phi}})}{H_n'^{(2)}(ka\sin(\theta))} + \sum_{n=0}^{\infty} \frac{nj^ne^{jn\bar{\phi}}}{H_n'^{(2)}(ka\sin(\theta))} \right]$$

$$(2.136)$$

Factorizing the summation in (2.136) and applying the Euler's identity, (2.136) can be simplified as

$$G_{e2}^{\theta\phi} \sim \frac{e^{-jRk_0}}{k_0R} \frac{j2k_0\cos(\theta)e^{jk\cos(\theta)z'}}{(2\pi)^2(ka\sin(\theta))^2} \left[\sum_{n=0}^{\infty} \frac{nj^n(e^{jn\overline{\phi}} - e^{-jn\overline{\phi}})}{H_n'^{(2)}(ka\sin(\theta))} \right] \frac{2j}{2j}$$

$$\sim \frac{e^{-jRk_0}}{k_0R} \frac{(-4)k_0\cos(\theta)e^{jk\cos(\theta)z'}}{(2\pi)^2(ka\sin(\theta))^2} \left[\sum_{n=0}^{\infty} \frac{nj^n\sin(n\overline{\phi})}{H_n'^{(2)}(ka\sin(\theta))} \right]$$
(2.137)

We can use the same procedure in (2.133) to obtain

$$G_{e2}^{\theta z} \sim \frac{e^{-jRk_0}}{k_0 R} \frac{j2e^{jk\cos(\theta)z'}}{(2\pi)^2 a} \left[\sum_{n=-\infty}^{0} \frac{e^{jn\frac{\pi}{2}}e^{jn\overline{\phi}}}{H_n^{\prime(2)}(ka\sin(\theta))} + \sum_{n=0}^{\infty} \frac{e^{jn\frac{\pi}{2}}e^{jn\overline{\phi}}}{H_n^{\prime(2)}(ka\sin(\theta))} - \frac{1}{H_0^{\prime(2)}(ka\sin(\theta))} \right]$$

$$\sim \frac{e^{-jRk_0}}{k_0 R} \frac{j2e^{jk\cos(\theta)z'}}{(2\pi)^2 a} \left[\sum_{n=0}^{\infty} \frac{j^n(e^{jn\overline{\phi}} - e^{-jn\overline{\phi}})}{H_n^{\prime(2)}(ka\sin(\theta))} \frac{2}{2} - \frac{1}{H_0^{\prime(2)}(ka\sin(\theta))} \right]$$

$$(2.138)$$

The last term in (2.138) can be introduced to the summation by introducing the term ε_n (called the Neumann's constant [37]) when $\varepsilon_n = 1$ for n = 0 and $\varepsilon_n = 2$ for $n \neq 0$ as

$$G_{e2}^{\theta z} \sim \frac{e^{-jRk_0}}{k_0 R} \frac{j2e^{jk}\cos(\theta)z'}{(2\pi)^2 a} \left[\sum_{n=0}^{\infty} \frac{\varepsilon_n j^n \cos(n\overline{\phi})}{H_n'^{(2)}(ka\sin(\theta))} \right]$$
(2.139)

The process for obtaining $G_{e2}^{\phi\phi}$ in (2.133) is exactly the same as the one for $G_{e2}^{\theta z}$

$$G_{e2}^{\phi\phi} \sim \frac{e^{-jRk_0}}{k_0R} \frac{2k_0 e^{jk\cos(\theta)z'}}{(2\pi)^2 ka\sin(\theta)} \left[\sum_{n=0}^{\infty} \frac{\varepsilon_n j^n \cos(n\overline{\phi})}{H_n^{(2)}(ka\sin(\theta))} \right]$$
(2.140)

At this point, an asymptotic approximation for the electric dyadic Green's function is found when the observation point is far way from the origin. However, this approximation works for circular cylinders with an electrically small diameter. For a large radius of curvature, this approximation converges poorly. As it was mentioned in Section 2.2, to obtain a good convergence, the order of the Hankel function has to be bigger than $k_{\rho}\rho$ $(n >> 2k_{\rho}\rho)$. As in Section 2.2, Watson transform has to be derived for this specific case, and is done as follows

$$2j\sum_{-\infty}^{\infty} f(n)e^{-jn\pi} = \int_{c_1+c_2} \frac{f(v)}{\sin(v\pi)} dv$$

$$2j\sum_{-\infty}^{\infty} f(n)e^{jn\overline{\phi}}e^{-jn\pi} = \int_{c_1+c_2} \frac{f(v)e^{jv\overline{\phi}}}{\sin(v\pi)} dv$$

$$2j\sum_{-\infty}^{\infty} f(n)e^{jn\overline{\phi}}e^{-jn\pi}e^{jn\frac{3\pi}{2}} = \int_{c_1+c_2} \frac{f(v)e^{jv\overline{\phi}}e^{jv\frac{3\pi}{2}}}{\sin(v\pi)} dv$$

$$\sum_{-\infty}^{\infty} f(n)e^{jn(\overline{\phi}+\frac{\pi}{2})} = \frac{1}{2j}\int_{c_1+c_2} \frac{f(v)e^{jv(\overline{\phi}+\frac{3\pi}{2})}}{\sin(v\pi)} dv \qquad (2.141)$$

Simplifying (2.133) and replacing $ka\sin(\theta)$ by γ , we obtain

$$G_{e2}^{\theta z} \sim \frac{e^{-jRk_0}}{Rk_0} \frac{jk\sin(\theta)e^{jk\cos(\theta)z'}}{2\pi^2\gamma} \sum_{n=-\infty}^{\infty} \frac{e^{jn(\overline{\phi} + \frac{\pi}{2})}}{H_n^{\prime(2)}(\gamma)}$$
(2.142)

Apply Watson transform in (2.142), with $f(v) = \frac{1}{H_v'^{(2)}(\gamma)}$

$$G_{e2}^{\theta z} \sim \frac{e^{-jRk_0}}{Rk_0} \frac{jk \sin(\theta)e^{jk} \cos(\theta)z'}{2\pi^2 \gamma} \left(\frac{1}{2j} \int_{c_1+c_2} \frac{e^{jv(\overline{\phi} + \frac{3\pi}{2})}}{\sin(v\pi)H_v'^{(2)}(\gamma)} \right)$$
(2.143)

Expanding the integrals, changing ν to $-\nu$ in the third integral of (2.143), it may be rewritten as

$$G_{e2}^{\theta z} \sim \frac{k \sin(\theta) e^{jk} \cos(\theta) z'}{4\pi^2 \gamma} \int_{c_1 + c_2} \frac{e^{jv(\overline{\phi} + \frac{3\pi}{2})}}{\sin(v\pi) H_v^{\prime(2)}(\gamma)} dv$$

$$\sim \frac{k \sin(\theta) e^{jk} \cos(\theta) z'}{4\pi^2 \gamma} \int_{-\infty - j\sigma}^{\infty - j\sigma} \frac{e^{jv(\overline{\phi} + \frac{3\pi}{2})}}{\sin(v\pi) H_v^{\prime(2)}(\gamma)} dv + \int_{\infty + j\sigma}^{-\infty + j\sigma} \frac{e^{jv(\overline{\phi} + \frac{3\pi}{2})}}{\sin(v\pi) H_v^{\prime(2)}(\gamma)} dv$$

$$\sim \frac{k \sin(\theta) e^{jk} \cos(\theta) z'}{4\pi^2 \gamma} \int_{-\infty - j\sigma}^{\infty - j\sigma} \frac{e^{jv(\overline{\phi} + \frac{3\pi}{2})}}{\sin(v\pi) H_v^{\prime(2)}(\gamma)} dv + \int_{\infty - j\sigma}^{-\infty - j\sigma} \frac{e^{-jv(\overline{\phi} + \frac{3\pi}{2})}}{\sin(-v\pi) H_{-v}^{\prime(2)}(\gamma)} dv$$

$$(2.144)$$

Replacing $H'^{(2)}_{-v}(\gamma) = e^{-jv\pi}H'^{(2)}_{v}$, and $\sin(-v\pi)$ with $-\sin(v\pi)$ and inverting the integration limits in (2.144) we have

$$G_{e2}^{\theta z} \sim \frac{k \sin(\theta) e^{jk \cos(\theta) z'}}{4\pi^{2} \gamma}$$

$$\begin{bmatrix} \int_{-\infty - j\sigma}^{\infty - j\sigma} \frac{e^{jv(\overline{\phi} + \frac{3\pi}{2})}}{\sin(v\pi) H'_{v}^{\prime(2)}(\gamma)} dv - \int_{-\infty - j\sigma}^{\infty - j\sigma} \frac{e^{-jv(\overline{\phi} + \frac{3\pi}{2})}}{-\sin(v\pi) e^{-jv\pi} H'_{v}^{\prime(2)}(\gamma)} dv \end{bmatrix}$$

$$\sim \frac{k \sin(\theta) e^{jk \cos(\theta) z'}}{4\pi^{2} \gamma} \int_{-\infty - j\sigma}^{\infty - j\sigma} \frac{e^{jv(\overline{\phi} + \frac{3\pi}{2})}}{\sin(v\pi) H'_{v}^{\prime(2)}(\gamma)} dv + \int_{-\infty - j\sigma}^{\infty - j\sigma} \frac{e^{-jv(\overline{\phi} + \frac{\pi}{2})}}{\sin(v\pi) H'_{v}^{\prime(2)}(\gamma)} dv$$

$$\sim \frac{k \sin(\theta) e^{jk \cos(\theta) z'}}{4\pi^{2} \gamma} \int_{-\infty - j\sigma}^{\infty - j\sigma} \frac{e^{jv(\overline{\phi} + \frac{3\pi}{2})} + e^{-jv(\overline{\phi} + \frac{\pi}{2})}}{\sin(v\pi) H'_{v}^{\prime(2)}(\gamma)} dv$$

$$\sim \frac{k \sin(\theta) e^{jk \cos(\theta) z'}}{4\pi^{2} \gamma} \int_{-\infty - j\sigma}^{\infty - j\sigma} \frac{e^{jv(\overline{\phi} + \frac{3\pi}{2})} + e^{-jv(\overline{\phi} + \frac{\pi}{2})}}{\sin(v\pi) H'_{v}^{\prime(2)}(\gamma)} dv$$

$$(2.145)$$

Following the same procedure as in Section 2.2, using the Poisson sum, we need to factorize the term $e^{jv\pi}$ in (2.145). Thus results in

$$G_{e2}^{\theta z} \sim \frac{k \sin(\theta) e^{jk \cos(\theta) z'}}{4\pi^2 \gamma} \int_{-\infty - j\sigma}^{\infty - j\sigma} \frac{e^{jv\pi}}{\sin(v\pi)} \frac{\left(e^{jv(\overline{\phi} + \frac{\pi}{2})} + e^{-jv(\overline{\phi} + \frac{3\pi}{2})}\right)}{H_v'^{(2)}(\gamma)} (2\pi 146)$$

For path C_1 when $\sigma < 0$, the Poisson sum that it is used is

$$\frac{e^{jv\pi}}{\sin(v\pi)} = 2j\sum_{l=0}^{\infty} e^{-j2lv\pi}$$
(2.147)

Replacing (2.147) in (2.146), and just retaining the lowest term of l, (2.146) is simplified as

$$G_{e2}^{\theta z} \sim \frac{k \sin(\theta) e^{jk \cos(\theta) z'}}{4\pi^2 \gamma} \int_{-\infty - j\sigma}^{\infty - j\sigma} 2j \sum_{l=0}^{\infty} e^{-j2lv\pi} \frac{\left(e^{jv(\overline{\phi} + \frac{\pi}{2})} + e^{-jv(\overline{\phi} + \frac{3\pi}{2})}\right)}{H_v'^{(2)}(\gamma)} dv$$

$$\sim \frac{jk \sin(\theta) e^{jk \cos(\theta) z'}}{2\pi^2 \gamma} \sum_{l=0}^{\infty} \int_{-\infty - j\sigma}^{\infty - j\sigma} \frac{\left(e^{-jv(2l\pi - \overline{\phi} - \frac{\pi}{2})} + e^{-jv(2l\pi + \overline{\phi} + \frac{3\pi}{2})}\right)}{H_v'^{(2)}(\gamma)} dv$$

$$(2.148)$$

$$G_{e2}^{\theta z} \sim \frac{jk\sin(\theta)e^{jk\cos(\theta)z'}}{2\pi^2\gamma} \int_{-\infty-j\sigma}^{\infty-j\sigma} \frac{\left(e^{-jv(-\overline{\phi}-\frac{\pi}{2})} + e^{-jv(\overline{\phi}+\frac{3\pi}{2})}\right)}{H_v^{\prime(2)}(\gamma)} dv \qquad (2.149)$$

With $\Phi_1 = -\overline{\phi} - \frac{\pi}{2}$ and $\Phi_2 = \overline{\phi} + \frac{3\pi}{2}$ and substituting $H_v^{\prime(2)}(\gamma)$ by (2.94) [8], we have

$$G_{e2}^{\theta z} \sim \frac{jk\sin(\theta)e^{jk\cos(\theta)z'}}{2\pi^{2}\gamma} \int_{-\infty-j\sigma}^{\infty-j\sigma} \frac{\left(e^{-jv\Phi_{1}} + e^{-jv\Phi_{2}}\right)}{-j\frac{w_{2}'(\tau)}{m^{2}\sqrt{\pi}}} dv$$

$$\sim \frac{-k\sin(\theta)e^{jk\cos(\theta)z'}}{2\pi\gamma} \int_{-\infty-j\sigma}^{\infty-j\sigma} \frac{m^{2}\left(e^{-jv\Phi_{1}} + e^{-jv\Phi_{2}}\right)}{\sqrt{\pi}w_{2}'(\tau)} dv \quad (2.150)$$

With $\tau = \frac{1}{m}(v - \gamma)$ and $m = (\frac{\gamma}{2})^{\frac{1}{3}}$ [33], we can find that $dv = md\tau$, replacing it in (2.150) yields

$$G_{e2}^{\theta z} \sim \frac{-k\sin(\theta)e^{jk}\cos(\theta)z'}{2\pi\gamma} \int_{\Gamma_{1}} \frac{m^{3}\left(e^{-jv\Phi_{1}} + e^{-jv\Phi_{2}}\right)}{\sqrt{\pi}w_{2}'(\tau)} d\tau$$

$$\sim \frac{-k\sin(\theta)e^{jk}\cos(\theta)z'}{4\pi} \int_{\Gamma_{1}} \frac{\left(e^{-jv\Phi_{1}} + e^{-jv\Phi_{2}}\right)}{\sqrt{\pi}w_{2}'(\tau)} d\tau \qquad (2.151)$$

This can be manipulated further to yield

$$G_{e2}^{\theta z} \sim \frac{-k\sin(\theta)e^{jk}\cos(\theta)z'}{4\pi} \int_{\Gamma_{1}} \frac{\left(e^{-j(m\tau+\gamma)\Phi_{1}} + e^{-j(m\tau+\gamma)\Phi_{2}}\right)}{\sqrt{\pi}w_{2}'(\tau)} d\tau$$

$$\sim \frac{-k\sin(\theta)e^{jk}\cos(\theta)z'}{4\pi} \left[e^{-j\gamma\Phi_{1}} \frac{1}{\sqrt{\pi}} \int_{\Gamma_{1}} \frac{e^{-jm\tau\Phi_{1}}}{w_{2}'(\tau)} d\tau + e^{-j\gamma\Phi_{2}} \frac{1}{\sqrt{\pi}} \int_{\Gamma_{1}} \frac{e^{-jm\tau\Phi_{2}}}{w_{2}'(\tau)} d\tau\right]$$

$$(2.152)$$

In (2.98), it is defined that $\beta = m\phi$, substituting $m\Phi_{1,2}$ by $\beta_{1,2}$, we have

$$G_{e2}^{\theta z} \sim \frac{-k\sin(\theta)e^{jk\cos(\theta)z'}}{4\pi} \left[e^{-j\gamma\Phi_1} \frac{1}{\sqrt{\pi}} \int_{\Gamma_1} \frac{e^{-j\beta_1\tau}}{w_2'(\tau)} d\tau + e^{-j\gamma\Phi_2} \frac{1}{\sqrt{\pi}} \int_{\Gamma_1} \frac{e^{-j\beta_2\tau}}{w_2'(\tau)} d\tau \right]$$

$$(2.153)$$

We can express (2.153) in terms of the complex conjugate far-zone hard Fock function $g^{(u)}(\beta)^*$ that is given by

$$g^{(u)}(\beta)^* = \frac{j^u}{\sqrt{\pi}} \int_{\Gamma_1} \frac{\tau^u e^{-j\beta\tau}}{w_1'(\tau)^*} d\tau$$
 (2.154)

Where "*" denotes complex conjugation, noting that $w_1'(\tau)^* = w_2'(\tau)$, and u is the function order, which for our case is zero. Equation (2.153) can be expressed as

$$G_{e2}^{\theta z} \sim \frac{-k \sin(\theta) e^{jk \cos(\theta) z'}}{4\pi} \left[e^{-j\gamma \Phi_1} g^{(0)} (m\Phi_1)^* + e^{-j\gamma \Phi_2} g^{(0)} (m\Phi_2)^* \right]$$

$$\sim \frac{-k \sin(\theta) e^{jk \cos(\theta) z'}}{4\pi} \sum_{n=1}^{2} e^{-j\gamma \Phi_n} g^{(0)} (m\Phi_n)^* \qquad (2.155)$$

Now, we will follow the same procedure with the $G_{e2}^{\phi\phi}$ component. We need to simplify (2.134) and replace $ka\sin(\theta)$ by γ to yield

$$G_{e2}^{\phi\phi} \sim \frac{e^{-jRk_0}}{Rk_0} \frac{k_0 e^{jk\cos(\theta)z'}}{2\pi^2 \gamma} \sum_{n=-\infty}^{\infty} \frac{e^{jn(\overline{\phi} + \frac{\pi}{2})}}{H_n^{(2)}(\gamma)}$$
 (2.156)

Applying the Watson transform results in

$$G_{e2}^{\phi\phi} \sim \frac{e^{-jRk_0}}{Rk_0} \frac{k_0 e^{jk\cos(\theta)z'}}{2\pi^2 \gamma} \left(\frac{1}{2j} \int_{c_1 + c_2} \frac{e^{jv(\overline{\phi} + \frac{3\pi}{2})}}{\sin(v\pi)H_v^{(2)}(\gamma)} \right)$$
(2.157)

Expanding the integrals, changing ν to $-\nu$, (2.157) may be rewritten as:

$$G_{e2}^{\phi\phi} \sim \frac{ke^{jk\cos(\theta)z'}}{j4\pi^{2}\gamma} \int_{c_{1}+c_{2}} \frac{e^{jv(\overline{\phi}+\frac{3\pi}{2})}}{\sin(v\pi)H_{v}^{(2)}(\gamma)} dv$$

$$\sim \frac{ke^{jk\cos(\theta)z'}}{j4\pi^{2}\gamma} \int_{-\infty-j\sigma}^{\infty-j\sigma} \frac{e^{jv(\overline{\phi}+\frac{3\pi}{2})}}{\sin(v\pi)H_{v}^{(2)}(\gamma)} dv + \int_{\infty+j\sigma}^{-\infty+j\sigma} \frac{e^{jv(\overline{\phi}+\frac{3\pi}{2})}}{\sin(v\pi)H_{v}^{(2)}(\gamma)} dv$$

$$\sim \frac{ke^{jk\cos(\theta)z'}}{j4\pi^{2}\gamma} \int_{-\infty-j\sigma}^{\infty-j\sigma} \frac{e^{jv(\overline{\phi}+\frac{3\pi}{2})}}{\sin(v\pi)H_{v}^{(2)}(\gamma)} dv + \int_{\infty-j\sigma}^{-\infty-j\sigma} \frac{e^{-jv(\overline{\phi}+\frac{3\pi}{2})}}{\sin(-v\pi)H_{-v}^{(2)}(\gamma)} dv$$

$$(2.158)$$

We replace $H_{-v}^{(2)}(\gamma) = e^{-jv\pi}H_v^{(2)}$ and $\sin(-v\pi)$ with $-\sin(v\pi)$, and invert the integration limits in (2.158) to yield

$$G_{e2}^{\phi\phi} \sim \frac{ke^{jk\cos(\theta)z'}}{j4\pi^{2}\gamma} \int_{-\infty-j\sigma}^{\infty-j\sigma} \frac{e^{jv(\overline{\phi}+\frac{3\pi}{2})}}{\sin(v\pi)H_{v}^{(2)}(\gamma)} dv - \int_{-\infty-j\sigma}^{\infty-j\sigma} \frac{e^{-jv(\overline{\phi}+\frac{3\pi}{2})}}{-\sin(v\pi)e^{-jv\pi}H_{v}^{(2)}(\gamma)} dv$$

$$\sim \frac{ke^{jk\cos(\theta)z'}}{j4\pi^{2}\gamma} \int_{-\infty-j\sigma}^{\infty-j\sigma} \frac{e^{jv(\overline{\phi}+\frac{3\pi}{2})}}{\sin(v\pi)H_{v}^{(2)}(\gamma)} dv + \int_{-\infty-j\sigma}^{\infty-j\sigma} \frac{e^{-jv(\overline{\phi}+\frac{\pi}{2})}}{\sin(v\pi)H_{v}^{(2)}(\gamma)} dv$$

$$\sim \frac{ke^{jk\cos(\theta)z'}}{j4\pi^{2}\gamma} \int_{-\infty-j\sigma}^{\infty-j\sigma} \frac{e^{jv(\overline{\phi}+\frac{3\pi}{2})} + e^{-jv(\overline{\phi}+\frac{\pi}{2})}}{\sin(v\pi)H_{v}^{(2)}(\gamma)} dv \qquad (2.159)$$

Following the same procedure as in Section 2.2, applying the Poisson sum, we need to factorize the term $e^{jv\pi}$ in (2.159) to get

$$G_{e2}^{\phi\phi} \sim \frac{ke^{jk\cos(\theta)z'}}{j4\pi^2\gamma} \int_{-\infty-j\sigma}^{\infty-j\sigma} \frac{e^{jv\pi}}{\sin(v\pi)} \frac{\left(e^{jv(\overline{\phi}+\frac{\pi}{2})} + e^{-jv(\overline{\phi}+\frac{3\pi}{2})}\right)}{H_v^{(2)}(\gamma)} dv (2.160)$$

Replacing (2.147) in (2.160), and just leaving the lowest term of l (2.160) is simplified as

$$G_{e2}^{\phi\phi} \sim \frac{ke^{jk\cos(\theta)z'}}{j4\pi^{2}\gamma} \int_{-\infty-j\sigma}^{\infty-j\sigma} 2j \sum_{l=0}^{\infty} e^{-j2lv\pi} \frac{\left(e^{jv(\overline{\phi}+\frac{\pi}{2})} + e^{-jv(\overline{\phi}+\frac{3\pi}{2})}\right)}{H_{v}^{(2)}(\gamma)} dv$$

$$\sim \frac{ke^{jk\cos(\theta)z'}}{2\pi^{2}\gamma} \sum_{l=0}^{\infty} \int_{-\infty-j\sigma}^{\infty-j\sigma} \frac{\left(e^{-jv(2l\pi-\overline{\phi}-\frac{\pi}{2})} + e^{-jv(2l\pi+\overline{\phi}+\frac{3\pi}{2})}\right)}{H_{v}^{(2)}(\gamma)} dv$$

$$(2.161)$$

$$G_{e2}^{\phi\phi} \sim \frac{ke^{jk}\cos(\theta)z'}{2\pi^2\gamma} \int_{-\infty-j\sigma}^{\infty-j\sigma} \frac{\left(e^{-jv(-\overline{\phi}-\frac{\pi}{2})} + e^{-jv(\overline{\phi}+\frac{3\pi}{2})}\right)}{H_v^{(2)}(\gamma)} dv \tag{2.162}$$

With $\Phi_1 = -\overline{\phi} - \frac{\pi}{2}$ and $\Phi_2 = \overline{\phi} + \frac{3\pi}{2}$ and substituting $H_v^{(2)}(\gamma)$ by (2.93)[8], we have:

$$G_{e2}^{\phi\phi} \sim \frac{ke^{jk\cos(\theta)z'}}{2\pi^{2}\gamma} \int_{-\infty-j\sigma}^{\infty-j\sigma} \frac{\left(e^{-jv\Phi_{1}} + e^{-jv\Phi_{2}}\right)}{j\frac{w_{2}(\tau)}{m\sqrt{\pi}}} dv$$

$$\sim \frac{ke^{jk\cos(\theta)z'}}{j2\pi\gamma} \int_{-\infty-j\sigma}^{\infty-j\sigma} \frac{m\left(e^{-jv\Phi_{1}} + e^{-jv\Phi_{2}}\right)}{\sqrt{\pi}w_{2}(\tau)} dv \qquad (2.163)$$

With $\tau = \frac{1}{m}(v - \gamma)$ and $m = (\frac{\gamma}{2})^{\frac{1}{3}}$ [33] we find that $dv = md\tau$, and replace it in (2.163) to give

$$G_{e2}^{\phi\phi} \sim \frac{ke^{jk\cos(\theta)z'}}{j2\pi\gamma} \int_{\Gamma_1} \frac{m^2 \left(e^{-jv\Phi_1} + e^{-jv\Phi_2}\right)}{\sqrt{\pi}w_2(\tau)} d\tau$$

$$\sim \frac{m^2ke^{jk\cos(\theta)z'}}{j2\pi\gamma} \int_{\Gamma_1} \frac{\left(e^{-jv\Phi_1} + e^{-jv\Phi_2}\right)}{\sqrt{\pi}w_2(\tau)} d\tau \qquad (2.164)$$

This equation can then be simplified as

$$G_{e2}^{\phi\phi} \sim \frac{m^2 k e^{jk} \cos(\theta) z'}{j2\pi\gamma} \int_{\Gamma_1} \frac{\left(e^{-j(m\tau+\gamma)\Phi_1} + e^{-j(m\tau+\gamma)\Phi_2}\right)}{\sqrt{\pi} w_2(\tau)} d\tau$$

$$\sim \frac{m^2 k e^{jk} \cos(\theta) z'}{j2\pi\gamma} \left[e^{-j\gamma\Phi_1} \frac{1}{\sqrt{\pi}} \int_{\Gamma_1} \frac{e^{-jm\tau\Phi_1}}{w_2(\tau)} d\tau + e^{-j\gamma\Phi_2} \frac{1}{\sqrt{\pi}} \int_{\Gamma_1} \frac{e^{-jm\tau\Phi_2}}{w_2(\tau)} d\tau\right]$$

$$(2.165)$$

In (2.98), we defined that $\beta = m\phi$, substituting $m\Phi_{1,2}$ by $\beta_{1,2}$, we have

$$G_{e2}^{\phi\phi} \sim \frac{m^2 k e^{jk\cos(\theta)z'}}{j2\pi\gamma} \left[e^{-j\gamma\Phi_1} \frac{1}{\sqrt{\pi}} \int\limits_{\Gamma_1} \frac{e^{-j\beta_1\tau}}{w_2(\tau)} d\tau + e^{-j\gamma\Phi_2} \frac{1}{\sqrt{\pi}} \int\limits_{\Gamma_1} \frac{e^{-j\beta_2\tau}}{w_2(\tau)} d\tau \right]$$

$$(2.166)$$

We can express (2.166) in terms of the complex conjugate far-zone soft Fock function $f^{(u)}(\beta)^*$ given by

$$f^{(u)}(\beta)^* = \frac{j^u}{\sqrt{\pi}} \int_{\Gamma_1} \frac{\tau^u e^{-j\beta\tau}}{w_1(\tau)^*} d\tau$$
 (2.167)

Having $w_1(\tau)^* = w_2(\tau)$ and u is the function order, which for our case is zero, (2.166) can be expressed as:

$$G_{e2}^{\phi\phi} \sim \frac{m^2 k e^{jk \cos(\theta)z'}}{j2\pi\gamma} \left[e^{-j\gamma\Phi_1} f^{(0)}(m\Phi_1)^* + e^{-j\gamma\Phi_2} f^{(0)}(m\Phi_2)^* \right]$$
$$\sim \frac{m^2 k e^{jk \cos(\theta)z'}}{j2\pi\gamma} \sum_{p=1}^2 e^{-j\gamma\Phi_p} f^{(0)}(m\Phi_p)^* \tag{2.168}$$

Next, Watson transform can be used to accelerate the computation of $G_{e2}^{\theta\phi}$. Replacing $ka\sin(\theta)$ by γ simplifies (2.132) as

$$G_{e2}^{\theta\phi} \sim \frac{e^{-jRk_0}}{Rk_0} \frac{jk\cos(\theta)e^{jk\cos(\theta)z'}}{2\pi^2\gamma^2} \sum_{n=-\infty}^{\infty} \frac{ne^{jn(\overline{\phi} + \frac{\pi}{2})}}{H_n'^{(2)}(\gamma)}$$
(2.169)

Applying, Watson transform but with $f(n) = \frac{n}{H_n'^{(2)}(\gamma)}$ (2.169) can be written as

$$G_{e2}^{\theta\phi} \sim \frac{e^{-jRk_0}}{Rk_0} \frac{jk\cos(\theta)e^{jk\cos(\theta)z'}}{2\pi^2\gamma^2} \left(\frac{1}{2j} \int_{c_1+c_2} \frac{ve^{jv(\overline{\phi} + \frac{3\pi}{2})}}{\sin(v\pi)H_v'^{(2)}(\gamma)} \right)$$
(2.170)

Expanding the integrals, changing ν to $-\nu$, (2.170) yields

$$G_{e2}^{\theta\phi} \sim \frac{e^{-jRk_0}}{Rk_0} \frac{k\cos(\theta)e^{jk}\cos(\theta)z'}{4\pi^2\gamma^2} \int_{c_1+c_2} \frac{ve^{jv(\overline{\phi}+\frac{3\pi}{2})}}{\sin(v\pi)H_v'^{(2)}(\gamma)} dv$$

$$\sim \frac{k\cos(\theta)e^{jk}\cos(\theta)z'}{4\pi^2\gamma^2} \int_{-\infty-j\sigma}^{\infty-j\sigma} \frac{ve^{jv(\overline{\phi}+\frac{3\pi}{2})}}{\sin(v\pi)H_v'^{(2)}(\gamma)} dv + \int_{\infty+j\sigma}^{-\infty+j\sigma} \frac{ve^{jv(\overline{\phi}+\frac{3\pi}{2})}}{\sin(v\pi)H_v'^{(2)}(\gamma)} dv$$

$$\sim \frac{k\cos(\theta)e^{jk}\cos(\theta)z'}{4\pi^2\gamma^2} \int_{-\infty-j\sigma}^{\infty-j\sigma} \frac{ve^{jv(\overline{\phi}+\frac{3\pi}{2})}}{\sin(v\pi)H_v'^{(2)}(\gamma)} dv + \int_{\infty-j\sigma}^{-\infty-j\sigma} \frac{-ve^{-jv(\overline{\phi}+\frac{3\pi}{2})}}{\sin(-v\pi)H_{-v}'^{(2)}(\gamma)} dv$$

$$(2.171)$$

We replace $H_{-v}^{\prime(2)}(\gamma) = e^{-jv\pi}H_v^{\prime(2)}$ and $\sin(-v\pi)$ with $-\sin(v\pi)$, and invert the integration limits in (2.171)

$$G_{e2}^{\theta\phi} \sim \frac{k\cos(\theta)e^{jk\cos(\theta)z'}}{4\pi^{2}\gamma^{2}}$$

$$\begin{bmatrix} \int_{-\infty-j\sigma}^{\infty-j\sigma} \frac{ve^{jv(\overline{\phi}+\frac{3\pi}{2})}}{\sin(v\pi)H'_{v}^{\prime(2)}(\gamma)} dv - \int_{-\infty-j\sigma}^{\infty-j\sigma} \frac{-ve^{-jv(\overline{\phi}+\frac{3\pi}{2})}}{-\sin(v\pi)e^{-jv\pi}H'_{v}^{\prime(2)}(\gamma)} dv \end{bmatrix}$$

$$\sim \frac{k\cos(\theta)e^{jk\cos(\theta)z'}}{4\pi^{2}\gamma^{2}} \int_{-\infty-j\sigma}^{\infty-j\sigma} \frac{ve^{jv(\overline{\phi}+\frac{3\pi}{2})}}{\sin(v\pi)H'_{v}^{\prime(2)}(\gamma)} dv - \int_{-\infty-j\sigma}^{\infty-j\sigma} \frac{ve^{-jv(\overline{\phi}+\frac{\pi}{2})}}{\sin(v\pi)H'_{v}^{\prime(2)}(\gamma)} dv$$

$$\sim \frac{k\cos(\theta)e^{jk\cos(\theta)z'}}{4\pi^{2}\gamma^{2}} \int_{-\infty-j\sigma}^{\infty-j\sigma} \frac{ve^{jv(\overline{\phi}+\frac{3\pi}{2})} - ve^{-jv(\overline{\phi}+\frac{\pi}{2})}}{\sin(v\pi)H'_{v}^{\prime(2)}(\gamma)} dv$$

$$\sim \frac{k\cos(\theta)e^{jk\cos(\theta)z'}}{4\pi^{2}\gamma^{2}} \int_{-\infty-j\sigma}^{\infty-j\sigma} \frac{ve^{jv(\overline{\phi}+\frac{3\pi}{2})} - ve^{-jv(\overline{\phi}+\frac{\pi}{2})}}{\sin(v\pi)H'_{v}^{\prime(2)}(\gamma)} dv$$

$$(2.172)$$

As in the two other components, we factorize the term $e^{jv\pi}$ to apply the Poisson sum and obtain

$$G_{e2}^{\theta\phi} \sim \frac{-k\cos(\theta)e^{jk}\cos(\theta)z'}{4\pi^2\gamma^2} \int_{-\infty-j\sigma}^{\infty-j\sigma} \frac{e^{jv\pi}}{\sin(v\pi)} \frac{v\left(e^{jv(\overline{\phi}+\frac{\pi}{2})} - e^{-jv(\overline{\phi}+\frac{3\pi}{2})}\right)}{H_v'^{(2)}(\gamma)} dv$$

$$(2.173)$$

Replacing (2.147) in (2.173), and just leaving lowest term of l, (2.173) is simplified as

$$G_{e2}^{\theta\phi} \sim \frac{-k\cos(\theta)e^{jk}\cos(\theta)z'}{4\pi^{2}\gamma^{2}} \int_{-\infty-j\sigma}^{\infty-j\sigma} 2j \sum_{l=0}^{\infty} e^{-j2lv\pi} \frac{v\left(e^{jv(\overline{\phi}+\frac{\pi}{2})} - e^{-jv(\overline{\phi}+\frac{3\pi}{2})}\right)}{H'^{(2)}_{v}(\gamma)} dv$$

$$\sim \frac{-jk\cos(\theta)e^{jk}\cos(\theta)z'}{2\pi^{2}\gamma^{2}} \sum_{l=0}^{\infty} \int_{-\infty-j\sigma}^{\infty-j\sigma} \frac{v\left(e^{-jv(2l\pi-\overline{\phi}-\frac{\pi}{2})} - e^{-jv(2l\pi+\overline{\phi}+\frac{3\pi}{2})}\right)}{H'^{(2)}_{v}(\gamma)} dv$$

$$(2.174)$$

$$G_{e2}^{\theta\phi} \sim \frac{-jk\cos(\theta)e^{jk}\cos(\theta)z'}{2\pi^2\gamma^2} \int_{-\infty-j\sigma}^{\infty-j\sigma} \frac{v\left(e^{-jv(-\overline{\phi}-\frac{\pi}{2})} - e^{-jv(\overline{\phi}+\frac{3\pi}{2})}\right)}{H_v'^{(2)}(\gamma)} dv \quad (2.175)$$

With $\Phi_1 = -\overline{\phi} - \frac{\pi}{2}$ and $\Phi_2 = \overline{\phi} + \frac{3\pi}{2}$ and substituting $H_v'^{(2)}(\gamma)$ by (2.94)[8], we have

$$G_{e2}^{\theta\phi} \sim \frac{jk\cos(\theta)e^{jk\cos(\theta)z'}}{2\pi^{2}\gamma^{2}} \int_{-\infty-j\sigma}^{\infty-j\sigma} \frac{v\left(e^{-jv\Phi_{2}} - e^{-jv\Phi_{1}}\right)}{j\frac{w_{2}'(\tau)}{m^{2}\sqrt{\pi}}} dv$$

$$\sim \frac{k\cos(\theta)e^{jk\cos(\theta)z'}}{2\pi\gamma^{2}} \int_{-\infty-j\sigma}^{\infty-j\sigma} \frac{m^{2}v\left(e^{-jv\Phi_{2}} - e^{-jv\Phi_{1}}\right)}{\sqrt{\pi}w_{2}'(\tau)} dv \quad (2.176)$$

Using $v = m\tau + \gamma$ and $dv = md\tau$, (2.176) simplifies to

$$G_{e2}^{\theta\phi} \sim \frac{k\cos(\theta)e^{jk\cos(\theta)z'}}{2\pi\gamma^2} \int_{\Gamma_1} \frac{m^3(m\tau+\gamma)\left(e^{-j\Phi_2(m\tau+\gamma)} + e^{-j\Phi_1(m\tau+\gamma)}\right)}{\sqrt{\pi}w_2'(\tau)} d\tau$$
(2.177)

Expanding (2.177), we have

$$G_{e2}^{\theta\phi} \sim \frac{k\cos(\theta)e^{jk}\cos(\theta)z'}{2\pi\gamma^{2}}$$

$$\left\{m^{4}\left[e^{-j\gamma\Phi_{2}}\frac{1}{\sqrt{\pi}}\int_{\Gamma_{1}}\frac{\tau e^{-jm\tau\Phi_{2}}}{w_{2}'(\tau)}d\tau - e^{-j\gamma\Phi_{1}}\frac{1}{\sqrt{\pi}}\int_{\Gamma_{1}}\frac{\tau e^{-jm\tau\Phi_{1}}}{w_{2}'(\tau)}d\tau\right]\right\}$$

$$+ m^{3}\gamma\left[e^{-j\gamma\Phi_{2}}\frac{1}{\sqrt{\pi}}\int_{\Gamma_{1}}\frac{e^{-jm\tau\Phi_{2}}}{w_{2}'(\tau)}d\tau - e^{-j\gamma\Phi_{1}}\frac{1}{\sqrt{\pi}}\int_{\Gamma_{1}}\frac{e^{-jm\tau\Phi_{1}}}{w_{2}'(\tau)}d\tau\right]\right\}$$

$$(2.178)$$

Equation (2.178) can be expressed in terms of the first and second order, u = 1 and u = 2, complex conjugate far-zone soft Fock function $g^{(u)}(\beta)^*$. Replacing m^3 by $\frac{\gamma}{2}$, results in

$$G_{e2}^{\theta\phi} \sim \frac{k\cos(\theta)e^{jk\cos(\theta)z'}}{2\pi\gamma^2} \left\{ \frac{m\gamma}{2} \left[e^{-j\gamma\Phi_2} jg^{(1)} (m\Phi_2)^* - e^{-j\gamma\Phi_1} jg^{(1)} (m\Phi_1)^* \right] + \frac{\gamma}{2} \left[e^{-j\gamma\Phi_2} g^{(0)} (m\Phi_2)^* - e^{-j\gamma\Phi_1} g^{(0)} (m\Phi_1)^* \right] \right\}$$

$$(2.179)$$

Simplifying (2.179), we have

$$G_{e2}^{\theta\phi} \sim \frac{k\cos(\theta)e^{jk}\cos(\theta)z'}{4\pi} \sum_{p=1}^{2} (-1)^{p} e^{-j\gamma\Phi_{p}} \left[g^{(0)}(m\Phi_{p})^{*} + \frac{jm}{\gamma}g^{(1)}(m\Phi_{p})^{*} \right]$$
(2.180)

This is the remaining component of our asymptotic solution. The expressions for $G_{e2}^{\theta z}$, $G_{e2}^{\phi \phi}$ and $G_{e2}^{\theta \phi}$ work very well at azimuth. Although, as the elevation angle θ changes from $\frac{\pi}{2}$ to 0 the accuracy and convergence decreases significatively. An alternative solution for this problem is proposed in the next chapter.

CHAPTER 3

MODIFIED MODAL SOLUTION FOR THE DYADIC GREEN'S FUNCTION

In this Chapter, the analytic modal solution, and the steepest descent solution are studied and discussed in detail for a magnetic source on a PEC circular cylinder for observation points far away from the source point $(\vec{r} - \vec{r}') \gg 10\lambda$. The exact dyadic Green's function of the second kind, $\overline{G}_{e2}^{(2)}$, for the infinite PEC circular cylinder will be the starting point of the analysis. The $\hat{\phi}\hat{\phi}'$ component of $\overline{G}_{e2}^{(2)}$ would be the focus of this work, because the axial singularities that are presented when using the steepest descent method becoming indeterminate when evaluated at the vertical axis. In Section 3.1, an efficient way of implementing the modal solution is obtained using the integration around the branch cuts. These will be related to using an steepest descent path approximation to evaluate this integral. The convergence of the exact and the modified modal solution will be studied in this Chapter. Plots of the relative error between the solutions will be also shown.

3.1 Exact Modal and Asymptotic Solutions

The dyadic Green's function of the second kind for a infinite PEC circular cylinder of radius a, was obtained for a magnetic source was obtained as

$$\overline{G}_{e2}^{(2)}(\rho,\phi,z|a,\phi',z') = \frac{1}{(2\pi)^2} \sum_{n=-\infty}^{\infty} e^{jn\overline{\phi}} \int_{-\infty}^{\infty} dk_z e^{-jk_z\overline{z}} \\
\left\{ \left[\frac{-jnH_n^{(2)}(k_{\rho}\rho)}{k_{\rho}ak_{\rho}\rho H_n^{(2)}(k_{\rho}a)} + \frac{jn}{(k_{\rho}a)^2} \left(\frac{k_z}{k_0}\right)^2 \frac{H_n^{\prime(2)}(k_{\rho}\rho)}{H_n^{\prime(2)}(k_{\rho}a)} \right] \hat{\rho}\hat{\phi}' - j \left[\frac{k_z k_{\rho} H_n^{\prime(2)}(k_{\rho}\rho)}{k_{\rho}ak_0^2 H_n^{\prime(2)}(k_{\rho}a)} \right] \hat{\rho}\hat{z}' \\
+ \left[\frac{H_n^{\prime(2)}(k_{\rho}\rho)}{k_{\rho}aH_n^{(2)}(k_{\rho}a)} - \left(\frac{nk_z}{k_0k_{\rho}a}\right)^2 \frac{H_n^{(2)}(k_{\rho}\rho)}{(k_{\rho}\rho)H_n^{\prime(2)}(k_{\rho}a)} \right] \hat{\phi}\hat{\phi}' + \left[\frac{nk_z k_{\rho} H_n^{(2)}(k_{\rho}\rho)}{k_{\rho}a(k_{\rho}\rho)k_0^2 H_n^{\prime(2)}(k_{\rho}a)} \right] \hat{\phi}\hat{z}' \\
+ \left[\frac{nk_z k_{\rho} H_n^{(2)}(k_{\rho}\rho)}{(k_{\rho}a)^2 k_0^2 H_n^{\prime(2)}(k_{\rho}a)} \right] \hat{z}\hat{\phi}' - \frac{1}{k_{\rho}a} \left[\left(\frac{k_{\rho}}{k_0}\right)^2 \frac{H_n^{(2)}(k_{\rho}\rho)}{H_n^{\prime(2)}(k_{\rho}a)} \right] \hat{z}\hat{z}' \right\} \tag{3.1}$$

As stated earlier, this exact modal solution is very difficult to evaluate when the radius of the cylinder is electrically large $(ka \gg 1)$ and when the observation point is far away from the source point. The $\hat{\phi}\hat{\phi}'$ component of the Green's function is

$$G_{\phi\phi}(\rho,\phi,z|a,\phi',z') = \frac{1}{(2\pi)^2} \sum_{n=-\infty}^{\infty} e^{jn\overline{\phi}} \int_{-\infty}^{\infty} dk_z e^{-jk_z\overline{z}} f(k_z,k_\rho)$$
(3.2)

where $f(k_z, k_\rho)$ is written as

$$f(k_z, k_\rho) = \frac{H_n^{\prime(2)}(k_\rho \rho)}{k_\rho a H_n^{(2)}(k_\rho a)} - \left(\frac{nk_z}{k_0 k_\rho a}\right)^2 \frac{H_n^{(2)}(k_\rho \rho)}{(k_\rho \rho) H_n^{\prime(2)}(k_\rho a)} \hat{\phi} \hat{\phi}^{\prime}$$
(3.3)

As shown if Figure 3.1, the integral on the real axis of the $\hat{\phi}\hat{\phi}'$ component is very difficult to evaluate, because as the integral being evaluated the complex argument $(jk_z\bar{z})$ of the exponential part become very oscillatory. As shown in Chapter 2, the

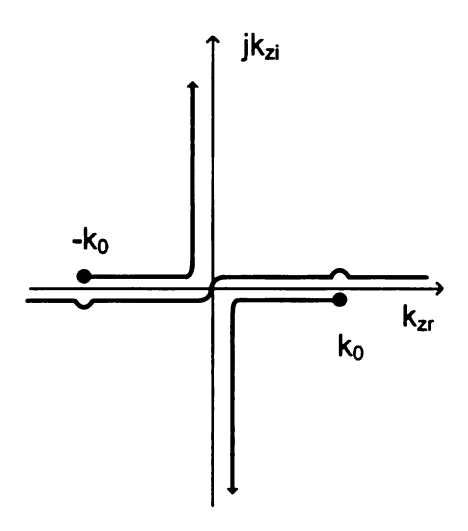


Figure 3.1. Complex k_z plane

steepest descent method could be implemented, but it was shown, this method has convergence problems near to the paraxial zone due to the branch point singularities in k_z . Instead of fixing the steepest descent problem, this solution will try to deform the contour of integration. The first problem is to close the correct contour of integration. The radiation condition in the \hat{z} and the $\hat{\rho}$ direction must be satisfied. Expressing k_z as a complex number, $k_z = k_{zr} + jk_{zi}$, with k_{zr} as the real part and k_{zi} the imaginary part, the plane wave with propagation constant k_z in the \hat{z} direction can be expressed as

$$e^{-jk_z\bar{z}} = e^{-j(k_{zr}+jk_{zi})\bar{z}}$$

= $e^{-jk_{zr}(z-z')}e^{k_{zi}(z-z')}$ (3.4)

As seen in Figure 3.2, if (z-z')>0 the contour of integration must be closed in the lower half plane, represented by a dashed line. In this way, k_{zi} will take only negative values and attenuation of $e^k_{zi}(z-z')$ will be guaranteed. For (z-z')<0 the upper half plane is chosen. The two branch points of the integrand $(k_{\rho}=\pm\sqrt{k_0^2-k_z^2})$ at

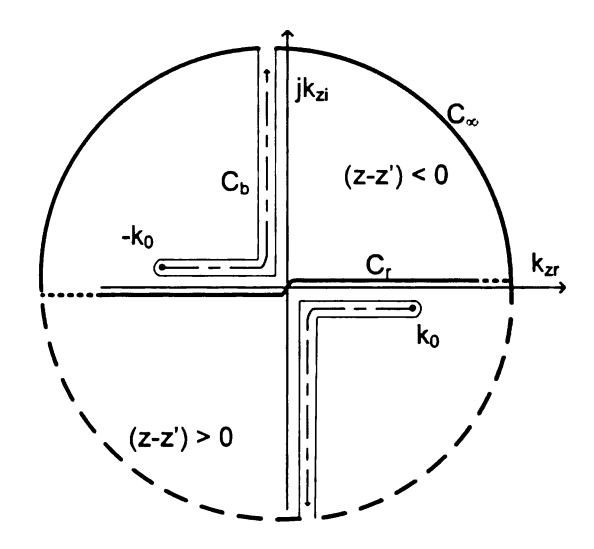


Figure 3.2. Contour of integration dictated by the radiation condition

 $k_z = \pm k_0$, indicated us the two possible Riemann surfaces k_z could be at, during the contour of integration. Therefore, the contour of integration must be chosen in such a manner that the inverse transform of (3.2) exists. According to Cauchy theorem, closing the contour of integration as in Figure 3.2, the original integration in the k_z plane could be changed by two integrals, one around the branch cut, and the other one closing the contour at infinity as

$$\int_{-\infty}^{\infty} e^{-jk_z\overline{z}} f(k_z, k_\rho) dk_z = -\int_{C_\infty} e^{-jk_z\overline{z}} f(k_z, k_\rho) dk_z - \int_{C_b} e^{-jk_z\overline{z}} f(jk_z, k_\rho) dk_z$$
(3.5)

As it is shown in Figure 3.3, we have different options for setting the branch cut of $k_{\rho} = \pm \sqrt{k_0^2 - k_z^2}$; however, the proper Riemman sheet is the one that leads to satisfaction of the radiation condition for large values of ρ for each part of the contour of integration. Also, the correct topology of the branch cut chosen guarantees the contribution of $\int_{C_{\infty}}$ goes to zero [34]. In order to chose the appropriated Riemman

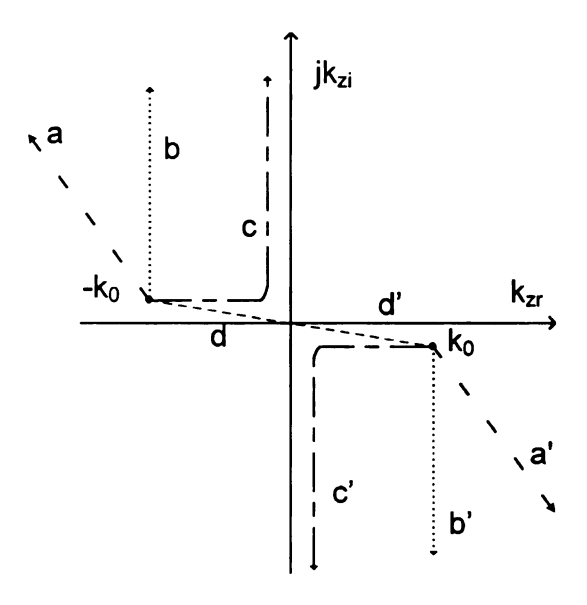


Figure 3.3. Definition of the Branch Cut

sheet, the $k_{
ho}$ component can be expressed in polar coordinates

$$k_{\rho} = \pm \sqrt{k_{0}^{2} - k_{z}^{2}}$$

$$= \pm j \sqrt{k_{z} - k_{0}} \sqrt{k_{z} + k_{0}}$$

$$= \pm j \sqrt{r + r^{-}} e^{j \frac{(\varphi^{+} + \varphi^{-})}{2}}$$

$$= \pm \sqrt{r + r^{-}} e^{j \left[\frac{(\varphi^{+} + \varphi^{-})}{2} + \frac{\pi}{2}\right]}$$
(3.6)

Looking at Figure 3.4, it seem that r^+ and r^- represent the magnitude contribution of the branch cut singularities $-k_0$ and k_0 , respectively, as well as, φ^+ and φ^- contribute to the phase for a given point on the contour of integration around the branch cut. Taking the first case, when the contour of integration is coming from $j\infty$ down to a value close to zero, and evaluating the angle contribution for different points using (3.6), as shown in Figure 3.4(a), the phase for k_ρ is calculated as 2π which means the points are located at the first Riemman sheet. Looking at Figure 3.4(b), and following the same procedure, it is found out the k_ρ phase for this case is

 π selecting the second Riemman sheet.

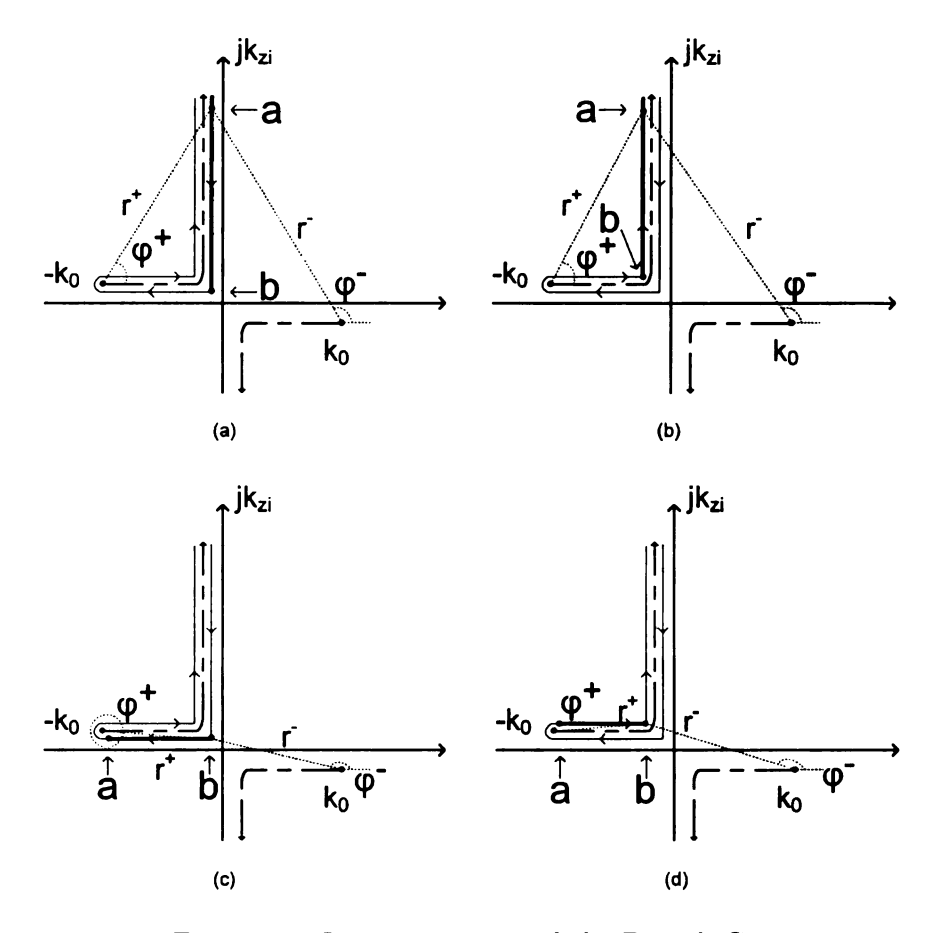


Figure 3.4. Integration around the Branch Cut

$$\int_{C_{b}} e^{-jk_{z}\overline{z}} f(k_{z}, k_{\rho}) dk_{z} = \int_{\infty}^{0} e^{k_{z}i\overline{z}} f(jk_{zi}, \beta) j dk_{zi} + \int_{0}^{-k_{0}} e^{-jk_{z}r\overline{z}} f(k_{zr}, -\alpha) dk_{zr} + \int_{0}^{\infty} e^{-jk_{z}r\overline{z}} f(k_{zr}, \alpha) dk_{zr} + \int_{0}^{\infty} e^{k_{z}i\overline{z}} f(jk_{zi}, -\beta) j dk_{zi} + \int_{0}^{\infty} e^{-jk_{z}\overline{z}} f(k_{z}, k_{\rho}) dk_{z} + \int_{0}^{\infty} e^{-jk_{z}\overline{z}} f(k_{z}, k_{\rho}) dk_{z}$$

$$(3.7)$$

Where $\alpha = \sqrt{k_0^2 - k_{zr}^2}$, $\beta = \sqrt{k_0^2 + k_{zi}^2}$, \int_{\odot} is the integral around the branch cut singularity. When evaluating the integral around the branch cut singularity, the small argument approximation for the Hankel function could be used, and it can be shown that at the limit closed to the singularity, the contribution of the integral vanishes. Thus,

$$\int_{C_b} e^{-jk_z\overline{z}} f(k_z, k_\rho) dk_z = \int_{0}^{\infty} e^{k_z i\overline{z}} \left[f(jk_{zi}, -\beta) - f(jk_{zi}, \beta) \right] j dk_{zi}
+ \int_{0}^{-k_0} e^{-jk_{zr}\overline{z}} \left[f(k_{zr}, \alpha) - f(k_{zr}, -\alpha) \right] dk_{zr}$$
(3.8)

Using the identities $H_n^{(2)}(\varsigma e^{-j\pi}) = -e^{jn\pi}H_n^{(1)}(\varsigma)$ and $H_n^{\prime(2)}(\varsigma e^{-j\pi}) = e^{jn\pi}H_n^{\prime(1)}(\varsigma)$ from [38] we obtain

$$\int_{C_{b}} e^{-jk_{z}\overline{z}} f(k_{z}, k_{\rho}) dk_{z} = \int_{0}^{\infty} e^{k_{z}i\overline{z}} \psi(jk_{z}i, \beta) j dk_{z}i
+ \int_{0}^{-k_{0}} e^{-jk_{z}r\overline{z}} \psi(k_{z}r, \alpha) dk_{z}r$$
(3.9)

$$\psi(k_z, \gamma) = \left[\frac{-H_n^{\prime(1)}(\gamma \rho)}{\gamma a H_n^{(1)}(\gamma a)} + \frac{H_n^{\prime(2)}(\gamma \rho)}{\gamma a H_n^{(2)}(\gamma a)} \right] + \left(\frac{n k_z}{k_0 \gamma a} \right)^2 \left[\frac{-H_n^{(1)}(\gamma \rho)}{\gamma \rho H_n^{\prime(1)}(\gamma a)} + \frac{H_n^{(2)}(\gamma \rho)}{\gamma \rho H_n^{\prime(2)}(\gamma a)} \right]$$
(3.10)

Substituting $H_n^{(1)}(\varsigma) = J_n(\varsigma) + jY_n(\varsigma)$ and $H_n^{(2)}(\varsigma) = J_n(\varsigma) - jY_n(\varsigma)$ over (3.3), evaluation the contour integral, and after some mathematical manipulation, the $G_{\phi\phi}$

can be written as in (3.11), with $\psi(k_z, \gamma)$ shown in 3.12.

$$G_{\phi\phi}(\rho,\phi,z|a,\phi',z') = \frac{-1}{(2\pi)^2} \sum_{n=-\infty}^{\infty} e^{jn\overline{\phi}} \left\{ \int_{0}^{-k_0} dk_{zr} 2j e^{-jk_{zr}\overline{z}} \psi(k_{zr},\alpha) + \int_{0}^{\infty} dk_{zi} 2e^{k_{zi}\overline{z}} \psi(jk_{zi},\beta) \right\}$$
(3.11)

$$\psi(k_z, \gamma) = \frac{J'_n(\gamma \rho) Y_n(\gamma a) - Y'_n(\gamma \rho) J_n(\gamma a)}{\gamma a \left(J_n(\gamma a)^2 + Y_n(\gamma a)^2\right)} - \left(\frac{nk_z}{k_0 \gamma a}\right)^2 \frac{J_n(\gamma \rho) Y'_n(\gamma a) - Y_n(\gamma \rho) J'_n(\gamma a)}{\gamma \rho \left(J'_n(\gamma a)^2 + Y'_n(\gamma a)^2\right)}$$
(3.12)

The infinite and finite integrals in expression (3.11) converge more rapidly for increasing \bar{z} as well as the index n. However, for cylinder with large radius, the modified modal solution converges relatively slower with respect to the steepest descent solution.

3.2 Numerical Results and Discussions

In this Subsection, the convergence of the exact modal solution (EMS) and the modified modal solution (MMS) will be studied for a circular cylinder of radius $a = 0.05\lambda$. After proving a good agreement between the EMS and the MMS, we will compare the steepest decent solution with the MMS for an infinite circular cylinder with large radius ($a = 10\lambda$). Values of the magnitude for different indexes n, from 1 - 7, for EMS and MMS are shown in Figure 3.5, showing the convergence of the magnitude for the $\hat{\phi}\hat{\phi}'$ components represented by (3.2) and (3.11).

Three observation points where analyzed for $R = 100\lambda$. The first case when $\theta = 90^{o}$ is seen in Figure 3.5(a) where EMS and MMS start converging at n = 3. Figure 3.5(b) with $\theta = 45^{o}$ and Figure 3.5(c) with $\theta = 0^{o}$ have a similar behavior to

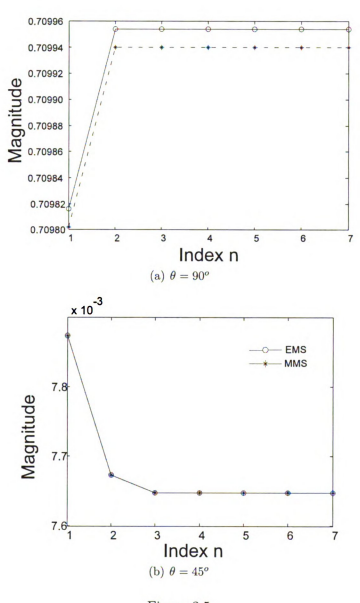


Figure 3.5

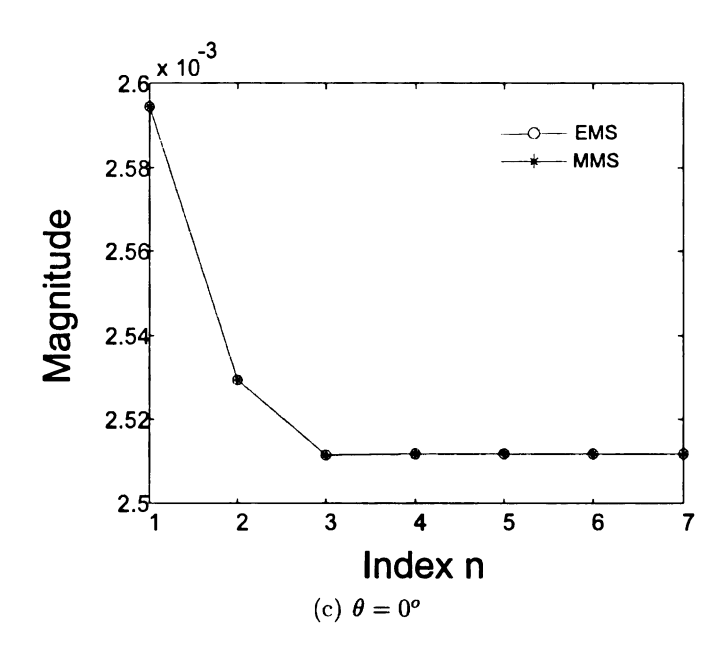


Figure 3.5. Magnitude convergence for exact modal solution and modified modal solution

the previous Figure 3.5(a) where the solution converges for indexes of n greater than 2, which was expected because the size of the cylinder and wave number $n \gg 2ka$. The small error on Figure 3.5(a) is explained by the following: The second integral term in (3.11)that goes form 0 to ∞ and involves an attenuation factor represented by $e^k z i^{\overline{z}}$. As $\theta \to 90^o$, z gets closer to z', $\overline{z} \to 0$, and the attenuation factor goes to 1, therefore the integral will not be attenuated fast enough and errors introduced by $\psi(jk_{zi},\beta)$ will have more impact in the final solution. Figure 3.6 shows phase values for different index of EMS and MMS that converges when n > 2 and different values of $\theta = 0^o, 45^o, 90^o$. As seen MMS and EMS show good agreement in magnitude as well in phase.

Figure 3.7 shows values of magnitude and relative error when n = 3, $R = 50\lambda$ and $0^{o} < \theta < 90^{o}$. Figure 3.7(b) presents the relative error. As seen the error is very small in order of 10^{-6} and does not show a big variation along the scan. This is because

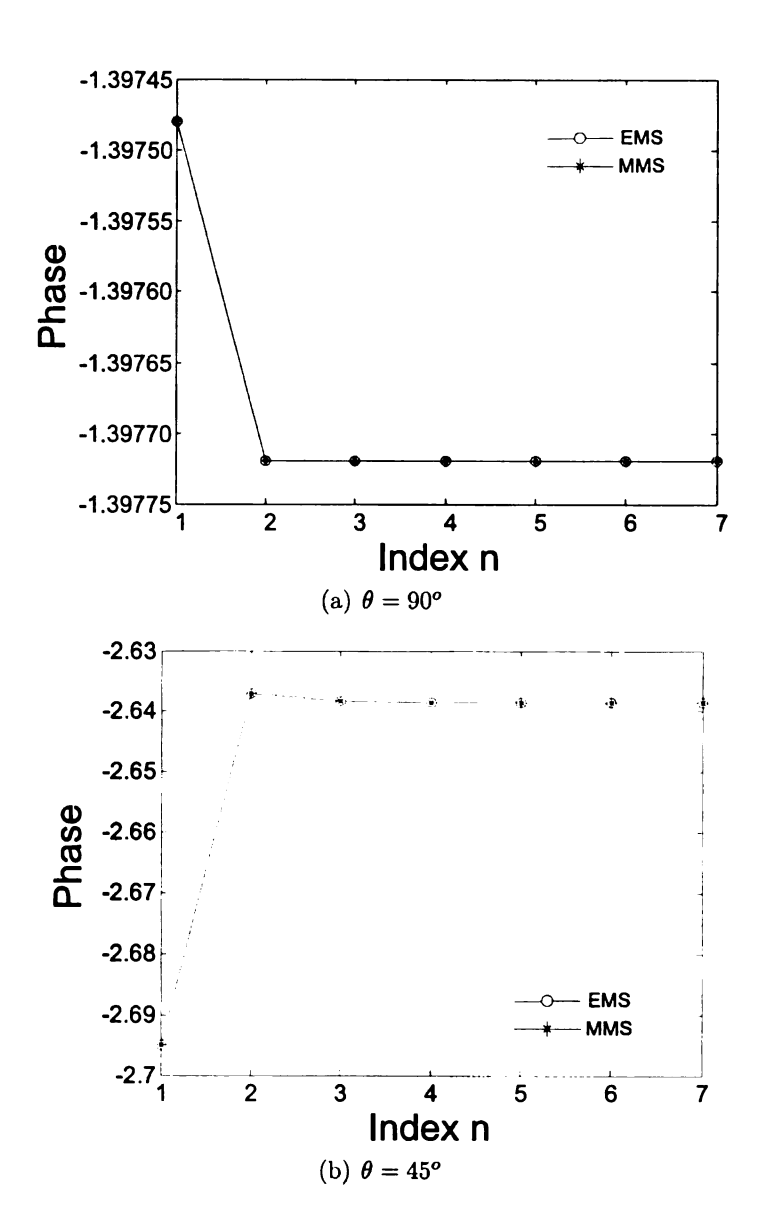


Figure 3.6

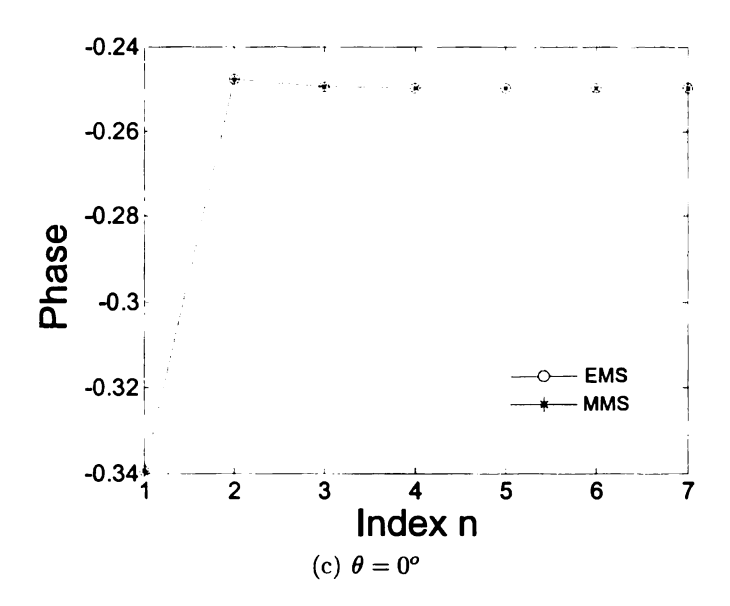


Figure 3.6. Phase convergence for exact modal solution and modified modal solution

the radius of the circular cylinder is small enough to obtain a reasonable answer with both solutions and the observation point is not far away from the source. Figure 3.8 shows the same results as Figure 3.7 but when $R = 100\lambda$. Comparing Figure 3.7(b) with Figure 3.8(b) it is noticed a maximum error occurs when $\theta = 90^{\circ}$; this is because $\psi(jk_{zi},\beta)$ is composed by Bessel functions, which arguments are proportional to $k_{\rho}\rho$ and at $\theta = 90^{\circ}$ $\rho \simeq R = 100\lambda$ thus making it a large argument.

Figure 3.9 presents values of the phase for EMS and MMS and relative errors between them when n=3 and $R=50\lambda$. As seen in Figure 3.9(b) the behavior of the relative error for the phase is similar to the relative error of the magnitude. It is an error of a very small order, 10^{-5} , and it remains constant though $0^o < \theta < 90^o$. The results when $R=100\lambda$ can be seen in Figure 3.10. For Figure 3.10(b) the error increases near $\theta=0^o$ and $\theta=90^o$. The error when $\theta=0^o$ is produced as a result of high oscillations within the first integral of (3.11). Those oscillations exist because when $\theta=0^o$, \bar{z} becomes a big oscillatory argument for $e^{-jk_{Zr}\bar{z}}$. The second error,

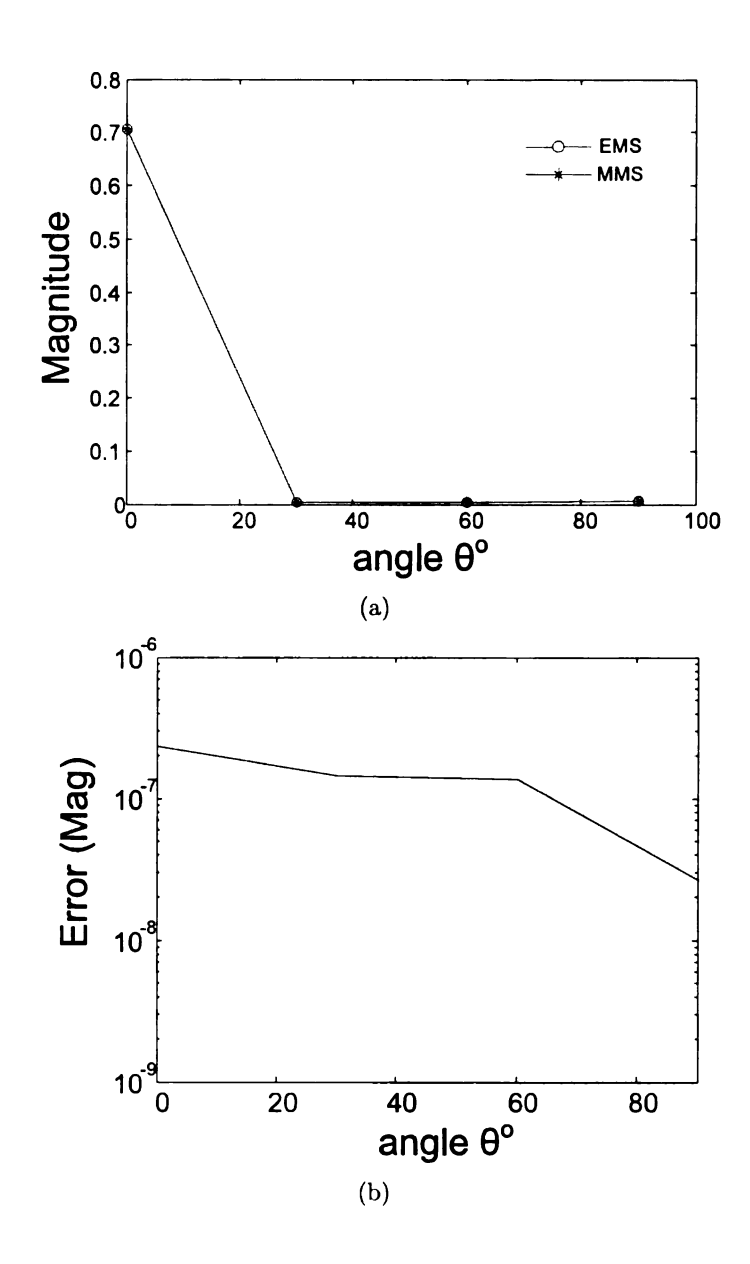


Figure 3.7. (a) Magnitude for exact modal solution and modified modal solution; (b) Relative Error; n=3 and $R=50\lambda$

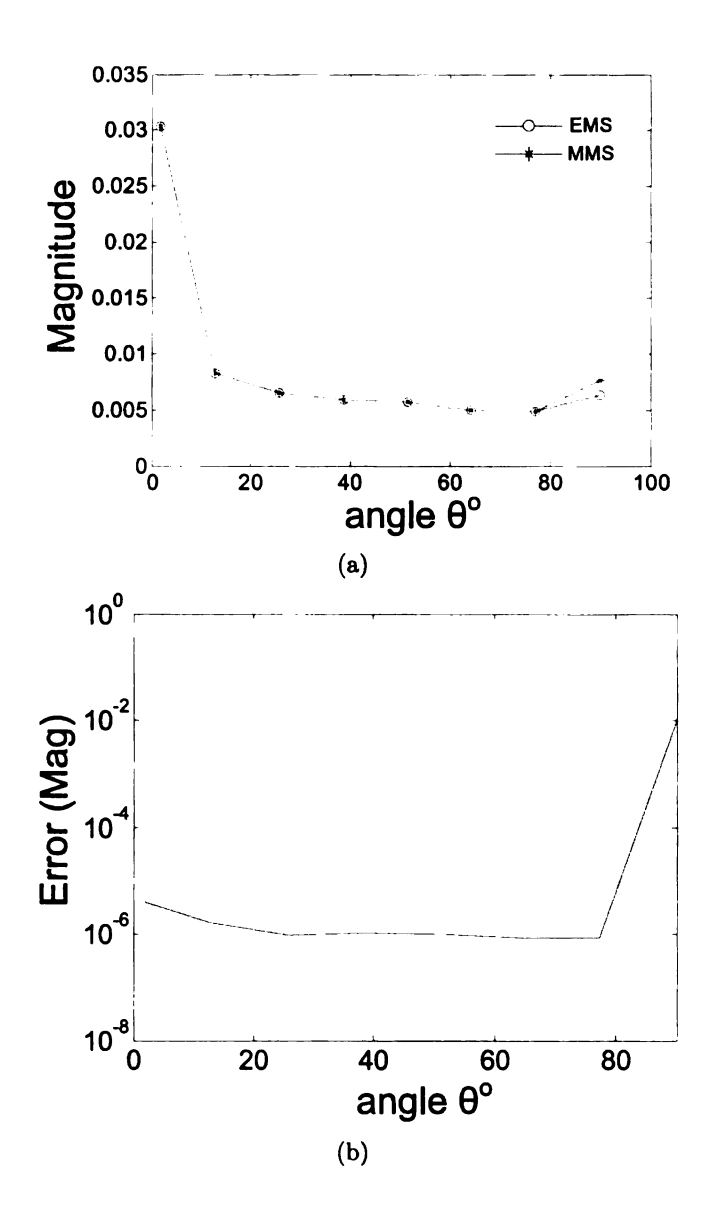


Figure 3.8. (a) Magnitude for exact modal solution and modified modal solution; (b) Relative Error; n=3 and $R=100\lambda$

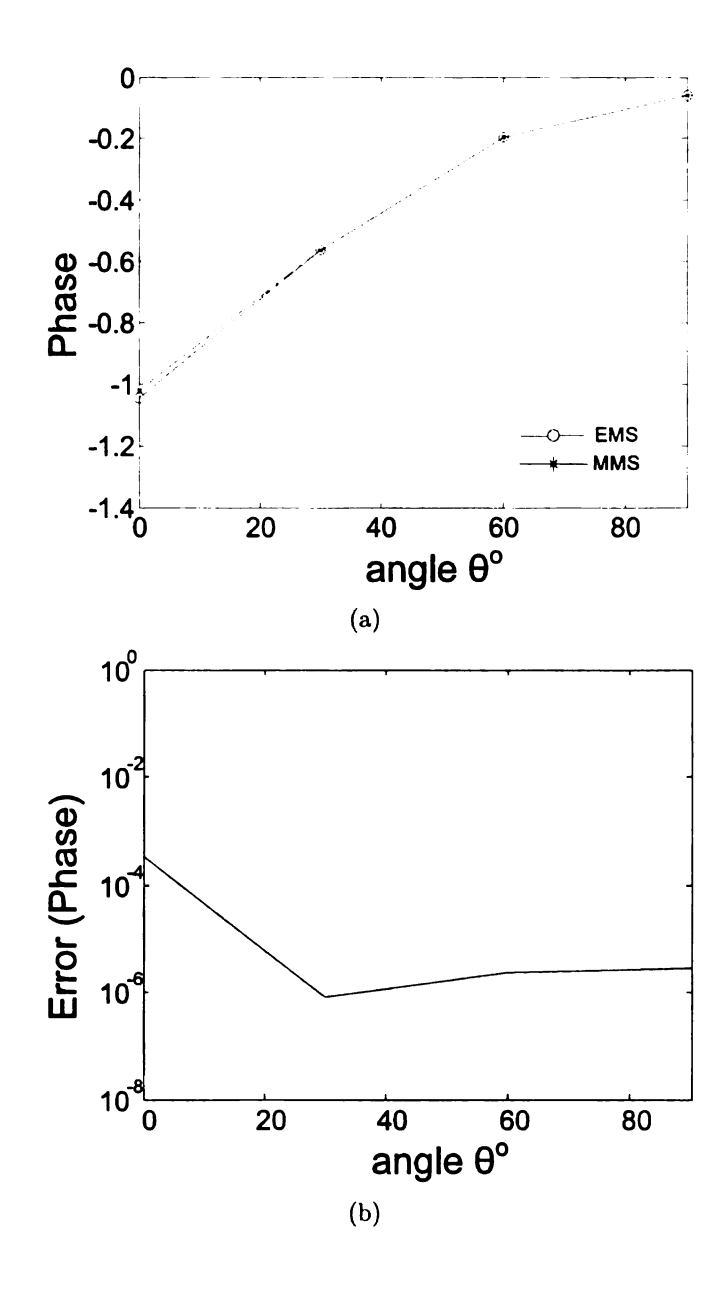


Figure 3.9. (a) Phase for exact modal solution and modified modal solution; (b) Relative Error; n=3 and $R=50\lambda$

when $\theta = 90^{\circ}$ is caused by the same issues as the magnitude relative error, which was discussed for Figure 3.8(b).

Numerical calculations, for different values of R and θ , have been executed to obtain the convergence of the magnitude and phase for both, the steepest descent solution. (SPD), and the modified modal solution and only the most important results have been shown here. The $\hat{\phi}\hat{\phi}'$ component of the dyadic Green's function was computed for $\theta = 0.0572938^o$, $\theta = 46.10219^o$ and $\theta = 89.42706^o$ for a cylinder of radio $a = \lambda$ and $R = 100.0049\lambda$. Comparing Figure 3.11 and Figure 3.12, it is noticed the fast convergence and likeliness of the magnitude and phase when the observation angle $\theta \simeq 90^{\circ}$. For $\theta \simeq 45^{\circ}$ we can see a good agreement of the magnitude and phase. As shown in Figure 3.11(a) and Figure 3.12(a), SPD values do not agree with values obtained using the modal solution ($\theta \sim 0^{\circ}$). Near the paraxial zone, the axial singularities show up, the difference in the magnitudes is bigger and the convergence in the SPD method is not as good as the convergence using the modified modal solution. The lack of convergence of the SPD and the disagreement between the solutions increases because as we get closer to the $\theta = 0$ or $\theta = \pi$ in the k_z plane, saddle point in the α plane is getting near to $\alpha_r = \frac{\pi}{2}$ or $\alpha_r = \frac{-\pi}{2}$, we have the branch cut singularities represented at these points.

Figure 3.13 and Figure 3.14 contain values of magnitude and its relative error for $R = \lambda$ and $R = 100\lambda$ respectively. Both figures were obtained with index n = 10 and $0^{\circ} < \theta < 90^{\circ}$. Comparing Figure 3.13(b) and Figure 3.14(b) it can be seen that both figures present very high errors when $\theta = 0^{\circ}$. The order of the error decreases as the distance from the observation point to the paraxial zone increases. The same behavior is observed on Figure 3.15 and Figure 3.16 where the values of the phase and its relative error for both SDP and MMS are shown.

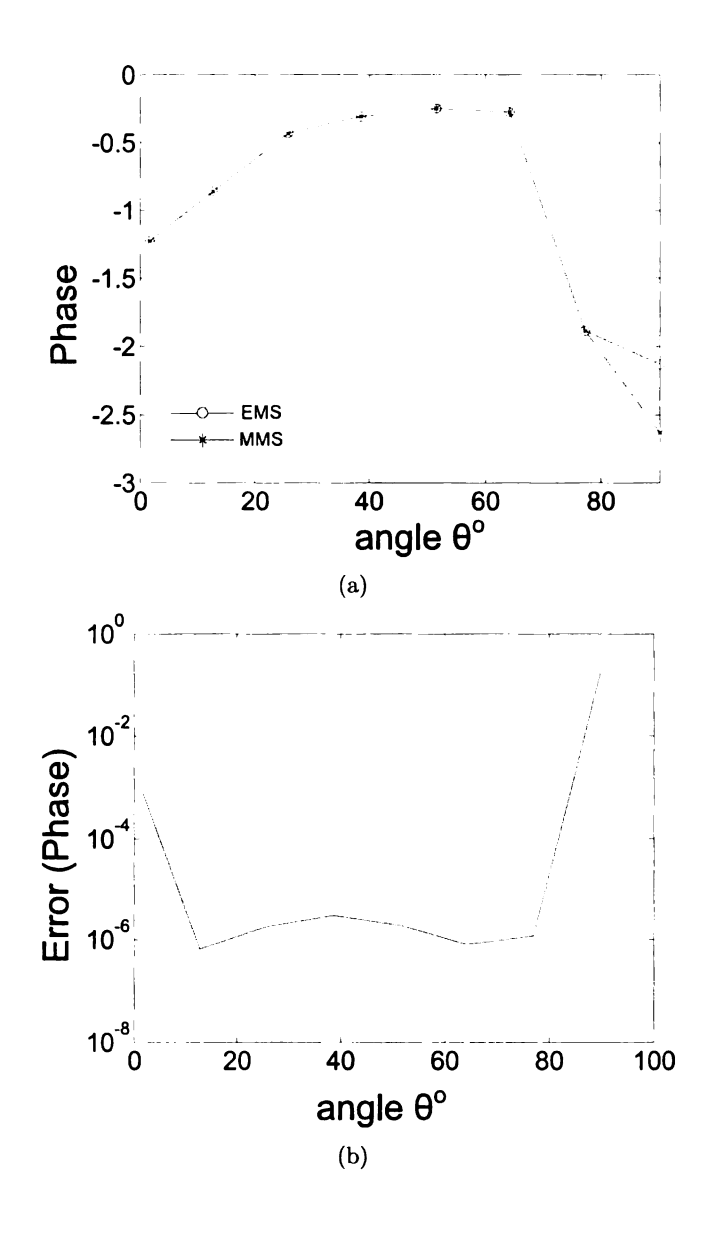


Figure 3.10. (a) Phase for exact modal solution and modified modal solution; (b) Relative Error; n=3 and $R=100\lambda$

3.3 Singly Surface Periodic Structure in \hat{z}

Many applications require the analysis of periodic antennas over structures such as infinite plates [39] and circular cylinders [40]. Looking at Figure 3.17, it can be stated that computationally, it is more efficient to analyze a single unit cell containing information about the periodicity of the structure than simulating the complete periodic structure. The periodic Green's functions have been the focus of many studies similar to the previous [41, 42, 43].

In this section, the development of a periodic Green's function that relates the field produced by magnetic currents due to periodic antennas in \hat{z} over the surface of an infinite circular cylinder will be explained. The periodic phased array of antennas must be expressed in terms of one unit cell and the fields produced by it will be expressed in terms of Floquet modes. The infinite array of magnetic current sources is written in terms of a singular magnetic current term as

$$\mathbf{M}(\rho = a, \phi', z' + \frac{2m\pi}{L}) = \mathbf{M}(\rho = a, \phi', z')e^{-jk_z}\frac{2m\pi}{L}$$
 (3.13)

where L is the distance between array elements in the \hat{z} direction, and the field due to this infinite periodic magnetic currents is expressed as

$$\mathbf{H}(\mathbf{r}) = jw\epsilon_0 \sum_{m=-\infty}^{\infty} \iint_{\mathbf{R}_{\mathbf{q}}} \mathbf{M}(\mathbf{r}') \cdot \overline{\mathbf{G}}_{e2}(\mathbf{r}'|\mathbf{r}) e^{-jk_z \frac{2m\pi}{L}} dS'$$
 (3.14)

Periodic Green's functions are a common approach to attack these problems, the periodic infinite array can be translated as part of the Green's function such that

$$\overline{\mathbf{G}}_{Pe2}(\rho,\phi,z|a,\phi',z') = \sum_{m=-\infty}^{\infty} \overline{\mathbf{G}}_{e2}(\rho,\phi,z|a,\phi',z'-\frac{2m\pi}{L})e^{-jk_z\frac{2m\pi}{L}}$$
(3.15)

in this way (3.14) is re-written in the following known way

$$\mathbf{H}(\mathbf{r}) = jw\epsilon_0 \iint_{Sa} \mathbf{M}(\mathbf{r}') \cdot \overline{\mathbf{G}}_{Pe2}(\mathbf{r}'|\mathbf{r}) dS'$$
 (3.16)

and the periodic dyadic Green's function of the second kind for a infinite PEC circular cylinder of radius a is

$$\overline{G}_{Pe2}^{(2)}(\rho,\phi,z|a,\phi',z') = \frac{1}{(2\pi)^2} \sum_{m=-\infty}^{\infty} \sum_{n=-\infty}^{\infty} e^{jn\overline{\phi}} \int_{-\infty}^{\infty} dk_z e^{-jk_z\overline{z}} e^{-jk_z} \frac{2m\pi}{L} \\
\left\{ \left[\frac{-jnH_n^{(2)}(k_\rho\rho)}{k_\rho ak_\rho\rho H_n^{(2)}(k_\rho a)} + \frac{jn}{(k_\rho a)^2} \left(\frac{k_z}{k_0} \right)^2 \frac{H_n^{\prime(2)}(k_\rho\rho)}{H_n^{\prime(2)}(k_\rho a)} \right] \hat{\rho}\hat{\phi}' - j \left[\frac{k_z k_\rho H_n^{\prime(2)}(k_\rho\rho)}{k_\rho ak_0^2 H_n^{\prime(2)}(k_\rho a)} \right] \hat{\rho}\hat{z}' \\
+ \left[\frac{H_n^{\prime(2)}(k_\rho\rho)}{k_\rho aH_n^{(2)}(k_\rho a)} - \left(\frac{nk_z}{k_0 k_\rho a} \right)^2 \frac{H_n^{(2)}(k_\rho\rho)}{(k_\rho\rho) H_n^{\prime(2)}(k_\rho a)} \right] \hat{\phi}\hat{\phi}' + \left[\frac{nk_z k_\rho H_n^{(2)}(k_\rho\rho)}{k_\rho a(k_\rho\rho) k_0^2 H_n^{\prime(2)}(k_\rho a)} \right] \hat{\phi}\hat{z}' \\
+ \left[\frac{nk_z k_\rho H_n^{(2)}(k_\rho\rho)}{(k_\rho a)^2 k_0^2 H_n^{\prime(2)}(k_\rho\rho)} \right] \hat{z}\hat{\phi}' - \frac{1}{k_\rho a} \left[\left(\frac{k_\rho}{k_0} \right)^2 \frac{H_n^{(2)}(k_\rho\rho)}{H_n^{\prime(2)}(k_\rho a)} \right] \hat{z}\hat{z}' \right\} \tag{3.17}$$

Using Poisson summation formula [34]

$$\sum_{q=-\infty}^{\infty} \frac{1}{|T|} e^{jt} \frac{2q\pi}{T} = \sum_{p=-\infty}^{\infty} \delta(t-pT)$$
 (3.18)

with $t = k_z$ and T = L we have

$$\sum_{m=-\infty}^{\infty} \frac{1}{|-L|} e^{-jk_z \frac{2m\pi}{L}} = \sum_{p=-\infty}^{\infty} \delta(k_z + pL)$$
 (3.19)

using (3.19) into (3.17)

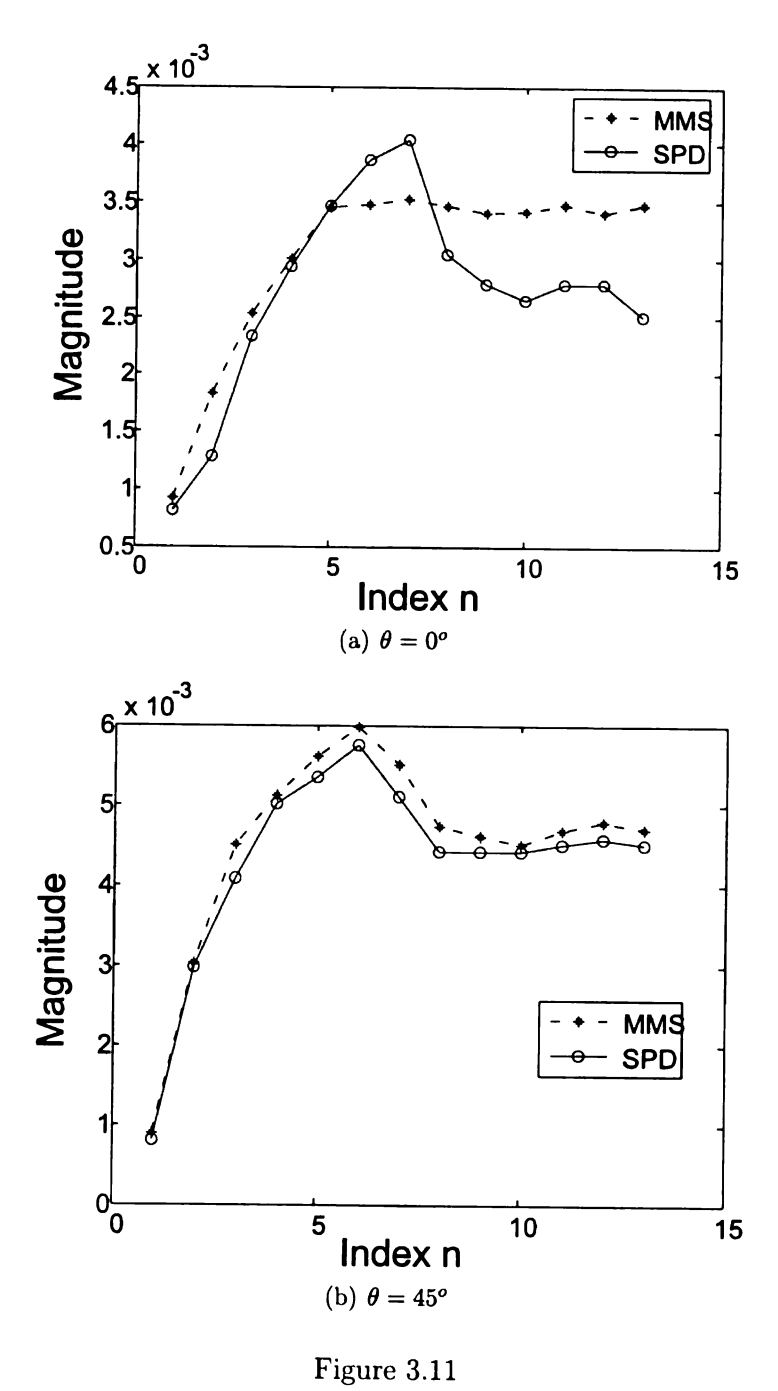
$$\overline{G}_{Pe2}^{(2)}(\rho,\phi,z|a,\phi',z') = \frac{L}{(2\pi)^2} \sum_{n=-\infty}^{\infty} e^{jn\overline{\phi}} \int_{-\infty}^{\infty} dk_z e^{-jk_z\overline{z}} \sum_{m=-\infty}^{\infty} \delta(k_z + mL)
\left\{ \left[\frac{-jnH_n^{(2)}(k_\rho\rho)}{k_\rho ak_\rho\rho H_n^{(2)}(k_\rho a)} + \frac{jn}{(k_\rho a)^2} \left(\frac{k_z}{k_0} \right)^2 \frac{H_n^{\prime(2)}(k_\rho\rho)}{H_n^{\prime(2)}(k_\rho a)} \right] \hat{\rho}\hat{\phi}' - j \left[\frac{k_z k_\rho H_n^{\prime(2)}(k_\rho\rho)}{k_\rho ak_0^2 H_n^{\prime(2)}(k_\rho a)} \right] \hat{\rho}\hat{z}'
+ \left[\frac{H_n^{\prime(2)}(k_\rho\rho)}{k_\rho aH_n^{(2)}(k_\rho a)} - \left(\frac{nk_z}{k_0 k_\rho a} \right)^2 \frac{H_n^{(2)}(k_\rho\rho)}{(k_\rho\rho) H_n^{\prime(2)}(k_\rho a)} \right] \hat{\phi}\hat{\phi}' + \left[\frac{nk_z k_\rho H_n^{(2)}(k_\rho\rho)}{k_\rho a(k_\rho\rho) k_0^2 H_n^{\prime(2)}(k_\rho a)} \right] \hat{\phi}\hat{z}'
+ \left[\frac{nk_z k_\rho H_n^{(2)}(k_\rho\rho)}{(k_\rho a)^2 k_0^2 H_n^{\prime(2)}(k_\rho\rho)} \right] \hat{z}\hat{\phi}' - \frac{1}{k_\rho a} \left[\left(\frac{k_\rho}{k_0} \right)^2 \frac{H_n^{(2)}(k_\rho\rho)}{H_n^{\prime(2)}(k_\rho a)} \right] \hat{z}\hat{z}' \right\}$$
(3.20)

Solving the integrand of (3.20), the periodic Green's function is not a spectral solution anymore and it becomes a modal solution with eigenvalues dictated by the periodicity of the array elements as seen

$$\overline{G}_{Pe2}^{(2)}(\rho,\phi,z|a,\phi',z') = \frac{L}{(2\pi)^2} \sum_{n=-\infty}^{\infty} e^{jn\overline{\phi}} \sum_{m=-\infty}^{\infty} e^{jmL\overline{z}} \\
\left\{ \left[\frac{-jnH_n^{(2)}(k_{m\rho}\rho)}{k_{m\rho}ak_{m\rho}\rho H_n^{(2)}(k_{m\rho}a)} + \frac{jn}{(k_{m\rho}a)^2} \left(\frac{mL}{k_0} \right)^2 \frac{H_n^{\prime(2)}(k_{m\rho}\rho)}{H_n^{\prime(2)}(k_{m\rho}a)} \right] \hat{\rho}\hat{\phi}' \\
+j \left[\frac{mLk_{m\rho}H_n^{\prime(2)}(k_{m\rho}\rho)}{k_{m\rho}ak_0^2 H_n^{\prime(2)}(k_{m\rho}a)} \right] \hat{\rho}\hat{z}' - \left[\frac{nmLk_{m\rho}H_n^{(2)}(k_{m\rho}\rho)}{k_{m\rho}a(k_{m\rho}\rho)k_0^2 H_n^{\prime(2)}(k_{m\rho}a)} \right] \hat{\phi}\hat{z}' \\
+ \left[\frac{H_n^{\prime(2)}(k_{m\rho}\rho)}{k_{m\rho}aH_n^{(2)}(k_{m\rho}a)} - \left(\frac{nmL}{k_0k_{m\rho}a} \right)^2 \frac{H_n^{(2)}(k_{m\rho}\rho)}{(k_{m\rho}\rho)H_n^{\prime(2)}(k_{m\rho}a)} \right] \hat{\phi}\hat{\phi}' \\
- \left[\frac{nmLk_{m\rho}H_n^{(2)}(k_{m\rho}\rho)}{(k_{m\rho}a)^2 k_0^2 H_n^{\prime(2)}(k_{m\rho}a)} \right] \hat{z}\hat{\phi}' - \frac{1}{k_{m\rho}a} \left[\left(\frac{k_{m\rho}}{k_0} \right)^2 \frac{H_n^{(2)}(k_{m\rho}\rho)}{H_n^{\prime(2)}(k_{m\rho}a)} \right] \hat{z}\hat{z}' \right\} \tag{3.21}$$

where $k_{m\rho} = \sqrt{k_0^2 - (mL)^2}$. The next step is the efficient implementation of this

periodic Green's function. This is a very changeling problem because the summation of Floquet modes usually converges very slowly, and this is left for future works.



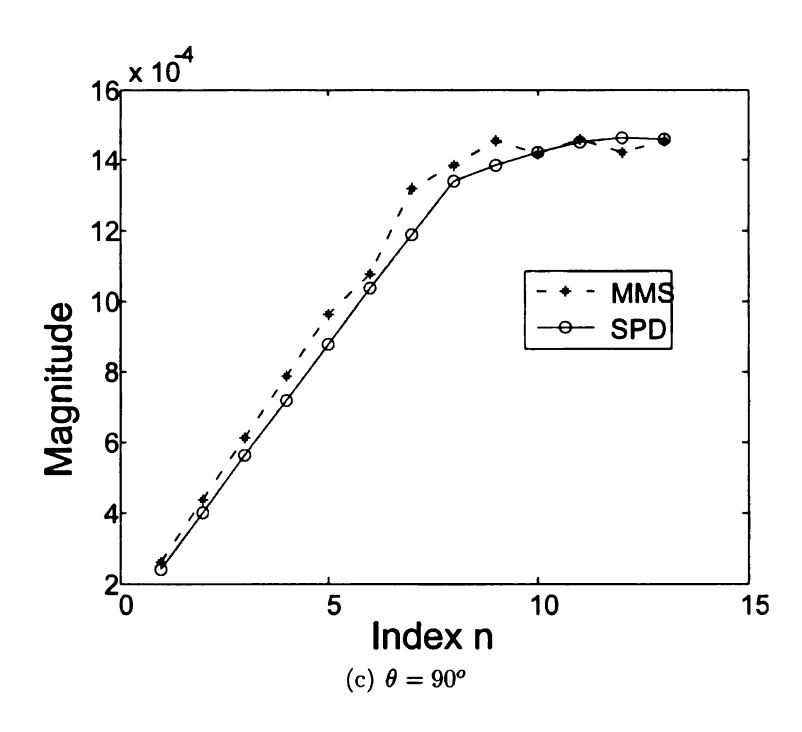


Figure 3.11. Magnitude convergence for modified modal solution and steepest descent solution $\,$

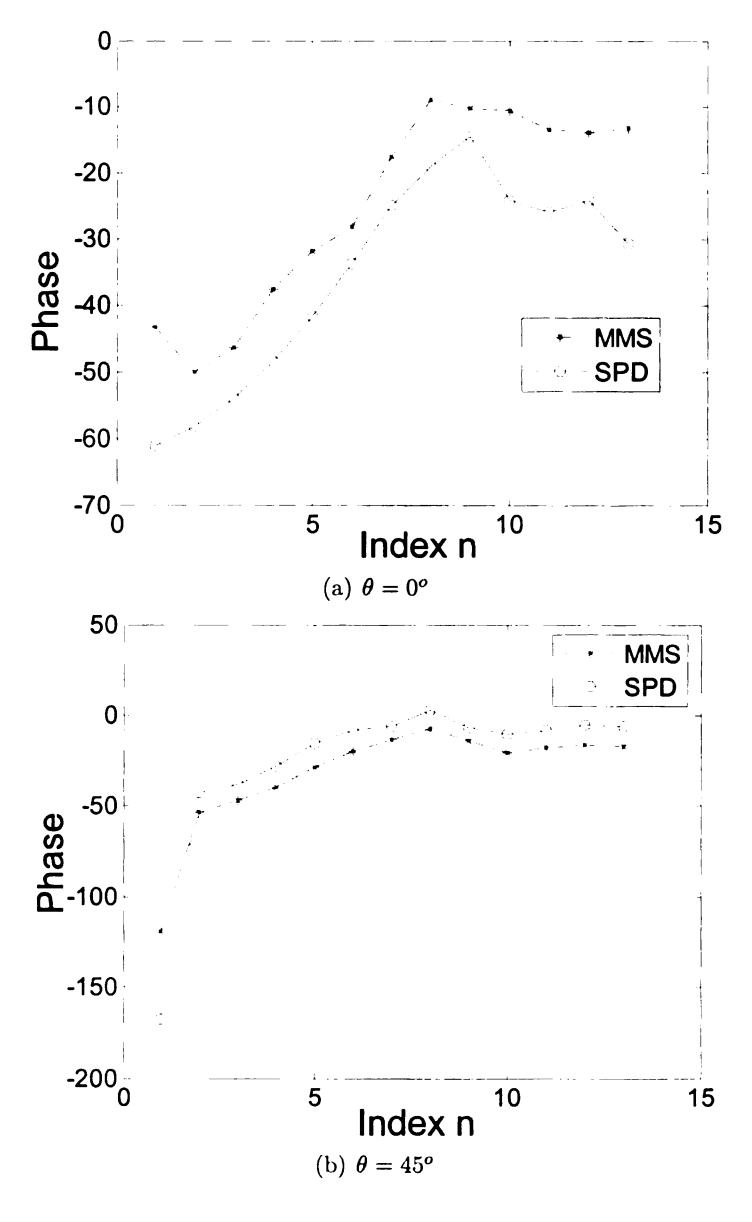


Figure 3.12

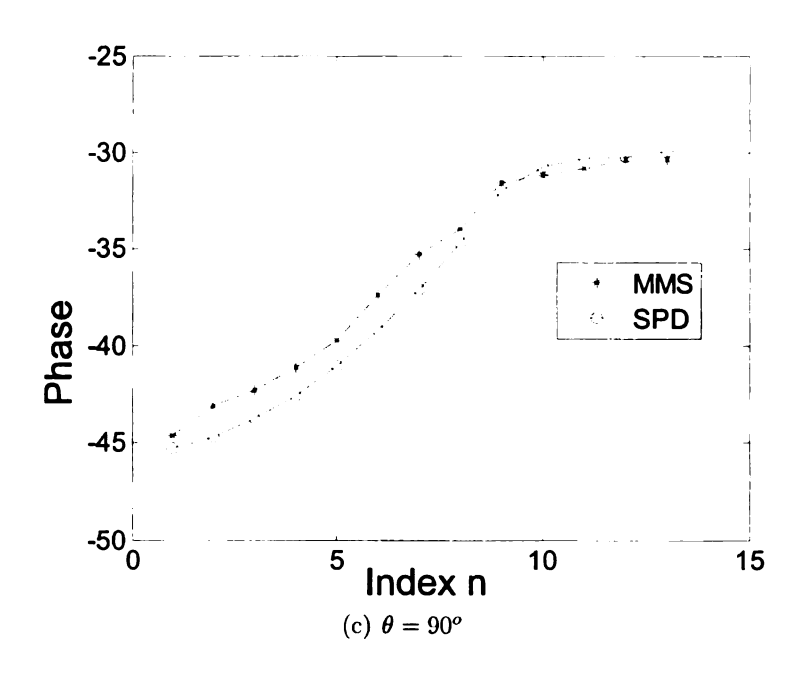


Figure 3.12. Phase convergence for modified modal solution and steepest descent solution

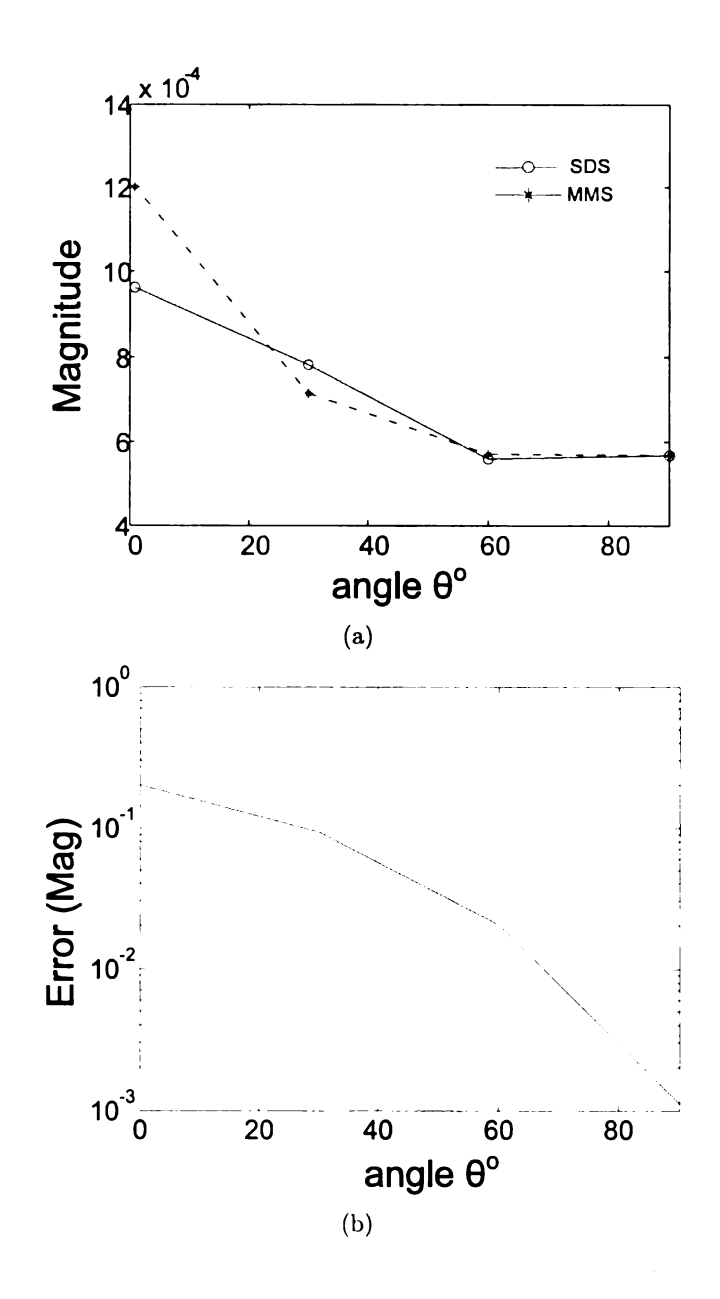


Figure 3.13. (a) Magnitude for modified modal solution and steepest descent solution; (b) Relative error; $n=10,\ R=50\lambda$

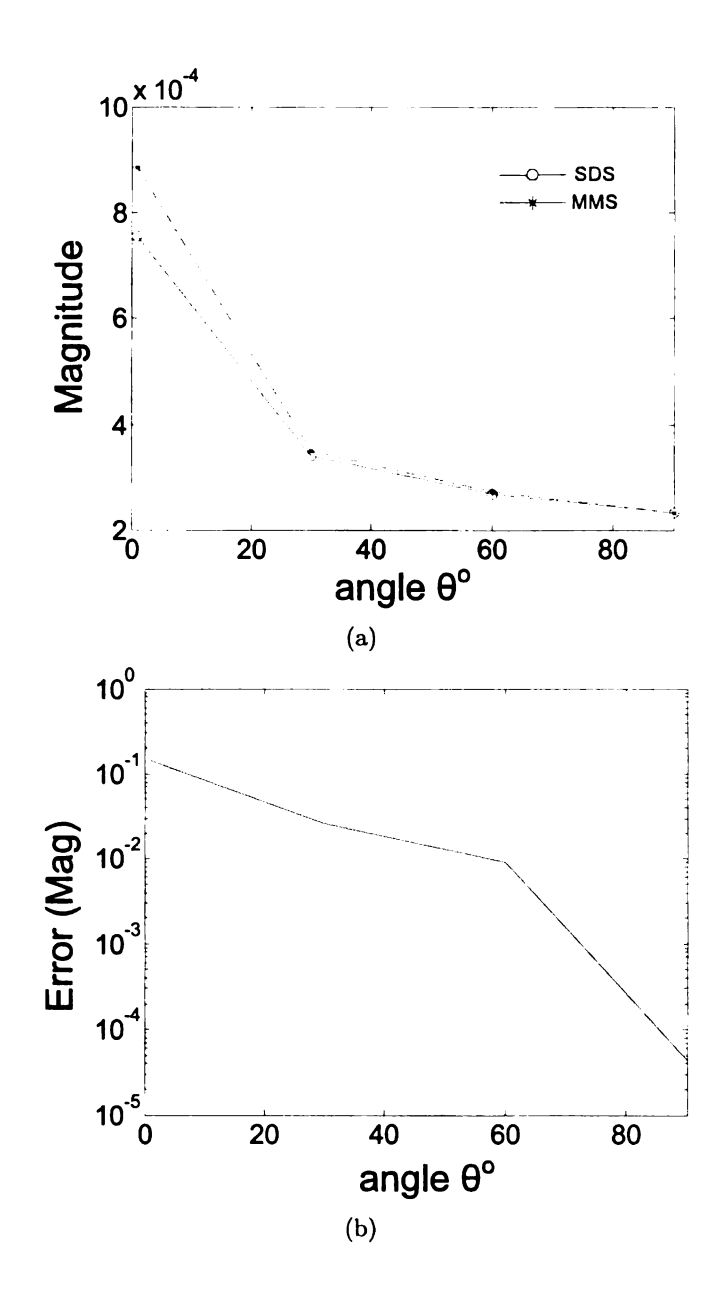


Figure 3.14. (a) Magnitude for modified modal solution and steepest descent solution; (b) Relative error; $n=10,~R=100\lambda$

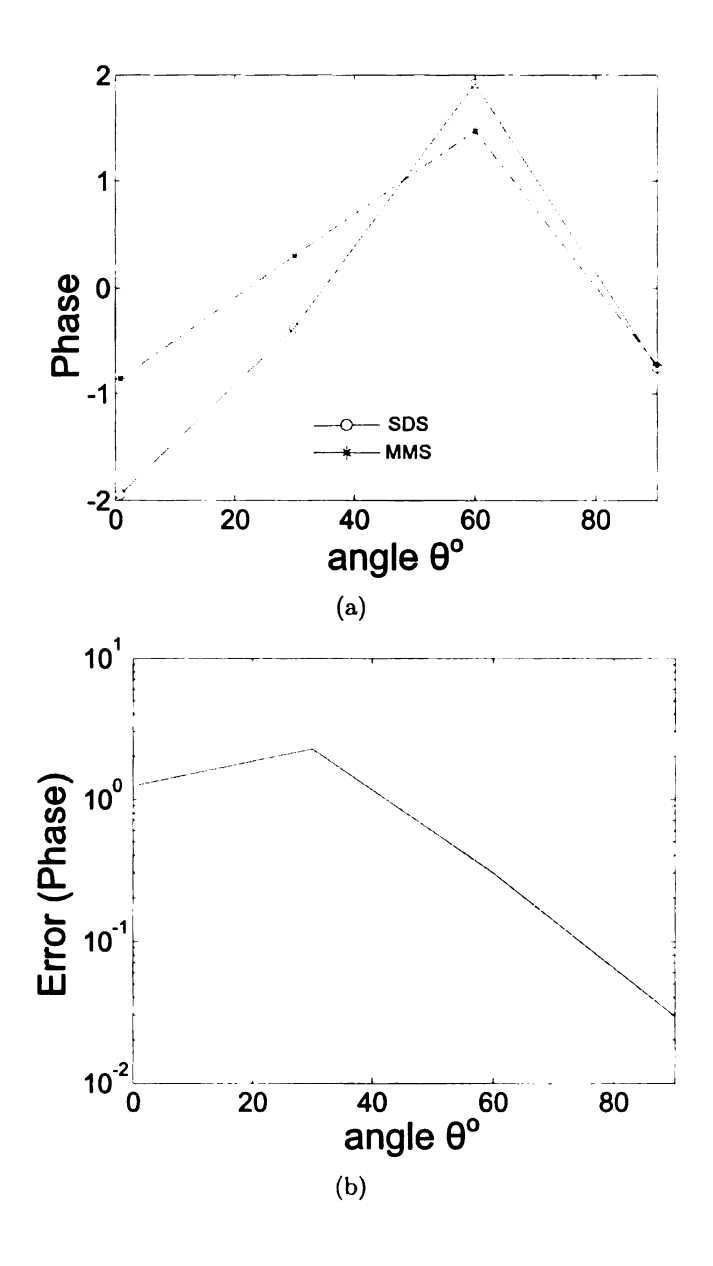


Figure 3.15. (a) Phase for modified modal solution and steepest descent solution; (b) Relative error; $n=10,\,R=50\lambda$

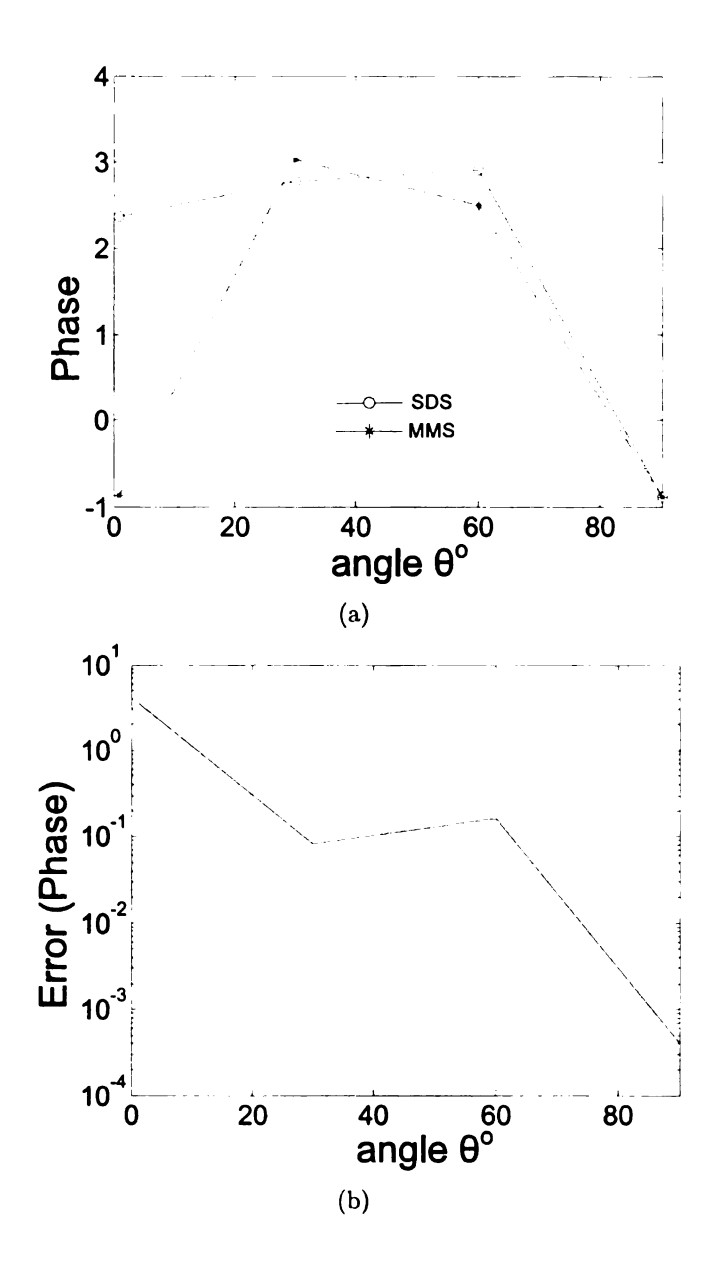


Figure 3.16. (a) Phase for modified modal solution and steepest descent solution; (b) Relative error; $n=10,\,R=100\lambda$

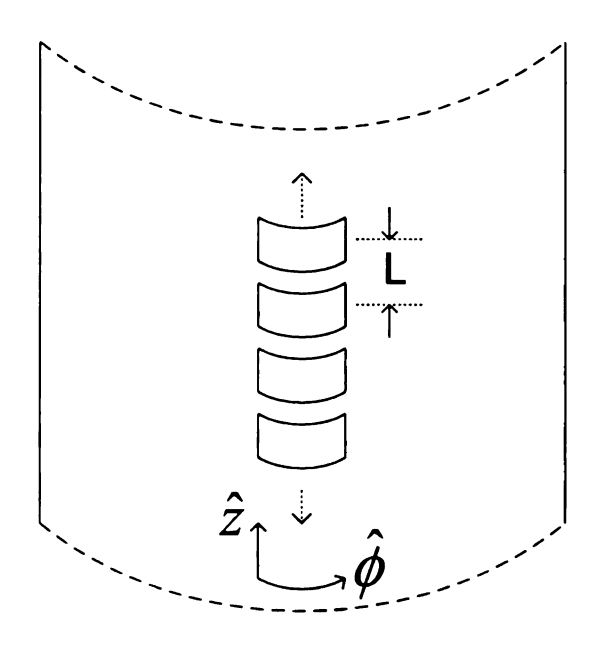


Figure 3.17. Singly surface periodic structure in \hat{z}

CHAPTER 4

CONCLUSIONS AND FUTURE WORK

A modified modal solution for obtaining the field due to magnetic currents as an aperture on an infinite circular cylinder was obtained. Validation of this solution was made by comparing the MMS with the exact modal solution for the same problem. The agreement between both methods, as expected, was very good for cylinders with small radius ($a < 0.01\lambda$) and the distance between the source and the observation points no larger than 50λ , obtaining a relative error between the solution around order of 10^{-6} . For distances grater than 50λ the relative error between them increases due to convergence problems with the exact modal solution, specifically at $\theta = 90^{\circ}$.

A deep analysis of the steepest descent solution was made concluding that the solution was not accurate for the paraxial zone due to axial singularities in the k_z plane, omitted when the saddle point technique was implemented. Those axial singularities where detected to show up when the angle θ of the observation point was close to 0^o and 180^o .

The MMS was found to be a good solution to over come the lack of accuracy around the paraxial zone for circular cylinders of larger radius ($a = \lambda$). It was demonstrated this solution provides the same accuracy as the steepest descent solution near the azimuth region $35^{\circ} < \theta < 135^{\circ}$. For angles smaller or greater than those, the steepest descent method fails converging to an accurate solution. Although steepest descent remains faster converging at the azimuth zone, the MMS provides a smooth transition between the paraxial region and the azimuth region.

Although MMS was found for an infinite circular cylinder, this solution can be expanded for an infinite elliptical cylinder by multiplying the MMS with the specific torsion factor and radius of curvature for an elliptical cylinder. These coefficients

could be found by using UTD.

As a future work, a FE-BI code could be implemented using the MMS as boundary integral for truncating the computational domain, this code can be validated by using analytic solutions for the radar cross section of an antenna embedded in an infinite circular or elliptical cylinder. Diffraction and attenuation coefficients for prolate spheroids can be found to expand this solution for arbitrary shapes with doubly surface.

Additionally, a periodic Green's function that relates the field produced by magnetic currents due to periodic array antennas on \hat{z} and over the surface of an infinite circular cylinder was obtained using Floquet's theorem and the Poisson summation equation. The efficient implementation of this solution is left for future works.

BIBLIOGRAPHY

BIBLIOGRAPHY

- [1] W. D. Burnside, "Analysis of on-aircraft antenna patterns," report 3390-1, Ohio State Univ. ElctroScience Lab., Columbus, August 1972.
- [2] P. H. Pathak, A. Ghantous, C. W. Chuang, and O. M. Buyukdura, "A Preliminary Investigation of Conformal Antenna Phased Arrays on Perfectly-Conducting Convex Surfaces," Final Report 717060-2, The Ohio State University, ElectroScience Laboratory, Nov 1985.
- [3] B. Thors, L. Josefsson, and R. G. Rojas, "The rcs of a cylindrical array antenna coated with a dielectric layer," *IEEE Trans. Antennas Propagat.*, vol. 52, pp. 1851–1858, Jul 2004.
- [4] C. A. Macon and L. C. Kempel, "Modeling conformal antennas on metallic prolate spheroid surfaces using a hybrid finite element method," *IEEE Trans. Antennas Propagat.*, vol. 52, pp. 750–758, March 2002.
- [5] J. Shim and H. Kim, "Dominance of creeping wave modes of backscattered field from a conducting sphere with dielectric coating," *PIER*, vol. 21, pp. 293–306, 1999.
- [6] J. L. Volakis, A. Chatterjee, and L. C. Kempel, Finite Element Method for Electromagnetics. IEEE Press, New York, 1998.
- [7] J. Jin, The Finite Element Method in Electromagnetics. John Wiley and Sons, New York, 2002.
- [8] R. Mittra and S. Safavi-Naini, "Source Radiation in the Presence of Smooth Convex Bodies," *Radio Science*, vol. 14, pp. 217–237, March 1979.
- [9] A. Nakatini, N. Alexopoulus, N. Uzunoglu, and P. Uslenghi, "Accurate Greens Function Computation for Printed Circuit Antennas on Cylindrical Antennas," *Electromagnetics*, vol. 6, pp. 243–254, July 1986.

- [10] J. B. Keller, "Geometrical Theory of Diffraction," J. Opt. Soc. Amer., vol. 52, pp. 116–130, Feb 1962.
- [11] V. B. Erturk and R. G. Rojas, "Paraxial space-domain formulation for surface fields on a large dielectric coated circular cylinder," *IEEE Trans. Antennas Propagat.*, vol. 50, pp. 1577–1587, Nov 2002.
- [12] T. S. Bird, "Comparison of asymptotic solutions for the surface field excited by a magnetic dipole on a cylinder," *IEEE Trans. Antennas Propagat.*, vol. AP-32, pp. 1237–1244, Nov 1984.
- [13] D. Chatterjee, "Paraxial and source region behavior of a class of asymptotic and rigorous (mom) solutions in the high-frequency planar limit," *IEEE Antennas and Wirless Propagat Letters*, vol. 4, pp. 71–74, 2005.
- [14] C. Tokgoz, "A Heuristic Solution for the Surface Magnetic Field on a Source Excited Circular Cylinder with an Impedance Boundary Condition," Antennas and Propagation Society International Symposium, 2005 IEEE, vol. 1B, pp. 368– 371, 2005.
- [15] C. Tokgoz, P. H. Pathak, and R. J. Marhefka, "An Asymptotic Solution for the Surface Magnetic Field Within the Paraxial Region of a Circular Cylinder with an Impedance Boundary Condition," *IEEE Trans. Antennas Propagat.*, vol. 53, pp. 1435–1443, Aprl 2005.
- [16] S. R. Silver and W. K. Saunders, "The External Field Produced by a Slot on an Infinite Cylinder," J. Appl. Phys., vol. 21, pp. 153–158, Feb 1950.
- [17] J. R. Wait and S. H. Kahana, "Calculated Patterns of Circumferential Slots in a Circular Cylinder," *Can. J. Tech.*, vol. 33, pp. 77–79, Jan 1955.
- [18] L. L. Bailin, "Field Produced by a Slot on an Large Circular Cylinder," Trans. Inst. Radio Engrs., vol. AP-3, p. 128, July 1955.
- [19] G. N. Watson, "The Diffraction of Electric Waves by the Earth," *Proc. Roy. Soc.*, vol. A95, pp. 83–99, Oct 1918.
- [20] J. W. Crispin and A. L. Maffett, "Radar Cross-Sectionn Estimation for Simple Shapes," *Proc. IEEE*, vol. 53, pp. 833–843, 1965.
- [21] R. F. Goodrich, A. L. Maffett, N. Reitlinger, C. E. Schensted, and K. M. Siegel, "Studies in Radar Cross Sections xxii, Elementary Slot Radiators," final report, Engineering Res. Inst., Ann Arbor, Mich., Nov 1956.

- [22] H. Ikuno and L. Felsen, "Complex ray interpretation of reflection from concaveconvex surfaces," *IEEE Trans. Antennas Propagat.*, vol. 36, pp. 1260–1271, Sept 1988.
- [23] P. H. Pathak, N. Wang, W. D. Burnside, and R. G. Kouyoumjian, "A Uniform GTD Solution for the Radiation from Sources on a Convex Surface," *IEEE Trans. Antennas Propagat.*, vol. AP-29, pp. 609–622, Jul 1981.
- [24] C. Demirdag and R. Rojas, "Mutual coupling calculations on a dielectric coated pec cylinder using a utd-based green's function," *Antennas and Propagation Society International Symposium*, 1997 IEEE, vol. 3, pp. 1525–1528, Jul 1997.
- [25] P. H. Pathak and N. Wang, "Ray Analysis of Mutual Coupling Between Antennas on a Convex Surface," *IEEE Trans. Antennas Propagat.*, vol. AP-29, pp. 911–922, Nov 1981.
- [26] P. H. Pathak and R. G. Kouyoumjian, "An Analysis of the Radiation from Apertures in a Curved Surfaces by the Geometrical Theory of Diffraction," *Proc. IEEE*, vol. 62, pp. 1438–1447, Nov 1974.
- [27] B. R. Levy and J. B. Keller, "Diffraction by a Smooth Object," Comm. Pure Appl. Math., vol. 12, pp. 159–209, 1959.
- [28] V. A. Fock, *Electromagnetic Diffraction and Propagation Problems*. Pergamon Press, Oxford, 1965.
- [29] C. T. Tai, Dyadic Green Functions in Electromagnetic Theory. IEEE Press, New Jersey, 1994.
- [30] W. W. Hansen, "A New Type of Expansion in Radiation Problems," *Phys. Rev.*, vol. 47, pp. 139–146, Jan 1935.
- [31] A. Sommerfeld, Partial Differential Equations. Academic Press, New York, 1949.
- [32] R. F. Harrington, Time-Harmonic Electromagnetic Fields. McGraw-Hill, New York, 1961.
- [33] J. R. Wait, Electromagnetic Radiation from Cylindrical Structures. Pergamon Press, New York, 1959.
- [34] A. Ishimaru, Electromagnetic Wave Propagation, Radiation, and Scattering. Prentice Hall, Jersey, 1991.

- [35] N. Bleistein and R. A. Handelsman, Asymptotic Expansions of Integrals. Dover Publications, New York, 1975.
- [36] N. N. Lebedev, Special Functions and Their Applications. Dover, New York, 1972.
- [37] C. A. Macon, Modeling the Radiation From Cavity-Backed Antennas on Prolate Spheroids Using a Hybrid Finite Element-Boundary Integral Method. PhD thesis, Michigan State University, 2001.
- [38] M. Abramowitz and I. A. Stegun, *Handbook of Mathematical Functions*. Dover Publications, New York, 1972.
- [39] C. P. Wu, N. Amitay, and V. Galindo, Theory and Analysis of Phased Array Antennas. John Wiley and Sons Inc, New York, 1972.
- [40] D. Mastela, L. Reindl, L. Wiebking, and L. Zander, "Development of a Cylindrical Microstrip Phased Array Antenna for a Radio Tracking System," Antenna Technology Small Antennas and Novel Metamaterials, 2006 IEEE International Workshop on, pp. 381–383, March 6–8 2006.
- [41] J. Gao and B. Shanker, "Time domain weyl's identity and the causality trick based formulation of the time domain periodic green's function," *IEEE Trans. Antennas Propagat.*, vol. 55, pp. 1656–1666, June 2007.
- [42] R. Jorgenson and R. Mittra, "Efficient calculation of the free-space periodic green's function," *IEEE Trans. Antennas Propagat.*, vol. 38, pp. 633–642, May 1990.
- [43] R. Jorgenson and R. Mittra, "Oblique scattering from lossy strip structures with one-dimensional periodicity," *IEEE Trans. Antennas Propagat.*, vol. 38, pp. 212–219, Feb 1990.

